UNIVERSITÀ
DEGLI STUDI
DI PADOVA

Sede Amministrativa: Università degli Studi di Padova

Dipartimento di Ingegneria Idraulica Marittima Ambientale e Geotecnica

SCUOLA DI DOTTORATO DI RICERCA IN
SCIENZE DELL'INGEGNERIA CIVILE ED AMBIENTALE
CICLO XXIII

CATCHMENT-SCALE TRANSPORT PHENOMENA: RAINFALL INTERMITTENCY, AGE OF RUNOFF, ANTHROPIC CATCHMENT MANAGEMENT

Direttore della Scuola : Ch.mo Prof. Stefano Lanzoni

Supervisori : Ch.mo Prof. Andrea Rinaldo
Dott. Ing. Gianluca Botter

Dottorando : Stefano Zanardo

Abstract

Complexity of transport phenomena at the catchment scale arises from the interconnection of several processes over a range of spatial and temporal scales. The hydrologic and biogeochemical response of catchments is produced by the highly non-linear interaction between meteorological forcing, landscape heterogeneity, and human activity. As a result, a simple experimental analysis does not give significant insight into the processes involved and exploring such phenomena is a challenging task. Nevertheless, investigating these processes is important in order to evaluate the dominant controls on catchment-scale mechanisms as well as predict the response of the systems to human activities and climate-related perturbations. This is particularly relevant in changing environments, where a deep understanding of the systems is critical for a proper management of landscape and water resources. This thesis aims at exploring catchment-scale transport phenomena by applying novel modeling tools to relevant case studies. Both deterministic and probabilistic approaches are followed, as the latter are required by the random nature physical processes whereas the former allow for the analysis of the systems under certain, well defined conditions. Model evaluations are supported by robust analyses of extensive datasets, whose purpose is not simply to validate the approaches but rather to provide further insight into the processes. Long term effects of hydrologic fluctuations are captured by stochastic models in terms of steady state statistical distributions of relevant physical quantities. This modeling approach provides a causal relationship between daily rainfall random fluctuations and daily stream flow variability, this, in turn, relates to the variability of stream stage, and in-stream nutrients removal. The stochastic approach is further extended to evaluate the effect of the daily variability of precipitation on the inter-annual variability of water balance. The application of the model to a large amount of experimental catchment across the United States shows how there exist regions where the daily variability of water partitioning is the major control on inter-annual variability of water balance, and regions where the inter-annual variability arises from controls other than the simple scaling-up of short term processes. A deterministic approach, namely Mass Response Function (MRF), is used to evaluate the effect of soil heterogeneities, as well as the effect of water-mixing mechanisms on the hydrologic and biogeochemical response of catchments. The main idea underlying this framework is that the evolution of solute and water pulses moving within the soil largely depends on their residence time. The application of the MRF model to a tracer study on nitrates and lithium suggests that runoff is composed by a collection of water particles with a mixture of ages and that, in this case, the effect of unmixed preferential flow can be ruled out. The MRF is then coupled with a 'source zone' model suitable to describe pesticides release from the top soil layer in intensively

managed catchments. This additional module proves necessary to properly simulate the pesticides transport mechanisms. The application of the model to a decade-long water-quality monitoring dataset suggests that the prediction of the agro-chemical response requires an accurate knowledge of the management practices. In particular, the interval between the occurrence of large rainfall events and the pesticide application dates seems to constitute the main control on the pesticide release dynamics. These considerations are of particular interest when modeling pesticides as they are exclusively of anthropic origin. Whereas, when considering other types contaminant such as nutrients, the anthropic component may be clouded by the effect of chemical soil production.

Sommario

La complessità dei fenomeni di trasporto alla scala di bacino deriva dall'interconnessione di diversi processi su diverse scale temporali e spaziali. La risposta idrologica e biogeochimica dei bacini è il prodotto di interazioni altamente non lineari tra le forzanti meteorologiche, le eterogeneità del territorio e le attività umane. Di conseguenza, semplici analisi sperimentali non permettono un'adeguata comprensione dei processi coinvolti, e l'analisi di questi fenomeni rappresenta un obiettivo ambizioso. Tuttavia, l'esplorazione di questi processi è importante per valutare i controlli dominanti su meccanismi di trasporto alla scala di bacino e predirne la risposta idrologica e biogeochimica a perturbazioni climatiche ed alla gestione del territorio. Questo è particolarmente importante nel caso di ecosistemi in cambiamento, dove una profonda comprensione dei processi è fondamentale per una corretta gestione del territorio e delle risorse idriche. Lo scopo di questa tesi è l'analisi di fenomeni di trasporto alla scala di bacino attraverso l'applicazione di nuovi approcci modellistici a casi studio di interesse. A questo scopo si è utilizzato sia un approccio probabilistico sia un approccio deterministico: il primo richiesto dalla natura casuale di numerosi processi fisici coinvolti, il secondo necessario per analizzare le dinamiche sotto condizioni ben definite. Lo studio è supportato da una robusta analisi dei dati disponibili, il cui scopo non è semplicemente quello di validare i modelli ma piuttosto di fornire una comprensione più approfondita delle dinamiche in gioco. Gli effetti di fluttuazioni idrologiche nel lungo termine sono simulati attraverso distribuzioni di probabilità stazionarie relative a grandezze fisiche rilevanti. Questo approccio modellistico fornisce una relazione causale tra la fluttuazione giornaliera della pioggia e la fluttuazione giornaliera dei deflussi, la quale, a sua volta, è messa in relazione con l'atezza di moto nei corsi d'acqua ed infine con i processi rimozione di nutrienti nelle reti idrografiche. Tale approccio stocastico è successivamente utilizzato per valutare l'effetto delle fluttuazioni giornaliere delle precipitazioni sulla variabilità inter-annuale del bilancio idrico alla scala di bacino. L'applicazione del modello ad un esteso numero di bacini sperimentali, distribuiti sul territorio degli Stati Uniti, mostra come esistano alcune regioni dove le fluttuazioni della pioggia giornaliera rappresentano il controllo principale sulla la variabilità inter-annuale del bilancio idrico, ed altre regioni dove questa variabilità è determinata da altri processi che non necessariamente avvengono alla scala giornaliera. Un modello deterministico, detto Mass Response Function (MRF), è utilizzato per valutare l'effetto delle eterogeneità del suolo e dei meccanismi di mescolamento sulla risposta idrologica e biogeochimica dei bacini. Il concetto principale che caratterizza questo approccio si basa sull'assunzione che l'evoluzione degli impulsi di acqua e soluti che si muovono nel suolo sia prevalentemente governata dal relativo tempo di residenza. L'applicazione del modello MRF ad uno studio di traccianti effettuato utilizzando

nitrati e litio suggerisce che i deflussi sono composti da un insieme di impulsi aventi differenti età e che, almeno nel caso in esame, l'effetto di flussi preferenziali non mescolati può essere trascurato. Il modello MRF è stato successivamente accoppiato con un modello detto 'source zone' atto a simulare il rilascio di pesticidi dallo strato superficiale del suolo in bacini intensamente antropizzati. L'aggiunta di questo secondo modello si è dimostrata necessaria per rappresentare accuratamente le dinamiche di trasporto dei pesticidi. L'applicazione ad un caso di studio sperimentale suggerisce come la previsione della risposta agro-chimica richieda un'accurata conoscenza della pratiche agricole utilizzate. In particolare, l'intervallo tra la data di applicazione dei pesticidi e i primi eventi di pioggia successivi sembra costituire il fattore principale nelle dinamiche di rilascio di contaminanti. Queste considerazioni sono di particolare interesse nella modellazione dei pesticidi in quanto di origine esclusivamente antropica. Nel caso invece della modellazione contaminanti quali i nutrienti, la componente antropica può venire oscurata dalla produzione chimica del suolo.

Contents

Chapter 1

Introduction

Catchments are complex hydrologic systems, subject to spatial and temporal variations in hydroclimatic controls (e.g. rainfall; net radiation), characterized by spatially heterogeneous landscape attributes (e.g. soil properties, land-use patterns and management practices), and even temporal changes in such attributes over both the short term (e.g. daily) and the long-term (e.g. seasonal; annual). To develop and implement models for predicting hydrologic and biogeochemical fluxes at a catchment, knowledge of such controls is required. Physical data describing the landscape features of a catchment are usually available in detailed soil characterization and mapping databases, at least within the US and Europe, such that the soil hydrologic and biogeochemical parameters can be estimated. On the other hand, climatic drivers are in general more difficult to handle as, given their characteristic unsteadiness, they require continuous monitoring as well as future forecast. In particular, among those, the precipitation forcing constitutes a major challenge, because of its random character as well as its high variability, relatively to the other climatic controls.
The unpredictable nature of precipitation entails its probabilistic characterization, usually in terms of frequency and intensity, when the long-term hydrologic or biogeochemical response of a catchment is to be described [*Rodriguez-Iturbe et al.*, 1999; *Botter et al.*, 2007; *McGrath et al.*, 2007]. Nonetheless, on the short run, the timing of rainfall events, in relationship with other system variables can be more important than the long-term statistics of the process. An example, which is extensively discussed in the thesis, is the process of pesticide losses from the soil, where the lag time between the time of pesticide application and the time of the first rainfall event constitutes one of the most important drivers for the process [*Chiovarou and Siewicki*, 2007; *Luo and Zhang*, 2009].
Overall, the aim of this thesis is to investigate the dominant controls on transport phenomena at the catchment scale, by providing and discussing novel tools for modeling catchment response on the basis of probabilistic as well as deterministic approaches.

Variability of catchment response is a natural consequence of a series of complex, intertwined ecohydrological and climatic processes that operate over various scales. These include recharge terms (due to infiltration from rainfall), losses (evapotranspiration and discharge) and storage variations related to the residence time distributions in channeled and unchanneled states [e.g.,

Chow, 1964; *Rodriguez-Iturbe and Rinaldo*, 1997; *Brutsaert*, 2005]. Given the typically random nature of these processes, stochastic methods prove extremely powerful tools when modeling the catchment system.

One important feature of analytical, process-based models is that they allow for a simple evaluation of the response of the system under different conditions. This proves indeed very useful when, for example, the impacts of hypothetical climate change scenarios are to be analyzed. The novel contribution of this work to the stochastic modeling in natural systems regards different processes typical of the catchment scale. The hydrologic response, in terms of daily streamflow is first considered and an analytical expression for the annual flow duration curve (FDC) is derived on the basis of phenomenological parameters [*Botter et al.*, 2008]. By means of general geomorphologic and biogeochemical relationships it was then possible to derive the analytical probability density function (pdf) of stream stage as well as the pdf of nutrient loss rate constant within the streams, as functions of the daily streamflow variability [*Botter et al.*, 2010b]. Indeed, understanding the coupling between transport and transformation processes that attenuate nutrient loads within the river networks is important, in order to minimize adverse ecological impacts due to nutrient export [*Boyer et al.*, 2006].

The results introduced above are all related to the variability of daily streamflow, which is a direct consequence of the daily variability of climatic drivers (i.e., rainfall). However, for certain physical variables the scale of variability may be larger. In fact, one of the many complicating factors in understanding the response of catchments in a changing environment is the role of vegetation, because, depending on climatic conditions, vegetation water use may be an important term of the overall catchment water balance. The variability of annual vegetation water use was recently shown to be strongly related to the competition between water availability and atmospheric demand [*Troch et al.*, 2009]. One may think that such inter-annual variability can arise straightforwardly through the inter-annual variability of climate drivers. However, intra-year (i.e., within-year) variability of such drivers and their nonlinear interactions with landscape properties can also manifest at the annual scale. The effect of short term fluctuation of the rainfall forcing on the long-term water balance variability [*Zanardo et al.*, 2011a, *in review*] is investigated here with the same stochastic approach introduced above.

Overall, the probabilistic framework proposed provides an interconnection of different hydrologic processes, such as stream flow, vegetation water use and nutrient losses. The linkage is characterized by a cascade of controls that spans from rainfall intermittency, to soil moisture dynamics, up to runoff production.

The episodic nature of hydrologic flows is a result of the nonlinearity of their triggering and the intermittency of rainfall [*McGrath et al.*, 2007]. For instance, fast surface runoff may result from the inability of the soil to infiltrate rainfall water with a certain intensity [*Horton*, 1993], or from soil saturation excess [*Dunne*, 1978], linking, in the latter case, the current rainfall event with the antecedent soil moisture conditions and therefore to the previous rainfall history, whereas in the former, the soil infiltration capacity to the rainfall intensity. As a further exemple, preferential flow through macropores, which constitutes another mechanism of fast runoff, is usually initiated when a certain threshold of rainfall intensity is exceeded [*Beven and Germann*, 1982] and, in turn,

represents one of the main triggers for the leaching process of strongly sorbing solutes, such as pesticides [*Flury*, 1996; *Kladivko et al.*, 2001]
Even though, the mobilization processes within the soil, whether solutes or simply water particles are under consideration, are strongly controlled by the timing and magnitude of rainfall events, the actual movement of solutes and water within the soil is also actively affected by the connectivity of flow pathways and, overall, by the heterogeneities of the soil. This in turn gives raise to the 'old water paradox' according to which a sizable part of the runoff within the hydrologic response of a hillslope is constituted by aged water particles. In other words, the runoff triggered by a certain rainfall event does not necessarily carry only the water of such event but may be constituted by water that infiltrated the soil during previous events [*Maloszewski and Zuber*, 1982; *McDonnell*, 1990; *Rodhe et al.*, 1996; *McGuire et al.*, 2007; *Botter et al.*, 2010c]. Lumped approaches are frequently employed to describe the overall behavior of hillslopes/catchments, as, with these methods, the underlying transport mechanisms of a hillslope/catchment are implicitly embedded within an assumed system response function. As an example, such function may be the solution of the advection-dispersion equation [*Stewart and McDonnel*, 1991], or the water travel time distribution [*Stewart and McDonnel*, 1991; *Rinaldo and Marani*, 1987; *Rinaldo et al.*, 1989, *Rinaldo et al.* 2006 a,b]. In particular, the water travel time distribution proves a robust descriptor of the whole transport mechanism and has the major advantage of blending all sources of uncertainty (e.g., the description of the spatial patterns of soil hydraulic properties) into a single curve [*Taylor*, 1921; *Dagan*, 1989], albeit this will, in the general case, be time variable [*Botter et al.*, 2010c].
Whether rainfall intermittency or soil heterogeneity exert the main control on transport phenomena within catchments is difficult to say, and, in general this depends on the problem under consideration; indeed, studies on solute transport in catchments are suitable to investigate this question. For example, a study by *Botter et al.* [2009] points out how the interactions between old and new water are central to understand the mechanisms driving the transfer of nitrates and lithium from the soil to stream water. On the other hand a different study [*Zanardo et al.*, 2011b (*in review*), *in review*] on atrazine, a highly sorbing pesticide, suggested that in managed catchments the mixing among water particles with different ages is not a major control of transport mechanisms, whereas the magnitude of rainfall events, relative to the pesticide application time, seems to represent the main driver. In Chapters 3 and 4 solutes transport within the soil is discussed with the help of simple hydrologic and biogeochemical models and their application to relevant case studies.

Understanding the relative roles of climate, soil, topography and vegetation in controlling the variability of the water balance in a catchment is important for assessing the effects of climate and landscape changes on water resources and ecological services.
Detailed models can optimize the characterization of a process through a series of proper descriptors of the system, when these are known. This may lead to very accurate predictions of the system response, even though, in many situations, critical data are not readily available. The conventional calibration-validation method, usually applied in such cases, leads to issues of equifinality [*Beven et al.*, 1996] where multiple combinations of model parameters lead to the same integrated response. Even though this procedure may still produce good predictions, the outcome is very poor in terms of true understanding of the system.

On the other hand, a parsimonious modeling approach, based on detailed data analyses, helps identifying the main drivers of the process. The models proposed in this thesis should be understood as 'learning', rather than 'predicting', tools; in particular, they are used here to investigate the role of rainfall intermittency in hydrologic and biogeochemical processes that typically occur at the catchment scale. This is very much consistent with the top-down framework [*Sivapalan et al.* 2003] where parsimonious models are used to learn from data and and test hypotheses.
Additionally, when it comes to large-scale (e.g., catchment-scale) analyses, detailed data are not readily available and there exist multiple sources of uncertainties [*Dubus et al.*, 2003] which may eventually affect their reliability. These types of difficulties and challenges provide a further motivation to pursue a minimalistic modeling approach that is based on a minimum level of possible model complexity, includes the major drivers, and uses pragmatic model assessments based on a set of hierarchical criteria. As an example related to hydrologic modeling, *Basu et al.* [2010] showed how in extensively managed cropping systems, a minimalistic, uncalibrated model (i.e. Threshold Exceedance Lagrangian Model, TELM) can predict the hydrologic response as well as the widely used and calibrated SWAT model, due to the functional homogeneity of those systems. Such an approach has been recently extended to the biogeochemical response, in terms pesticide loads and concentrations [*Zanardo et al.*, 2011b, *in review*].
A few studies have also recognized the value in studying patterns with an attempt to classify catchments and identify their dominant drivers and filters of hydrologic response [e.g., *Atkinson et al.*, 2002; *Wagener et al.*, 2007, *Zhang et al.*, 2008]. It is important to note that the dominant processes vary with scale; while local-scale soil characteristics may be important at the plot scale, geomorphology and climate may be the dominant controls on runoff response at the larger scales [*Atkinson et al.*, 2002; *Zhang et al.*, 2008]. Identifying and understanding dominant processes, through a parsimonious modeling approach, indeed helps in development of predictive tools that introduce complexity only when necessary, thus reducing the burden on calibration and parameter estimation [*Atkinson et al.*, 2002; *Sivapalan*, 2003; *Wagener et al.*, 2007].

The thesis is structured as follows:

- In Chapter 2, the long term effect of rainfall variability is discussed in terms of steady state probability distributions of catchment vegetation water use, streamflow, stream stage and nutrient losses. All the analytical results provided here are based on the pioneering works by *Rodriguez-Iturbe et al.* [1999] and *Rodriguez-Iturbe and Porporato* [2004] where the dynamics of water-controlled vegetation was tackled by studying the stationary probability distribution of soil moisture, and by *Botter et al.* [2007] where the leaching component of the hydrologic response was probabilistically characterized for the first time.

- Chapter 3 discusses a field experiment on solute transport relative to point as well as diffuse sources. The purpose is to analyze the processes determining the mobilization and transport of solutes driven by rainfall through runoff pathways at catchment scales. The hydrologic and biogeochemical response of a small catchment in Northern Italy was monitored in continuous during 4 weeks by properly measuring rainfall rates, streamflows, and stream flux concentrations. A modeling exercise simulating such responses gives some insight into the the scaling

of mobilization mechanisms and the mixing processes in terms of age of runoff water.

- In Chapter 4 the effect of precipitation timing is evaluated by applying a minimalistic model to the export of atrazine, one of the most used herbicides in the Midwestern US [*Baldock et al.*, 1993; *Belluck et al.*, 1991], in the Little Vermilion River watershed in Illinois (USA). This case study is suitable for this analysis because field observations in the Midwestern U.S. watersheds have repeatedly shown that the fraction of seasonal loads are closely related to the few major storm events subsequent to herbicide application [*Leonard*, 1990; *Kladivko et al.*, 2001; *Gish et al.*, 1991], as well as on their timing [*Chiovarou and Siewicki*, 2007; *Luo and Zhang*, 2009]. The model proposed [*Zanardo et al.*, 2011b, *in review*] is based on the coupling of a large-scale Mass Response Function approach [*Rinaldo and Marani*, 1987; *Rinaldo et al.*, 1989] to a 'source zone' model that describes near surface pesticide dynamics.

- The outcomes of the analyses carried out in Chapter 2, 3, and 4 are streamlined in Chapter 4, which also provides a synthesis and a discussion of the results.

- A list of the symbols used in each chapter is reported in the Appendix.

Chapter 2

Long Term Effects of Hydrologic Fluctuations

At the catchment scale, the partitioning of precipitation into runoff, water vapor (i.e., evaporation and transpiration) and soil moisture storage can be the result of ecohydrolgical processes operating at a range of different time scales. For example, the soil moisture storage prior to a storm can control the amount of runoff generated in a storm [*Ye et al.*, 1997]. These antecedent soil moisture conditions are in turn controlled by the previous history of rainfall and evapotranspiration. At the short time scale (say, daily) rainfall intermittency can be considered as the main source of variability for catchment water partitioning. At the catchment scale, such process can be characterized in a hierarchic way, where rainfall fluctuation generates variability in soil moisture dynamics which in turn affects runoff and water vapor production. Nevertheless, this characterization ceases to hold when the spatial scale is so large that regional feedbacks become important and precipitation becomes dependent on the soil moisture [*Rodriguez-Iturbe et al.*, 1991].
The linkage between soil moisture dynamics and stochastic rainfall fluctuations was analyzed in an extensive way by *Rodriguez-Iturbe et al.* [1999], who characterized the variability of soil moisture at a point in terms of its exact probability density function. This chapter is strongly founded on the pioneeristic work by *Rodriguez-Iturbe et al.* [1999] and, on the basis of the same framework provides further linkages between rainfall variability, streamflow production and vegetation water-use.

2.1 Probabilistic Characterization of Streamflow

Botter et al. [2007a] have recently analyzed the linkage existing between stochastic streamflow fluctuations and the relevant soil moisture dynamics in suitably defined geomorphic states contributing to streamflow. An exactly solved probabilistic model of streamflow dynamics was developed therein, where the steady state probability distribution of the subsurface contribution to streamflows is analytically expressed in terms of a few macroscopic rainfall properties, soil-vegetation parameters, and key geomorphological features. The approach was initially structured in a spatially lumped framework by assuming average properties, as in the related literature on soil moisture dynamics [see, e.g., *Rodriguez-Iturbe et al.*, 1999; *Rodriguez-Iturbe and Porporato*, 2004], but has been more

recently extended to tackle the effects of spatially distributed soils, vegetation and morphological features [*Botter et al.*, 2007b]. The probabilistic characterization proposed by *Botter et al.* [2007a] is here reported for clarity since all the results provided in the current chapter are based on this framework.

Following *Rodriguez-Iturbe et al.* [1999], the rainfall occurrence is modeled as a zero-dimensional Poisson process of rate λ_p $[T^{-1}]$ (Figure **??**). The latter assumption postulates catchments sizes smaller than the correlation scale of rainfall events and timescales greater than the characteristic duration of single rainfall events (e.g., daily), so that the internal spatial and temporal structure of rainfall events can be neglected. Moreover, the dynamics of catchment-averaged soil moisture (and the ensuing runoff production mechanisms) are modeled as a state-dependent point process taking place in the topsoil layer, which is assumed to be labeled by constant, spatially averaged properties (e.g., depth, Z_r $[L]$, porosity, n (dimensionless), soil moisture, s (dimensionless)). Lateral flows in the upper soil layer are neglected, possibly preventing the extension of the approach described in this paper to the case of steep mountain basins, where lateral flows play a decisive role in soil saturation dynamics during intense rainfall events. Daily rainfall depths, I $[L]$, are assumed to be exponentially distributed with parameter γ_p $[L^{-1}]$ (Figure 1a) and the dominant runoff production mechanism is supposed to be Dunnian (as typical in flat temperate regions). Furthermore, we neglect ecosystem dynamics, thus focusing on average, constant hydroecological parameters (i.e., representative of a whole season). Under the above assumptions, the procedure employed by *Rodriguez-Iturbe and Porporato* [2004] to derive the steady state probability distribution of soil moisture at a point can be interpreted and applied to heterogeneous catchments, where spatially averaged soil moisture pdfs can be described by macroscopic (rainfall, soil and vegetation) parameters [*Porporato et al.*, 2004; *Botter et al.*, 2006]. Under the above assumptions, the mass balance within the topsoil layer of a catchment can be written in terms of the spatially averaged (relative) soil moisture, $s(t)$, as

$$\frac{ds(t)}{dt} = -\rho(s(t)) + \xi_t, \tag{2.1}$$

where the last term on the right hand side defines the stochastic instantaneous inputs due to infiltration from rainfall. The latter is modeled as a marked Poisson process of rate λ_p and normalized depths, $I/(nZ_r)$, extracted from an exponential distribution of parameter $\gamma_p' = \gamma_p n Z_r$

$$\xi_t(\lambda_p, \gamma_p') = \sum_{i, t_i < t} \frac{I_i}{nZ_r} \delta(t - t_i), \tag{2.2}$$

where $\delta(\cdot)$ is the Dirac delta function. The term $\rho(s(t))$ in equation (**??**) is the (normalized) catchment-scale soil loss function, which is assumed to be linearly related to the maximum rate of evapotranspiration, PET (sometimes referred to as potential evapotranspiration):

$$\rho(s) = \frac{s - s_w}{s_1 - s_w} \frac{PET}{nZ_r}, \tag{2.3}$$

where s_1 is a critical soil moisture level the constitutes the threshold over which the rainfall is instantaneously lost as deep percolation and/or surface runoff [*Porporato et al.*, 2004]. According

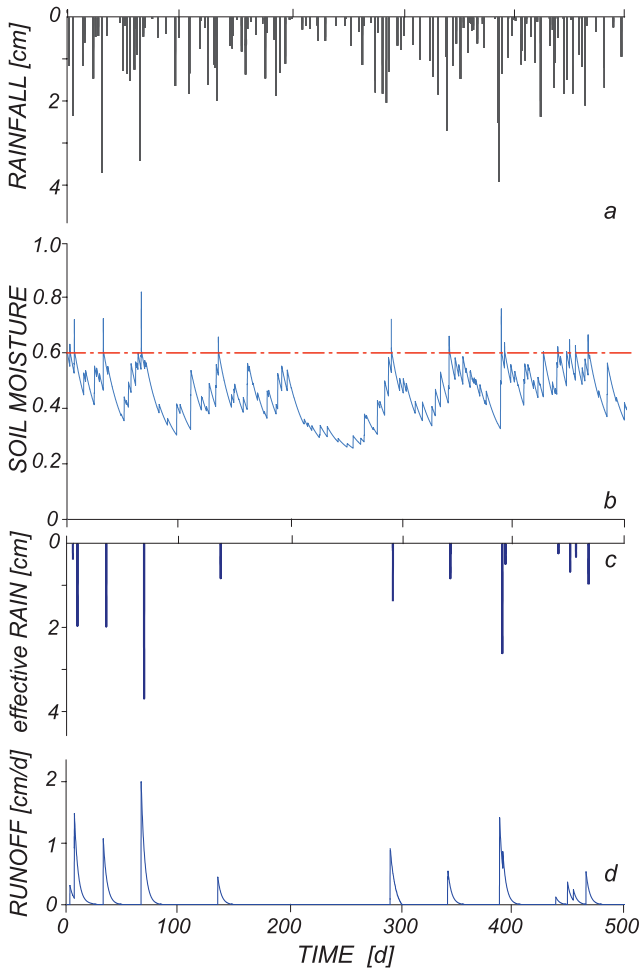

Figure 2.1: Schematic representation of the soil moisture and runoff models: (a) Temporal evolution of the overall rainfall depths (synthetic data). (b) Temporal evolution of the (catchment averaged) relative soil moisture, $s(t)$, which is commanded by the intermittent rainfall forcings shown in panel a and by the deterministic decay due to evapotranspiration process, according to equation (**??**). The dash-dotted line represents the threshold s_1, whose up crossing determines the triggering of runoff events. (c) Temporal sequence of effective rainfall, driven by the exceedance of the threshold s_1 for the soil moisture $s(t)$. (d) Temporal evolution of the overall, specific (i.e., for unit area) discharge [after *Botter et al.*, 2007a].

to equation (**??**), evapotranspiration is assumed to vanish below the wilting point, s_w, and linearly increasing above s_w up to the maximum rate, PET $[LT^{-1}]$.
The effective rainfall series resulting from the simplified soil moisture dynamics described above may be approximated by a new marked Poisson process [*Botter et al.*, 2007a] where the effective rainfall depths follow an exponential distribution the same parameter of total rainfall, γ_p, and the average frequency of effective rainfall (i.e., runoff) events, λ, may be expressed in terms of the underlying soil, vegetation and rainfall properties as [*Botter et al.*, 2007c]

$$\lambda = \eta \frac{exp[-\gamma_s]\gamma_s^{\frac{\lambda_p}{\eta}}}{\Gamma(\lambda_p/\eta, \gamma_s)}. \tag{2.4}$$

In equation (**??**) $\Gamma(a, b)$ is the incomplete gamma function of parameters a and b, $\eta = PET/(nZr(s_1 - s_w))$ is the normalized maximum evapotranspiration rate and $\gamma_s = \gamma_p n Z_r(s_1 - s_w)$ is the ratio between the soil storage capacity and the mean rainfall depth, which we will refer to as the storage index.
The effective rainfall pulses infiltrating beyond the root zone are assumed to propagate through deeper soil layers as subsurface and/or groundwater flow. Meanwhile, the effect of the presence of fast runoff components (e.g., surface flows possibly triggered by intense storms) is neglected; in fact, it is assumed that fast components of the hydrologic response (should they exist) are characterized by the same timescale of the slow subsurface/groundwater flow components. A residence time approach is then employed for modeling subsurface transport processes at the catchment scale.
Botter et al. [2006] adopt a simplified scheme, where the effects of the network structure (and of the spatial organization of the drainage pathways) on the ensuing basin-scale hydrologic response are neglected. This is consistent with the spatial and temporal scales considered in this study, that allow to model the rainfall as a sequence of uniform and instantaneous (i.e., daily) inputs. The whole catchment is simply modeled as a linear reservoir, where the outflowing flux is assumed proportional to the water storage. This is tantamount to assume that the catchment-scale subsurface flow is characterized by an exponential residence time distribution (i.e., $g(t) = kexp(-kt)$, if k $[T^{-1}]$ is the inverse of the mean residence time). The exponential distribution has been widely employed in the literature [e.g., *Boyd*, 1978; *Rinaldo et al.*, 2006a], because it allows one to reproduce the slow release of water from soil and it requires a single calibration parameter. Furthermore, extensive validations against field data have proved the robustness of the linear assumption in modeling subsurface flows at large spatial scales in many cases of practical interest [e.g., *Rinaldo et al.*, 2006b].
The overall catchment-scale runoff Q (in the sense specified above) is thus linked to the temporal evolution of the deep infiltration depths, $Y(t)$, according to the following relationship (see Figure **??**)

$$Q(t) = Ak \int_0^t Y(t - \tau) exp[-k\tau] d\tau, \tag{2.5}$$

where A is the basin surface. A Langevin equation for runoff can be obtained deriving both sides of equation (**??**) with respect to t,

$$\frac{dQ}{dt} = -kQ(t) + Ak\xi'_t, \tag{2.6}$$

where the first term on the right-hand side represents the deterministic (exponential) decay of the discharge due to the slow release of water from soil and the last term on the right-hand side represents the stochastic rate due to inputs by deep percolation

$$\xi'_t = \sum_{j,t_j<t} Y_j \delta(t - t_j). \tag{2.7}$$

Accordingly, the steady state pdf of Q, $p_Q(Q)$, is expressed by a Gamma distribution as [*Botter et al.*, 2007a, 2007c]

$$p_Q(Q, t \to \infty) = c^* Q^{\frac{\lambda}{k}-1} exp[-\gamma Q] \tag{2.8}$$

where $\gamma = \gamma_p/(kA)$ represents the mean runoff increment due to incoming rainfall events and $c^* = \gamma^{\lambda/k}/\Gamma(\lambda/k)$ is the normalizing constant.
The probability distribution of Q is thus related to the underlying soil and vegetation properties (through the parameter λ) and to key rainfall properties (through both the parameters γ and λ), but it also depends on important geomorphic factors such as the mean residence time of subsurface flow (λ/k) and the size of the basin (A). In particular, according to equation (**??**), the behavior of $p_Q(Q)$ is chiefly controlled by the ratio between the runoff frequency, λ, and the inverse of the mean residence time in subsurface, k. When $\lambda/k > 1$ ('wet conditions') the pdf of the runoff is bell shaped with $p_Q(Q \to 0) = 0$ (i.e., the absence of runoff is characterized by zero probability), while for $\lambda/k < 1$ ('dry conditions') $p_Q(Q)$ goes to infinity for $Q \to 0$ and monotonically decreases for $Q > 0$ [*Botter et al.*, 2007a].
The mean and the variance of the runoff pdf can be easily expressed in term of the parameters λ, k and γ as

$$\langle Q \rangle = \frac{\lambda}{k\gamma} \tag{2.9}$$

$$\langle Q^2 \rangle - \langle Q \rangle^2 = \frac{\lambda}{k\gamma^2} \tag{2.10}$$

In principle, the required statistical homogeneity of the underlying hydroecological and meteorological processes restricts the applicability of the approach presented in this section to single seasons, during which the system may be properly described by means of constant rainfall, soil, transport and vegetation parameters. However, the above framework may be suitably adapted to investigate also the structure of steady state, annual streamflow pdfs, which are an important indicator of the underlying streamflow variability in river basins. Note that in what follows the term annual is specifically designed to indicate those statistics which are evaluated on an annual basis (as opposed to 'seasonal'). Assuming that the specific value assumed by the discharge at the beginning of each season does not affect significantly the streamflow pdf during that season, the annual streamflow pdf can be expressed as a weighted average of the underlying seasonal pdf's (equation (**??**)), according to the following relationship [*Botter et al.*, 2008]:

$$p_\Sigma(t) = \sum_{i=1}^{N} d_i \left[\frac{\gamma_i^{\lambda_i/k_i}}{\Gamma(\lambda_i/k_i)} Q^{\left(\frac{\lambda_i}{k_i}-1\right)} exp[-\gamma_i Q] \right], \tag{2.11}$$

where the subscript i identifies one of the N seasons in the considered region and d_i represents its relative duration.

2.1.1 Effect of Seasonality

As the use of equation (**??**) produces an undesired increase of the number of parameters involved (from 3 to $3 \times N$), it is useful to investigate whether the validity of equation (**??**) can be extended directly to annual timescales via the definition of effective, temporally averaged parameters.
In the graphs reported in Figure **??** the effects of seasonally variable ecohydrological parameters on the annual streamflow pdf are investigated by analyzing the discrepancy between the gamma distributions obtained by applying equation (**??**) with temporally averaged parameters and the corresponding annual streamflow pdf evaluated via equation (**??**) under different climatic and ecohydrological conditions. In the illustrative examples reported in Figure **??**, each year is assumed to be composed of two 6-month seasons characterized by different parameters. In Figure **??**a the discrepancy between the two streamflow pdf's is evaluated by means of the absolute value of their integral difference, $E = \int_0^\infty \sqrt{[p_Q(x) - p_\Sigma(x)]^2} dx$ (where $p_Q(x)$ and $p_\Sigma(x)$ are given by equations (**??**) and (**??**), respectively). E measures the absolute value of the area comprising the considered distributions. For two exactly overlapping distributions one would have $E = 0$, whereas the maximum possible value of E (corresponding to the case of two distributions intersecting only for null values of p) is 2. The discrepancy between two distributions is thus directly proportional to the magnitude of E. Taking into account both theoretical considerations and numerical simulations, it is suggested that when the condition $E < 0.15$ is satisfied, the two pdfs exhibit an overall (i.e., general) agreement. Needless to say, this threshold has been selected somewhat arbitrarily, and should be considered only as an indicative value.
E is plotted in Figure **??**a as a function of the variation coefficients of λ/k ($CV_{\lambda/k}$) and γ (CV_γ), which represent the effects of the seasonal variability of the underlying climatic and ecohydrological parameters. In all the simulations explored in Figure **??**a the ratio λ/k is equal to 0.9, leading to a dry type average annual streamflow pdf. Further details on the parameters used in these simulations can be found in the caption of Figure **??**. As expected, E increases with $CV_{\lambda/k}$ and CV_γ. Moreover, the effect of the seasonal variability of the ratio λ/k on the agreement between $p_Q(Q)$ and $p_\Sigma(Q)$ is more pronounced than that produced by the seasonal variability of the parameter γ. Overall, the graph suggests that the temporal averaging of parameters leads to small errors in the estimate of the streamflow pdf when their seasonal variability is weak or moderate (e.g., $CV_{\lambda/k} + CV_\gamma \leq 0.5$, for which $E < 0.15$). The latter case is deemed to be rather frequent in several climatic areas of the world (e.g., humid subtropical, Mediterranean).
The effect of the seasonal variability of the parameters on the ensuing streamflow pdf is further analyzed in Figures **??**b and **??**c, where the difference between equation (**??**) (applied with temporally averaged parameters) and equation (**??**) is explored in detail in a number of cases chosen among the parameter combinations explored in Figure **??**a (points P1 - P5). The solid lines represent the gamma distribution obtained by applying equation (**??**) with temporally averaged values of λ, k and γ, whereas the other curves correspond to the annual pdfs evaluated via equation (**??**). The plot shown in Figure **??**b refers to cases where the ratio λ/k varies along the year while the parameter γ is assumed to be constant (points P1, P2 and P3). The plot considers three different coefficients of variation of the ratio λ/k: $CV_{\lambda/k} = 0.33$ ($E \approx 0.05$, dashed line); $CV_{\lambda/k} = 0.55$ ($E \approx 0.15$, dotted line) and $CV_{\lambda/k} = 0.77$ ($E \approx 0.30$, dash-dotted line). The above values of

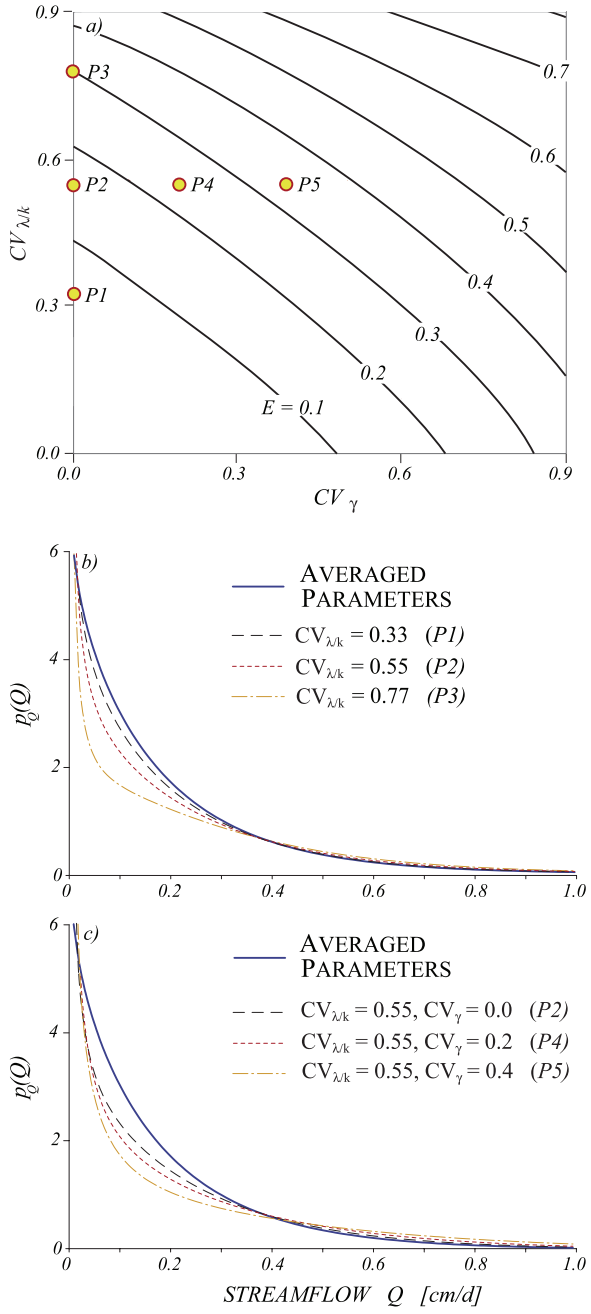

Figure 2.2: Analysis of the annual streamflow pdf in the case of seasonally variable ecohydrological parameters; each year is composed of two seasons (A and B) with different values of the parameters λ, k, and γ. (a) Contour plot of the integral difference between the annual streamflow pdf evaluated for seasonally variable parameters (equation (**??**)) and the corresponding Gamma distribution obtained with temporally averaged parameters (equation (**??**)), E, seen as a function of $CV_{\lambda/k}$ and CV_γ. In all the simulations $\bar{\lambda}/\bar{k} = 0.9$, $\bar{\gamma} = 5\ d\,cm^{-1}$ and $k_A = k_B = 0.5\ d^{-1}$. Also shown are some sample plots of the streamflow distributions resulting from five different parameter combinations used in Figure panel a ($P1 - P5$). The solid lines represent equation (**??**) with temporally averaged parameters, whereas the other curves correspond to the annual pdfs evaluated via equation (**??**): (b) $k_A = k_B = 0.5\ d^{-1}$, $\gamma_A = \gamma_B = 5\ d\,cm^{-1}$, and $\lambda = k = 0.9$. Three different coefficients of variations of λ/k are considered, namely, P1, $CV_{l/k} = 0.33$; P2, $CV_{l/k} = 0.55$; and P3, $CV_{\lambda/k} = 0.77$. (c) Same as for panel b except that both $CV_{\lambda/k}$ and CV_γ are positive: P2, $CV_\gamma = 0$; P4, $CV_\gamma = 0.2$; and P5, $CV_\gamma = 0.4$.

$CV_{\lambda/k}$ have been selected to illustrate how the agreement with the pdf correspondent to temporally averaged parameters progressively deteriorates as E becomes larger than 0.1.
In Figure **??**c the agreement/disagreement between $p_Q(Q)$ evaluated with temporally averaged parameters and $p_\Sigma(Q)$ is shown in the case when both $CV_{\lambda/k}$ and CV_γ are positive (points P2, P4 and P5). The plot reinforces the fact that the effect of temporal fluctuations in the value of the average rainfall rates is smaller than the corresponding effect due to the seasonal variability of the ratio λ/k. Indeed, until $CV_\gamma < 0.4$, the effect due to temporally variable values of γ on the overall annual pdf remains small (as shown by the agreement between the dashed and the dotted lines in Figure **??**c).
Note that, to assess the maximum possible effect of the seasonal variability of the parameters on the annual streamflow pdf, in all the cases discussed in Figure **??** the ratio λ/k fluctuates around its critical (unit) value and the smallest ratios λ/k are associated with the largest values of γ. Where these conditions relaxed, the differences among the various cases discussed above would certainly be smoothed out. Overall, it can be concluded that the temporal averaging of the climatic and ecohydrological parameters leads to robust estimates of the underlying annual streamflow pdf, provided that the seasonality of the underlying ecohydrological parameters is weak or moderate. In general, the same considerations developed above can be drawn also if the annual distribution of the streamflows is a wet-type pdf.

2.2 Flow Duration Curves and Annual Minima

Among the various indicators of streamflow variability in river basins, flow duration curves and the related probability distribution of annual minima have traditionally received most attention from hydrologists and engineers [e.g., *Chow et al.*, 1988]. The flow duration curve represents the relationship between magnitude and frequency of streamflows at a location on a river. It provides a synthesis of the relevant hydrological processes occurring at the basin scale, and allows a graphical synopsis of the foremost flow characteristics throughout the range of recorded discharges (albeit disregarding their sequence). Flow values close to the largest frequencies are commonly used as measures of the stream low-flow potential and of its groundwater contribution [*Searcy*, 1959; *Chow*, 1964; *Chow et al.*, 1988; *Dingman*, 2002]. Moreover, flow duration curves can be a useful tool to assess and evaluate minimum streamflow requirements to ensure the sustainability of biotic communities. Flow frequency curves are also important for the analysis of the flow values associated with principal transport of sediment and dissolved load [*Leopold et al.*, 1964].
Unlike flow duration curves, low flow frequency curves (and, in particular, the distribution of annual minima) provide precious information on the temporal distribution and the magnitude of extreme events. The probabilistic structure of low-flow events is influenced by several hydraulic, physiographic and climatic factors. The analysis of low flow frequency curves may be useful, for example, to water managers in predicting the probability of occurrence and the magnitude of critical droughts (and hence the related consequences on fluvial ecosystems). Different types of probability distributions (e.g., Gumbel, Pearson, Weibull, lognormal) are usually employed to fit historical observations of minimum flows and used to determine the occurrence probability of these extremes [e.g., *Vogel and Kroll*, 1989; *Nathan and McMahon*, 1990; *Dingman*, 2002]. However, the selection

of the tail of the probability distribution, i.e., characterizing extreme low flows from observations, is sometimes difficult (if not altogether impossible) owing to the large number of data required. Hence, the improvement of our ability to theoretically predict extreme low flows is recognized as a challenging and important task for hydrologists [*Milly*, 1993; *Smakhtin*, 2001].

2.2.1 Flow Duration Curves

In this section, the theoretical streamflow pdf (Equation **??**) is used to provide an analytical expression of the long-term flow duration curve on the basis of a few (physically based) climatic, ecohydrological and morphologic parameters. The flow duration curve of a river basin is a mathematical function associating to each possible discharge, Q, the percentage of time during which such discharge is equaled or exceeded during a year. In this paper we focus on the long-term flow duration curve of a river basin [e.g., *Vogel and Fennessey*, 1994], which can be related to the period-of-record flow duration curve by assuming steady state conditions [*Castellarin et al.*, 2004]. From a mathematical viewpoint, the flow duration curve $f(Q)$ may be expressed as the annual streamflow cumulative exceeding probability $P_Q(Q)$:

$$f(Q) = P_Q(Q) = \int_Q^\infty p_Q(x)dx \tag{2.12}$$

If the annual pdf is modeled via equation (**??**) applied with temporally averaged parameters, the substitution of equation (**??**) into (**??**) leads to the following expression of the flow duration curve [*Botter et al.*, 2008]:

$$f(Q) = \frac{\Gamma(\lambda/k, \gamma\, Q)}{\Gamma(\lambda/k)} \tag{2.13}$$

Equation (**??**) expresses the flow duration curve as a regularized gamma function [*Abramowitz and Stegun*, 1965], which takes a unit value for $Q = 0$ and monotonously decreases toward zero for $Q \to 0$. Moreover, depending on the value of the ratio λ/k, the analytical duration curve given by (**??**) may have a single inflexion point or no flexes. All these features are quite commonly observed in several experimental flow duration curves, suggesting a certain suitability of the regularized gamma function to mimic the long-term flow duration curve of a river basins. The appropriateness of equation (**??**) to reproduce observed flow duration curves will be further assessed by a proper comparison with the statistics obtained from discharge measurements in a relevant case study.

2.2.2 Probability Distribution Function of the Annual Minima

The exceedance probability of the annual minimum of (daily) discharges, $P_m(Q)$, is estimated analytically by using the trough under threshold (TUT) theory [*Önöz and Bayazit*, 2002]. The method is based on the identification of the local minima in the daily discharge series which do not exceed a given threshold Q_0 (named hereafter 'troughs under threshold' or TUTs). The basic assumptions of the method are the following: (1) TUTs must be distributed in time according to a Poisson point process and (2) TUTs magnitude must be mutually independent.
According to the modeling scheme shown in Figure **??** the local minima of streamflow are located immediately before each runoff event, and their interarrivals are distributed exponentially with

parameter λ. However, these minima are generally strongly correlated. This problem may be overcome by eliminating the local minima exceeding a given threshold Q_0 and focusing only on the troughs under Q_0. In fact, as prescribed by a noteworthy theorem of the extremes [*Kramer and Leadbetter*, 1967], when $Q_0 \to 0$ the TUTs tend to become mutually independent. However, when Q_0 approaches zero, the distribution of the interarrivals between the TUTs may be no longer exponential. In what follows it is therefore assumed the existence of a threshold Q_0 low enough to ensure the independence of the TUTs, but large enough to preserve the Poissonian distribution of the number of TUTs for a given time interval. The meaningfulness of the above approximation can be assessed via suitable numerical simulations of the simplified streamflow model described above, where the temporal dynamic of Q results from a deterministic exponential decay (of rate k) and a series of random increments (exponentially distributed with average γ^{-1}) in correspondence of runoff events randomly distributed in time according to a Poisson process of rate λ.
Figure **??** shows some relevant statistics computed from synthetic streamflow series of 10^4 years generated by means of suitable numerical Monte Carlo simulations. Each synthetic streamflow series has been generated by numerically simulating the dynamic of Q by randomly extracting a sequence of interarrivals between runoff events and the corresponding streamflow increments from exponential distributions of parameters λ and γ, respectively. The statistics analyzed in Figure **??** correspond to different climatic and geomorphic conditions, characterized by three different values of the ratio λ/k: 3 (Figure **??**a), 1 (Figure **??**b) and 0.5 (Figure **??**c). The graphs focus on the analysis of two different quantities: the autocorrelation among the TUTs magnitude, R, and the integral difference between the distribution of the TUTs interarrivals and the theoretical exponential distribution, $E = \int_0^\infty \sqrt{[I(x) - \lambda_0 exp(-\lambda_0 x)]^2} dx$, (where λ_0 is the average frequency of troughs under Q_0 and $I(x)$ is the numerical distribution of the interarrivals between the troughs). R (circles) and E (squares) are plotted in Figure **??** as a function of the corresponding threshold Q_0, suitably normalized with the average streamflow $\langle Q \rangle = \lambda/(k\gamma)$. As expected, the correlation among the TUTs magnitude, R, grows linearly with Q_0, with $R \to 0$ when $Q_0 \to 0$. Moreover, the ratio λ/k does not seem to affect dramatically the behavior of the correlation (even though R tends to decrease when the ratio λ/k decreases). Indeed, in all the cases investigated, the correlation falls below $5 \cdot 10^{-2}$ when $Q_0 \approx 0.5 \langle Q \rangle$. Conversely, the agreement between the distribution of the TUTs interarrivals and the corresponding exponential distribution is found to be much more sensitive to the ratio λ/k. In particular, the plots reported in Figure **??** show that, when $\lambda/k \approx 1$, the distribution of the troughs interarrivals is nearly exponential, independently on the threshold Q_0 (with $E \approx 0.1$ even for the smallest thresholds). Instead, when $\lambda/k \neq 1$, E proves strongly dependent on Q_0. In particular, when Q_0 becomes low enough to ensure the condition $R < 0.05$, the discrepancy between the distribution of the interarrivals of the TUTs and the theoretical exponential distribution grows significantly ($E = 0.6$ when $\lambda/k = 3$, $E = 0.4$ when $\lambda/k = 0.5$). The above analyses suggest that postulating the existence of a series of independent and Poisson-distributed minima is a realistic assumption when $\lambda/k \approx 1$, while it may require some further care when the ratio λ/k is larger than (or smaller than) unit. The effect of the above approximation on the resulting cumulative distribution of the annual minima is further discussed in *Botter et al.* [2008]. Their analysis suggests that the effect of the non-exponential nature of the distribution of the troughs' interarrivals is negligible when considering the exceedance probability of the smallest

minima (e.g., of the minima characterized by an exceedance probability larger than 0.5). However, for $\lambda/k \neq 1$ the effect can be significant when estimating the exceedance probability of minima having a relatively small exceedance probability, and the effect becomes particularly important when $\lambda/k >> 1$.
Let us now consider a sequence of independent and Poisson-distributed TUTs identified by the (suitably chosen) threshold Q_0. According to the Markovian nature of the process we have

$$\lambda_0 = \lambda \int_0^{Q_0} p_Q(q)dq = \lambda[1 - P_Q(Q_0)], \tag{2.14}$$

where λ and λ_0 are, respectively, the runoff frequency and the frequency of TUTs, $p_Q(Q)$ is the annual streamflow pdf and $P_Q(Q)$ the corresponding exceeding cumulative probability. The exceedance probability of the annual minimum (daily) discharges, $P_m(Q)$, can be thus expressed in terms of the exceedance probability of the magnitude of the TUTS, $P_T(Q|Q_0)$, according to the relationship

$$P_m(Q) = \sum_{m=0}^{\infty} \pi(m) P_T(Q|Q_0)^m, \tag{2.15}$$

where $\pi(m)$ is the probability of having m TUTs in 1 year. Because of the Poissonian nature of the process, m is a Poisson-distributed random variable, i.e.,

$$\pi(m) = \frac{\lambda_0^m exp(-\lambda_0)}{m!}. \tag{2.16}$$

By inserting Equation (**??**) into (**??**) and after some manipulations the following expression for the exceedance probability of the annual minima of (daily) discharges is obtained [*Botter et al.*, 2008]:

$$P_m(Q) = exp\left\{-\lambda_0[1 - P_T(Q|Q_0)]\right\} \tag{2.17}$$

If the TUTs are independent and identically distributed the non-exceedance cumulative probability of their magnitude, $\widetilde{P_T}(Q|Q_0)$ may be computed as [e.g., *Iacobellis et al.*, 2002]

$$\widetilde{P_T}(Q|Q_0) = 1 - P_T(Q|Q_0) = \frac{\lambda[1 - P_Q(Q)]}{\lambda_0}, \tag{2.18}$$

where $P_Q(Q) = f(Q)$ is the flow duration curve. Substituting equation (**??**) back into (**??**) and expressing $f(Q)$ via equation (**??**), the following expression of the exceedance probability of the annual minima, no longer a function of the threshold Q_0, is finally obtained [*Botter et al.*, 2008]:

$$P_m(Q) = exp\left[-\lambda\left(1 - \frac{\Gamma(\lambda/k, \gamma\, Q)}{\Gamma(\lambda/k)}\right)\right]. \tag{2.19}$$

Equation (**??**) expresses the cumulative distribution of the annual minima of daily discharges as a function of three (physically based) parameters embedding the underlying climatic and ecohydrological conditions: the average frequency of runoff events, λ (which depends on rainfall and ecohydrological features); the inverse of the mean residence time in subsurface/groundwater states,

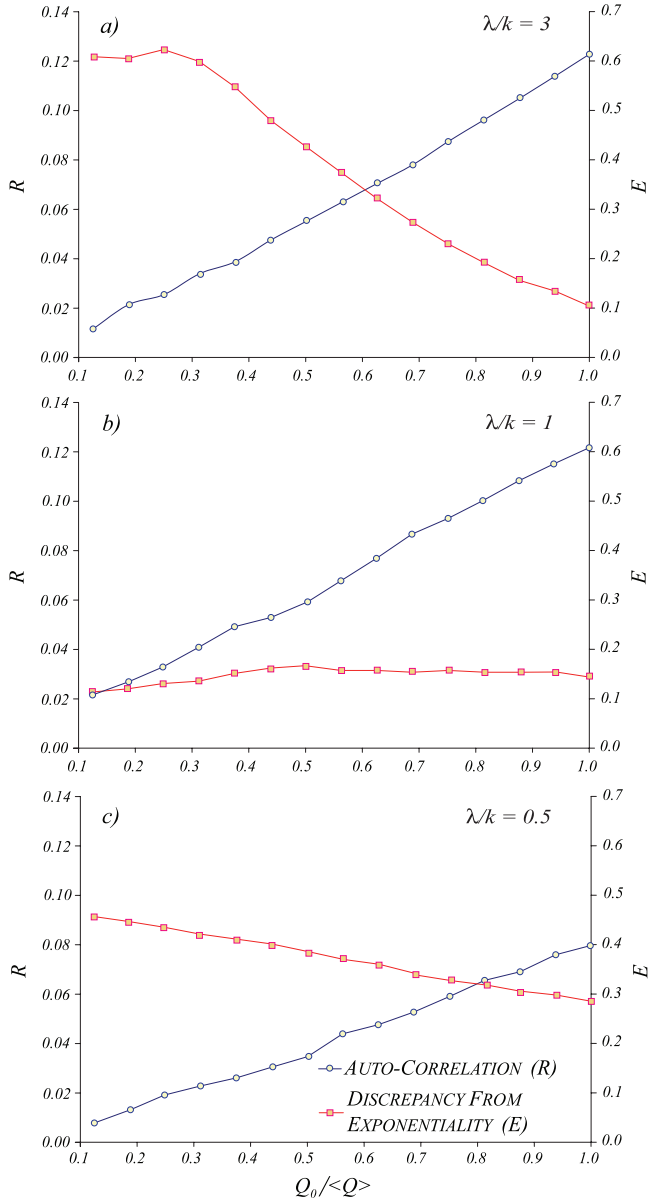

Figure 2.3: Relevant statistics computed from three synthetic streamflow series of 10^4 years generated by means of numerical Monte Carlo simulations, corresponding to different values of the ratio λ/k equal to (a) 3, (b) 1, and (c) 0.5. The plots show the autocorrelation among the troughs magnitude, R (circles), and the integral difference between the distribution of the troughs interarrivals and the theoretical exponential distribution, E (squares), as a function of the corresponding threshold Q_0, suitably normalized by the average streamflow $\langle Q \rangle = \lambda/(k\gamma)$. Note that $\gamma_p = 1\ cm^{-1}$ in all simulations.

k; and the mean streamflow increment during runoff events, γ^{-1} which depends on rainfall and geomorphic characteristics. As evident from equation (**??**) the parameter γ is simply a scale parameter, affecting the scale of the distribution but not its shape (that is, the increasing (decreasing) of γ simply leads to a compression (stretching) of the range of the distribution). The shape of the distribution is instead determined by the parameters λ and k. In particular, the increasing of λ leads to a shift of the inflection point toward larger values of streamflows (and smaller values of P_m). Accordingly, the 0.5 quantile of the distribution increases with λ as well. The parameter k exhibits a somewhat opposite effect with respect to that produced by λ: as k increases the inflection point moves toward the y axis and the 0.5 quantile decreases. Even though both λ and k significantly impact the shape of $P_m(Q)$, the distribution of the minima seems to be more sensitive to variations of the transport parameter k. Moreover, although the distribution of the minima depends on the parameters λ and k separately, the probability density of the minima in $Q = 0$ (i.e., the derivative of the cumulative distribution, dP_m/dQ evaluated in $Q = 0$) depends only on the ratio λ/k. When $\lambda/k > 1$ ('wet regime') dP_m/dQ in $Q = 0$ is zero, ensuring a relatively large exceedance probability for the smallest minimum discharges; conversely, the derivative of P_m with respect to Q evaluated in $Q = 0$ becomes $-\infty$ when $\lambda/k < 1$ ('dry regime').

2.2.3 Case Study

This section presents and discusses some results of the application of the analytical models described in the previous sections to the Jacob Fork catchment at Ramsey (Burke County, North Carolina). The Jacob Fork catchment has been already considered by *Botter et al.* [2007c] to compare the observed spring pdf of daily streamflows with a theoretical gamma distribution of the type expressed by equation (2). The analysis is extended in *Botter et al.* [2008] by considering the annual streamflow pdf, the long-term flow duration curve and the cumulative distribution of the annual minima.

The Jacob Fork catchment is a relatively flat basin, which has an overall drainage area of 67 km^2, an average elevation of 600 m above the see level, a maximum elevation of 800 m and is mainly covered by deciduous and evergreen forests (see inset of Figure **??**d). The climate is humid subtropical (as typical in the southeastern United States), with an average precipitation of about 2300 mm/y. While there are no distinct wet and dry seasons, average rainfall weakly fluctuates around the year, with relative maxima during the spring and the early summer. Rainfall measurements in the test catchment were available for the period $1980 - 1990$ at the station of Casar, whereas streamflow data have been recorded at the outlet during the last 50 years. Rainfall and hydrologic data have been collected by U.S. governmental agencies, and are freely accessible on the Web. In order to ensure the homogeneity of the data employed to validate the analytical model, the reference period was selected in correspondence to the decade where both rainfall and runoff measurements were simultaneously available ($1980 - 1990$), otherwise mentioned. Further details on the catchment geometry and on the set of hydrologic data available can be found in work by *Botter et al.* [2007c]. Figure **??** compares the seasonal pdf's of daily streamflows observed in the test catchment and the corresponding theoretical gamma distributions given by equation (**??**). The procedure used to determine the parameters of the analytical pdfs on the basis of climate, rainfall, soil use information has been described by *Botter et al.* [2007c], and is here briefly reviewed. The mean rainfall frequency

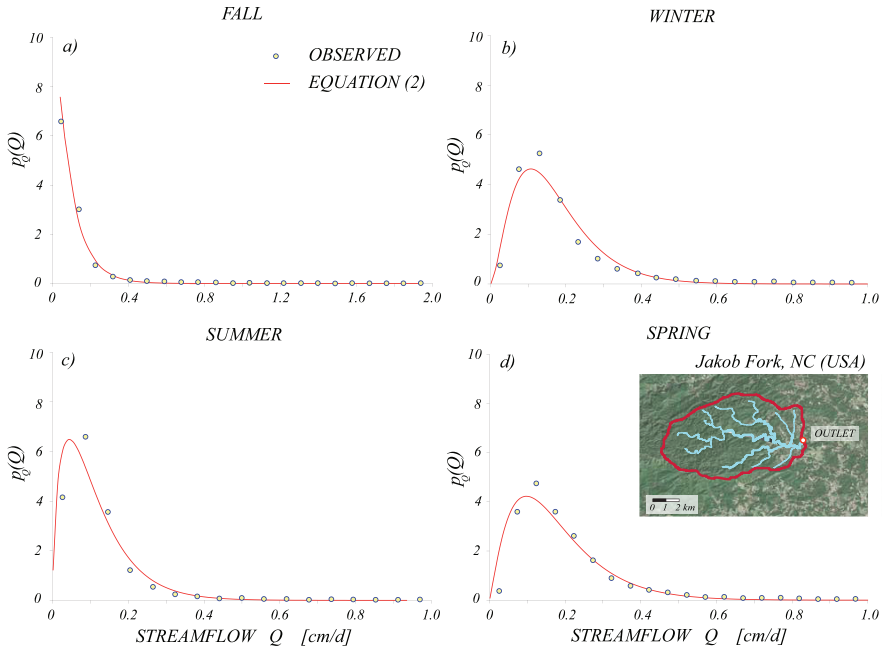

Figure 2.4: Comparison between the (seasonal) analytical streamflow pdfs (solid line, equation (**??**)) and the streamflow pdfs derived from field data (circles) in the Jacob Fork catchment (North Carolina) for (a) fall, (b) winter, (c) summer, and (d) spring. The inset in Figure 4d reproduces the channel network and the soil uses in the study catchment. The estimated soil, vegetation, climate, and transport parameters are listed in Table **??**.

λ_p, and the inverse of the mean daily rainfall depths, γ_p, are derived directly from the daily rainfall records. The runoff frequency, λ, is then estimated by means of equation (**??**) assuming reasonable values for the underlying soil and vegetation parameters (active soil depth nZ_r, wilting point s_w, soil moisture thresholds s_1 and maximum evapotranspiration PET), which are chosen in a narrow range physically meaningful on the basis of land use, soil and climate information. To ensure the reliability of the estimated runoff frequency we have also checked a posteriori the consistency of the estimated value of λ with the relative frequency of positive jumps observed in the recorded streamflow series. The inverse of the mean residence time in subsurface states, k, has been estimated by looking at the recession curves observed in the catchment at hand. The analytical model embeds the various subsurface and groundwater contributions to runoff into a single streamflow component [*Botter et al.*, 2007c]. The analysis of the recorded streamflows, however, seems to suggest the existence of a number of different timescales in the hydrologic response of the Jacob Fork catchment, namely, (1) a quick response with characteristic residence time smaller than 1 day (presumably related to surface flow components) and temporarily activated by rather intense rainfall events, (2) a relatively slow subsurface response with characteristic time in the range $13-15$ days, and (3) a long-term response characterized by large characteristic residence time (say, larger than 1 month), surely related to

Table 2.1: Seasonal Variability of Soil, Climate, Vegetation, and Transport Parameters in the Jacob Fork Catchment

	WINTER	*SPRING*	*SUMMER*	*FALL*
$PET\ [cm\,d^{-1}]$	0.15	0.19	0.30	0.28
$\gamma_p\ [cm^{-1}]$	1.0	0.9	0.9	0.9
$\lambda_p\ [d^{-1}]$	0.32	0.33	0.33	0.29
γ_s	13	11.7	11.9	11.2
$\lambda\ [d^{-1}]$	0.18	0.17	0.11	0.08
$k\ [d^{-1}]$	0.07	0.07	0.07	0.07
$\gamma\ [cm\,d^{-1}]$	16.2	13.1	14.6	11.5

slow groundwater release from soil. When considering the (seasonal or annual) streamflow pdfs, the medium-range subsurface response describes in a reasonable manner the average response of the catchment to precipitation, and indeed allows to reproduce the resulting streamflow pdf in a broad range of discharges. Obviously, the use of the mean subsurface residence time leads to sensibly underestimated high flows [see *Botter et al.*, 2007a, 2007c] and low flows. The probabilistic structure of the lowest flows is, in fact, primarily controlled by the long-term groundwater contribution to runoff.

The estimated values of the underlying soil, vegetation and transport parameters for the different seasons are reported in Table **??**. Owing to the lack of pronounced seasonality in the underlying rainfall and runoff regimes, the transport parameter k remains sensibly constant throughout the year, indicating that the relative importance of the different flow processes taking place is fairly constant in time. Conversely, the estimated values of maximum evapotranspiration rates show a certain variability along the year (due to the presence of seasonal fluctuations of the dominant climatic and ecological processes), with larger values observed during the summer and fall seasons. The graphs reported in Figure **??** show that a transition occurs along the year from a wet-type pdf (during the period December - August, Figures **??**b and **??**c) and a dry type pdf (during the Fall, Figure **??**a). Moreover, the plots also suggest that the model is able to accurately reproduce the observed streamflow statistics year round, except for a slight underestimation of the peaks of the streamflow distributions in winter and spring.

Figure **??** shows the comparison of the observed annual pdf of daily streamflows with the corresponding gamma distribution provided by equation (**??**), here used with temporally averaged parameters. The plot suggests that the analytical model applied at the annual timescale provides reasonable estimates of the observed streamflow pdf, even though notable discrepancies between the two curves can be observed in correspondence of the mode of the distribution. Note that at this site the seasonal variability of the ratioλ/k and of the parameter γ is relatively weak (i.e, $CV_{\lambda/k} = 0.3$ and $CV_\gamma = 0.1$), encouraging the use of temporally averaged parameters to model the annual streamflow statistics. Note that in this plot we avoid to report the curve representing the weighted average of the seasonal pdfs (equation (**??**)) as it results to be reasonably close to the theoretical gamma distribution applied with temporally averaged parameters. Figure **??** suggests that, in the case investigated, the definition of effective, temporally averaged parameters leads to

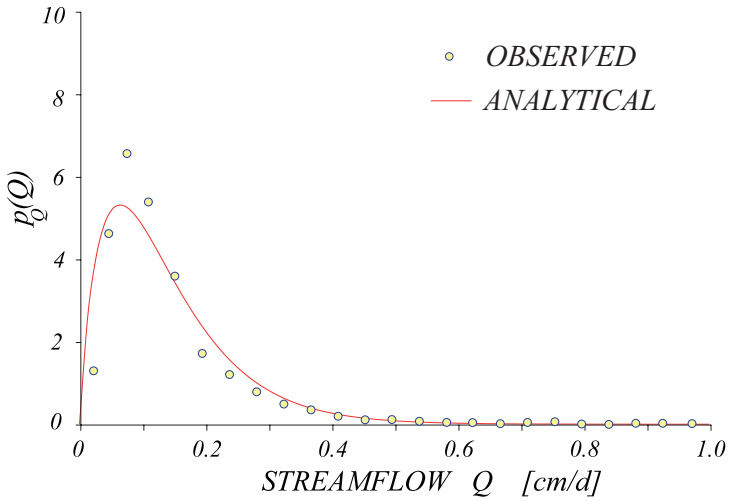

Figure 2.5: Comparison between the (annual) analytical streamflow pdf (solid line, equation **??**) and the corresponding streamflow pdf derived from field data (circles) in the Jacob Fork catchment. The parameters of the analytical distribution are derived as weighted averages of the corresponding seasonal values (Table **??**).

a significant reduction of the number of parameters without affecting negatively the performance of the model.

The behavior of the long-term flow duration curve in the Jacob Fork catchment is investigated in Figure **??**, where the analytical expression provided by equation (**??**) (solid line) is compared with the period-of-record flow duration curve during the period 19801990. The empirical flow duration curve of the Jacob Fork catchment has been evaluated by means of a nonparametric approach (a Weibull plotting position). In Figure **??**a the comparison is carried out in a normal plot, and the theoretical annual flow duration curve is estimated by applying equation (**??**) with the same set of parameters used in Figure **??**. The plot suggests that the analytical expression derived is able to reproduce the behavior of the observed flow duration curve in a broad range of durations (i.e., from 0.1 to 0.9 years). Notably, the duration of the highest flows (i.e., $Q > 0.5\ cm\,d^{-1}$) is significantly underestimated by the analytical model, because of the fact that fast (e.g., surface) runoff processes triggered by intense floods have been explicitly neglected. The analysis of the lognormal plot presented in Figure **??**b suggests that the analytical model slightly underestimates also the durations of the smallest streamflows (i.e., $Q < 0.05\ cm\,d^{-1}$). This is due to the fact that the low flows are primarily controlled by the slow groundwater component of the hydrologic response (the timescale of which are much larger than the characteristic time of subsurface processes). In fact, if we set $k = 0.03\ d^{-1}$ in equation (**??**), a value corresponding to the inverse of the mean residence time of groundwater flow (suitably estimated from the analysis of the sole recession curves falling in the range 00.05 $cm\,d^{-1}$), the ability of the analytical model to reproduce the low-flow portion of the duration curve significantly increases (dashed line in Figure **??**b). This suggests

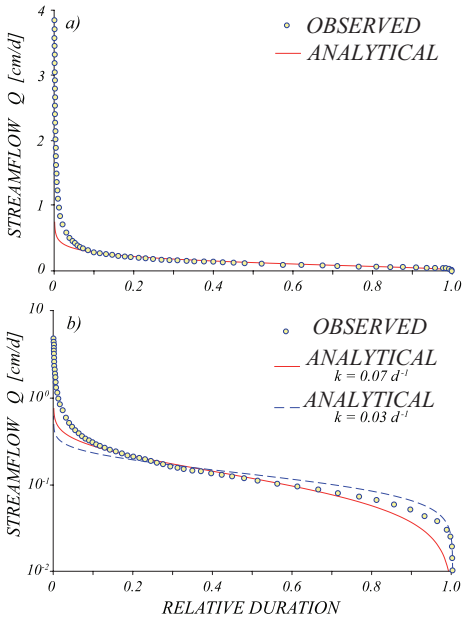

Figure 2.6: Comparison between analytical (solid and dashed lines, equation **??**) and experimental (circles) yearly flow duration curves in the Jacob Fork catchment: (a) normal plot and (b) semilog plot. The solid line refers to the case $k = 0.07\ d^{-1}$, and the dashed line in panel b refers to the case $k = 0.03\ d^{-1}$. The remaining parameters are the same as those used in Figure **??**.

that, when focusing only on the lowest flows and not on the whole streamflow pdf, the dominant process becomes the slow groundwater contribution to runoff as one expects.
Figure **??** shows the comparison between the observed probability distribution of the annual minima, $P_m(Q)$, and the theoretical distribution given by equation (**??**). The observed cumulative probability has been evaluated by means of a Weibull plotting position. As the annual minima strongly depend on the distribution of the streamflows for $Q \to 0$, the comparison is carried out by considering the mean residence time pertaining to the long-term groundwater contribution to runoff (i.e., $k = 0.03\ d^{-1}$), which allows the best fit between the theoretical and the observed duration curves for $Q \to 0$ (see Figure **??**b). The remaining parameters are the same as employed in Figures **??** and **??**. Because of the lack of pronounced seasonality in the underlying hydrologic regime, the annual minima do not occur always in the same season, but they are widespread along the year (from July to January). This circumstance encourages the use of the annual pdf to treat the distribution of the annual minima.
Remarkably, the experimental distribution of the annual minima in the decade 1980 - 1990 (dash-dotted line) shows a reasonable agreement with the predicted theoretical distribution. As expected, the analytical model tends to underestimate the cumulative probability of the largest minima owing to the fact that $\lambda/k > 1$. However, the analytical distribution provides a robust estimate of the observed $P_m(Q)$ for exceedance probabilities larger than 0.5. Also shown in Figure **??** (dotted line)

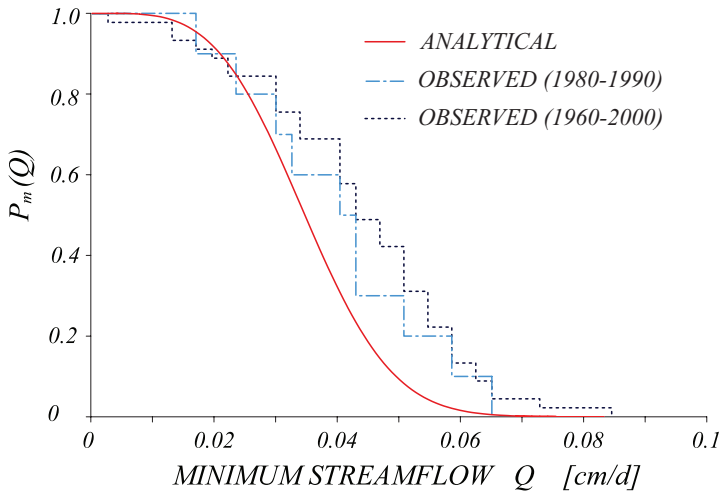

Figure 2.7: Comparison between analytical and experimental exceedance probability distributions for the annual minima in the Jacob Fork catchment. The parameters of the analytical distribution (equation **??**, solid line) are $\lambda = 0.13\ d^{-1}$, $\gamma = 13.8\ d\,cm^{-1}$, and $k = 0.03\ d^{-1}$. The experimental distributions shown in the plot refer to the decade 1980-1990 (dash-dotted line) and to the time period 1960-2000 (dotted line).

is the observed exceedance probability of daily streamflows in the period 1960 - 2000. The latter distribution exhibits a similar behavior with respect to that of the experimental distribution of the period 1980 - 1990 (even though the increased number of data obviously leads to a smoother curve). Overall, the agreement of the two experimental distributions of the annual minima suggests that no dramatic changes in the probabilistic structure of runoff have occurred in the last 50 years at Jacob Fork. Moreover, Figure **??** also indicates that the experimental exceedance probability in the period 1980 - 1990 can be considered as a reasonable estimate of the underlying probability distribution of the annual minima, despite of the limited number of data.

2.3 Long-term Variability of Stream Stage

Stochastic fluctuations in streamflow necessarily affect the temporal variability and the probability structure of the stage, h. As it will be extensively discussed in the next section, the stream stage modulates the impact of natural streamflow temporal fluctuations (induced by intermittent rainfall forcings) on the underlying biogeochemical processes and represents one of the major drivers for the nutrient removal processes within river networks [*Wollheim et al.*, 2006; *Alexander et al.*, 2009]. Therefore, given also the natural hydraulic and ecological risk related to fluctuations in stream stage, a proper probabilistic characterization of such variable is valuable.
To determine how stochastic fluctuations in streamflow, Q, influence the temporal variability and the probability structure of the stage, h, it is necessary to define a functional relationship between Q and h. In most cases of practical interest, the $Q - h$ dependence for a given reach can be

approximated by a power law [see, e.g., *Leopold and Maddock*, 1953; *Stall and Fok*, 1968; *Chow et al.*, 1988], i.e., $h = aQ^b$, where the constants a and b depend on the morphology of the stream (b is the discharge rating curve exponent). Seldom, in fact, the magnitude of inertial effects or convective terms impairs significantly the validity of such a relation [*Henderson*, 1963]. For simple geometries, exact relationships for a and b can be derived from uniform flow formulas. Note that the concave behavior of the rating curve usually implies $0 < b < 1$ (Figure **??**), while in most practical cases b is usually comprised in the range (0.3-0.9) [*Chow et al.*, 1988]. Note that larger values of the discharge rating curve exponent b are usually associated with less compact cross sections.

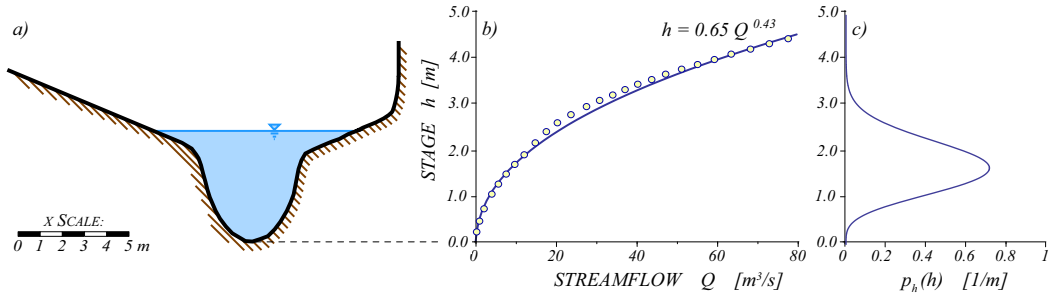

Figure 2.8: Example of derivation of the stage pdf, $p_h(h)$: (a) reach cross section, (b) rating curve in the considered section: values calculated by means of the Gauckler-Strickler formula valid for uniform flow (dots) and interpolation curve, and (c) stage pdf $p_h(h)$ for the section shown in panel a corresponding to a wet-typw streamflow pdf $p_Q(Q)$.

The pdf of the stage, $p_h(h)$, can be derived from the pdf of the discharge, p_Q, as [*Botter et al.* 2010b]

$$p_h(h) = p_Q(h^{1/b}/a)\left|\frac{dQ}{dh}\right| = \frac{\theta}{b\Gamma(\lambda/k)}(\theta h)^{(\frac{\lambda}{kb}-1)}exp[-(\theta h)^{1/b}], \tag{2.20}$$

where $\theta = \gamma^b/a$ represents the inverse of the stage observed when the discharge is equal to the mean streamflow jump produced by runoff events ($Q = 1/\gamma$). Thus, the pdf of the stage, p_h, is a generalized Gamma distribution with shape parameters $\lambda/k > 0$ and $1/b > 0$, and with scale parameter θ. The generalized Gamma distribution is a family of distributions widely employed in hydrology, with the Weibull, the lognormal, the Levy, the chi-square, the Gamma and the exponential distributions as special cases. An example of stage distribution derived from Equation (**??**) is shown in Figure **??**c. Therein, p_h is derived from the streamflow pdf via interpolation of $Q - h$ values obtained by assuming uniform flow with constant slope and roughness, and applying the Gauckler-Strickler (or Manning) uniform flow resistance formula (Figure **??**).
According to equation (**??**), p_h depends on geomorphologic, climatic and ecohydrological characteristics of the catchment, as well as on the geomorphologic features of the reach. Indeed, the distribution turns out to be monotonic or bell-shaped depending on the value of a dimensionless parameter, $\lambda/(kb)$. In particular, the pdf is monotonically decreasing (and the mode approaches zero) when $\lambda/(kb) < 1$, and becomes bell-shaped when $\lambda/(kb) > 1$. This circumstance reflects the

capability of the cross section geometry to affect the mode of the stage distribution, mitigating or enhancing the effects produced by low flows.
The behavior of the stage pdf $p_h(h)$ as a function of the climate-landscape interaction parameter λ/k, and the channel morphology shape factor b is explored in Figures **??**c and **??**d. Note that the stage pdfs are normalized with respect to the corresponding first moment of the distributions (i.e., the mean stage $\langle h \rangle$). When $\lambda/k < 1$ (Figure **??**c), the corresponding stage pdf can be monotonically decreasing (as the streamflow pdf) or bell-shaped depending on the value of the parameter b. For $\lambda/(kb) < 1$, the pdfs of both Q and h are monotonically decreasing, while for $\lambda/(kb) > 1$ and $\lambda/k < 1$ the pdf of Q is monotonically decreasing while that of h is bell-shaped. When $\lambda/k > 1$, the stage pdf is always bell-shaped similarly to the streamflow pdf (Figure **??**d). These results indicate that the transition from monotonic to bell-shaped stage pdf's does not depend only on the underlying catchment-scale hydrologic, morphologic and climate features, but is also affected by the shape of the cross section of the reach. In particular, when $b > \lambda/k$ and $\lambda/k < 1$, the section geometry induces a bell-shaped pdf of the stage regardless of the monotonically decreasing behavior of the streamflow pdf (Figure **??**).

2.3.1 Moments of $p_h(h)$

The mean and the variance of the stage h can be computed from equation (**??**), and their expressions are [*Botter et al.*, 2010b]

$$\langle h \rangle = \frac{\Gamma(\lambda/k + b)}{\theta \Gamma(\lambda/k)} \tag{2.21}$$

$$Var(h) = \langle h^2 \rangle - \langle h \rangle^2 = \frac{\Gamma(\lambda/k + 2b)\Gamma(\lambda/k) - [\Gamma(\lambda/k + b)]^2}{\theta^2 \Gamma(\lambda/k)^2}. \tag{2.22}$$

According to equations (**??**) and (**??**), and because of the implicit dependence of θ on other model parameters, the moments of the stage distributions depend on the following three types of parameters: i) channel cross section shape parameters: a and b (the scaling constant and the exponent of the rating curve); ii) climate and ecohydrological parameters embedding rainfall properties and soil-water dynamics: λ (the frequency of runoff events) and γ_p (the inverse of the mean rainfall depths); and iii) geomorphologic catchment attributes: k (the mean catchment residence time) and A (the catchment area). Note that the last three parameters define the value assumed by γ ($\gamma = \gamma_p/(kA)$), which, in turn, defines, jointly with a, the functional dependence of θ on b ($\theta = a\gamma^b$). Because of the intertwined variability of θ, λ, k and b along different climatic and geomorphic settings, exploring the full dependence of $\langle h \rangle$ and $Var(h)$ on all the independent parameters is a challenging task.
We focus on the dependence of the moments of the stage pdf on the channel cross-section shape (b) and on the ratio λ/k (which embeds rainfall and landscape features), assuming γ to be constant. This is justified (at least to first order) in the following cases: i) when λ is allowed to vary but k and A are kept constant, e.g., when the focus is to analyze the dependence of the stage pdf of a catchment with a certain area and prescribed features of its hydrologic response on the cross sectional shape, the rainfall frequency and the underlying soil properties; or ii) when the ratio λ/k varies as a result of variations of both λ and k, but without significant variations of the ratio

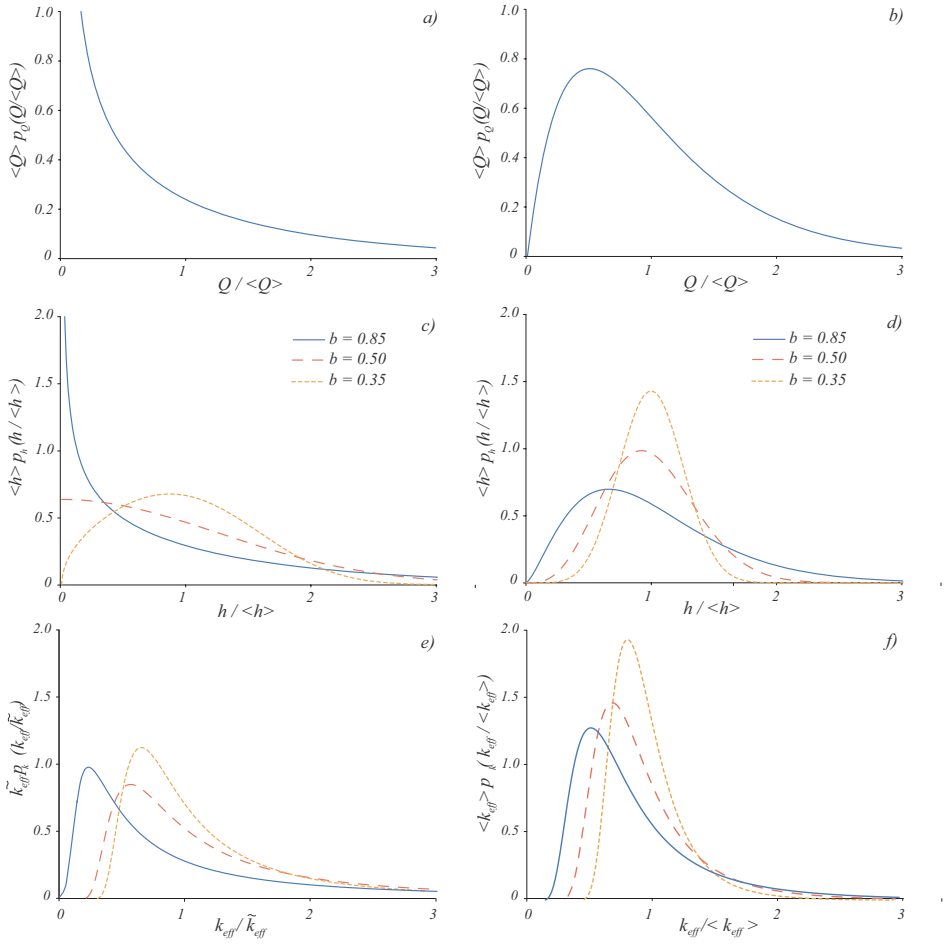

Figure 2.9: Sensitivity of the stage pdf ($p_h(h)$) and of the denitrification rate pdf ($p_k(k_e)$) to the discharge rating curve exponent b under two different hydrologic regimes: (left) dry-type $p_Q(Q)$ and (right) wet-type $p_Q(Q)$: (a) pdf of the normalized streamflow for $\lambda/k = 0.5$; (b) same as panel a but for $\lambda/k = 2$; (c) pdf of the normalized stage under the same hydrologic conditions shown in panel a ($\lambda/k = 0.5$); (d) pdf of the normalized stage under the same hydrologic conditions shown in panel b ($\lambda/k = 2$); (e) pdf of the normalized in-stream denitrification constant k_{eff} under the hydrologic conditions shown in panel a; and (f) pdf of the normalized in-stream denitrification constant k_{eff} under the hydrologic conditions shown in panel b. In panels c, d, e, and f the different curves refer to the following values of the parameter b: 0.85 (solid line); 0.5 (dashed line) and 0.35 (dotted line). Note that in all the graphs the normalizing factor is the mean, while in panel f the pdfs are normalized with respect to the median of k_{eff}. The other model parameters are: $a = 0.26$ $[s^{3b}/m^{3b-1}]$, $\gamma = 0.1$ $[s\,m^{-3}]$ and $v_f = 15$ $[mm\,d^{-1}]$.

$\gamma_p/(kA)$. Note also that, as the coefficient of variation (CV) proves to be independent of θ (on which both the mean and the standard deviation of the pdf depend linearly), the analysis of the

relative variability of h is unaffected by the latter simplification.
Figure **??** explores the behavior of the mean, the variance, and CV of the stage as a function of the dimensionless ratio λ/k and b, when $\gamma = 0.35\ s/m^3$ (corresponding to $\gamma_p = 80\ m^{-1}$, $k = 0.2\ d^{-1}$ and $A = 10^2\ km^2$). The specific value chosen for this parameter, which represents the mean of the values obtained in the literature for the different catchments examined by *Botter et al.* [2007c, 2010a], does not impact the trends evidenced here.
Three regions are identified in the plot depending on the relative value of λ/k and b. For $\lambda(kb) < 1$, the pdfs of both Q and h are monotonically decreasing. For $\lambda/(kb) > 1$ and $\lambda/k < 1$, the pdf of Q is still monotonically decreasing, while the pdf of h is bell-shaped. For $\lambda/(kb) > 1$, instead, the pdf's of both Q and h prove to be bell-shaped.
Over the entire range of λ/k, the mean stage increases along the gradient from dry ($\lambda/k < 1$) to wet ($\lambda/k > 1$) regimes (Figure **??**a). The rate of increase, however, it increases with larger values of b and appears to be larger in dry than in wet domains, particularly for small values of b. While $\langle h \rangle$ increases consistently with λ/k for a fixed value of b, the effect of b on $\langle h \rangle$ depends on the ratio λ/k. For small values of the ratio λ/k, indeed, larger b values reduce the mean stage. For large values of λ/k, increasing the shape parameter b leads to an increase in the mean stage. The sensitivity of the mean stage to changes in values of b decreases as λ/k approaches 1. For $b > 0.5$ and $\lambda/k < 1$, the mean stage becomes less sensitive to changes in b and depends chiefly on the parameter embedding climate]landscape interactions,λ/k. The variance of the stage increases with larger values of b, while it shows a more complex dependence on λ/k.
Two distinct domains of behavior exists depending on the relative magnitudes of λ/k and b. When $\lambda/k << 1$ the variance is extremely sensitive to λ/k and almost insensitive to b while when $\lambda/k > 1$, the variance is weakly sensitive to λ/k but highly sensitive to b (Figure **??**b). For large b, $Var(h)$ increases along with λ/k. For intermediate values of b, $Var(h)$ increases with λ/k in the dry domain, and then reaches a plateau in the wet domain ($\lambda/k > 1$). For low values of b, finally, $Var(h)$ increases with λ/k for low values of λ/k, and then decreases with λ/k for $\lambda/k > b$. The coefficient of variation of h increases with b and decreases with λ/k (Figure **??**c). The rate of change of both the variance and the CV is greater in the dry than in the wet domain. Thus, for a fixed value of γ, wet streamflow regimes (i.e., $\lambda/k > 1$) exhibit stages that have a greater mean, $\langle h \rangle$, are more stable over time (lower CV) and are in general less sensitive to changes in the climate-landscape controls. The opposite is true for dry domains. Conversely, larger values of b lead to stages that are less stable over time (higher CV's) and have a higher or a lower mean, depending on the underlying climate-landscape attributes.

2.4 Long-term Variability of Nutrient Removal in Streams

In this section the linkage between rainfall random variability to stream flow and stream depth fluctuations is further extended to characterize fluctuations in stream nutrient losses. To this end a relationship between the stream stage h and an effective, nutrient removal rate constant, k_{eff} $[T^{-1}]$, is provided and the pdf of k_{eff} is then derived on the basis of such relationship.
Nutrient losses in a stream can be characterized by several integrative metrics. Among the most widely employed is the nutrient delivery ratio (NDR), which is defined as the ratio of the nutrient

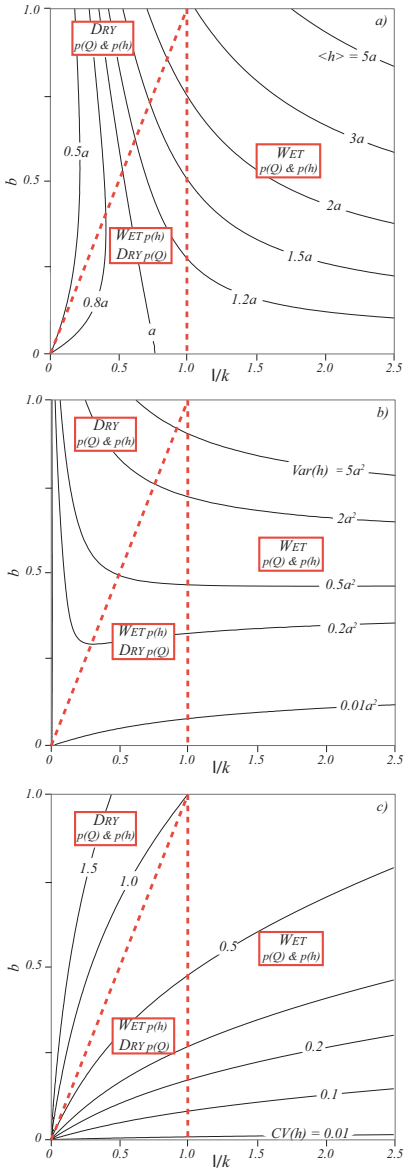

Figure 2.10: Mean, variance and coefficient of variation ($CV = Var(h)^{0.5}/\langle h \rangle$) of the stage as a function of λ/k and the discharge rating curve exponent b. $\gamma = 0.35$ $[s\,m^{-3}]$ and is constant with λ/k. The dashed lines highlight the following three regions: (1) a region where $p_Q(Q)$ and $p_h(h)$ are monotonic, (2) a region where $p_Q(Q)$ is monotonic but $p_h(h)$ is bell-shaped, and (3) a region where both $p_h(h)$ and $p_Q(Q)$ are bell-shaped.

flux that leaves the reach outlet and the flux that is delivered at the reach inlet. Nutrient losses can be characterized via k_{eff}, which is a measure of the relative rate of nutrient removal for unit stream

travel time. This approach implicitly assumes that the stream reach acts as a single, homogeneous compartment in which nutrient mass is transported by advective (and dispersive) flow, and is lost through the combined effects of interactions with the benthic sediments and biotic uptake in the water column [*Bencala et al.*, 1983]. According to the above scheme, the NDR for a single stream reach characterized can be expressed in terms of k_{eff} as $NDR = exp[-k_{eff}\tau_L]$, where τ_L is the in-stream average travel time. For a whole network, changes in NDR values along the network reflect the spatial and temporal variations in flow, nutrient inputs, and biogeochemical conditions. Temporal patterns of k_{eff}, induced by stage fluctuations have important implications for interpreting reach-scale experiments and for linking short-term nutrient loss rates estimates (which are frequently used for cross-scale comparisons) to long-term variations

2.4.1 Hydrogeomorphic Controls on Nutrient Losses

The model proposed conceptualizes the stream as a two compartment box, an advection-dominated zone (i.e., the water column) through which nutrient is transported (subscript w) coupled to a transient storage zone in which nutrient transformations dominate (subscript s). These two zones are linked by hyporheic exchange, represented as a first-order mass transfer process, which may be either by diffusion or hyporheic exchange [*Bencala and Walters*, 1983]. Figure **??** illustrates a schematic representation of this two-compartment conceptual model. This conceptualization is based on the Transient Storage Model (TSM), first proposed by *Bencala and Walters* [1983] and extensively used in stream denitrification studies [*Hart*, 1995; *Green et al.*, 1994; *Runkel and Chapra*, 1993; *Harvey et al.*, 1996; *Marion et al.*, 2008]. While recognizing the limitations of this conceptualization to describe tracer injection studies [*Harvey et al.*, 1996; *Wagner and Harvey*, 1996], the objective here is to apply it for providing a functional form for k_{eff} that can be used for comparison across systems. Since the focus of the work is to explore the variability in denitrification rates, biotic uptake term is neglected in our formulation. Moreover, we also neglect the dispersion term, and assume that the dominant transport mechanism is advection (an assumption which is satisfied in many practical applications in rivers [see, e.g., *Rinaldo et al.*, 1991; *Rutherford*, 1994; *Marion et al.*, 2008]). Under the above simplifications, the mathematical formulation of the TSM is given as follows:

$$\frac{\partial C_w}{\partial t} = -q\frac{\partial C_w}{\partial x} - \alpha(C_w - C_s), \tag{2.23}$$

$$\frac{\partial C_s}{\partial t} = \alpha\frac{S}{S_s}(C_w - C_s) - k_{sed}C_s, \tag{2.24}$$

where x $[L]$ is the distance along the stream; t $[T]$ is time; $C_w(x,t)$ and $C_s(x,t)$ $[ML^{-3}]$ are, respectively, the nutrient concentrations in the water column and the pore water. Moreover, q $[LT^{-1}]$ is the flow velocity; k_{sed} $[T^{-1}]$ is the site-specific first-order rate constant for nutrient loss in the benthic sediment; S_s is the cross sectional area of the storage zone $[L^2]$; S is the cross-sectional area of the channel $[L^2]$; and α is the stream storage exchange rate $[T^{-1}]$ expressing the exchange capacity between the two compartments.

The nutrient concentration at the downstream section of a reach may vary in time due to variations in the other model parameters, and because of transient effects induced by non-equilibrium

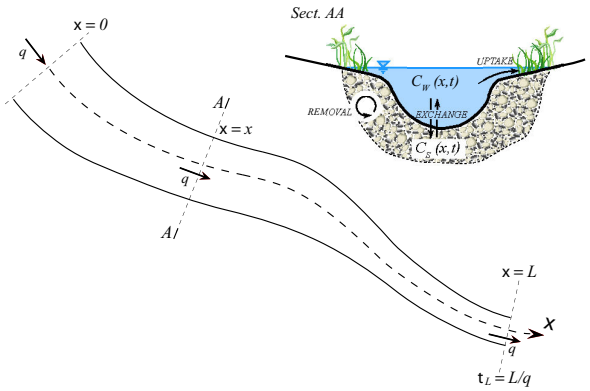

Figure 2.11: Conceptual representation of the Transient Storage Model in a stream reach (see text for symbol definitions).

conditions between the two compartments (driven, as they are, by temporally variable nutrient input rates). As the variation in the input concentration is weak (and usually relatively slow) when compared to the variations produced by temporally variable hydrologic conditions on the model parameters, possible transient effects due to temporally variable nutrient input rates will be neglected. The primary focus here is instead on the parameter fluctuations induced by intra-annual variation of the hydrologic conditions, embedded by variations of the stage (see below). Provided that in most cases the reactivity of the system to changes in these parameters is significant, the effect of the intra-annual variability of the hydrologic conditions on the overall nutrient removal will be described by deriving the steady state solution of equations (**??**) and (2.22) (with constant parameters), and then randomizing a posteriori the steady state solution.
The steady state expression for the nutrient concentration at the reach outlet is

$$C_w(x = L_x, t \to \infty) = C_{w,0} e^{-\kappa \tau_L}, \tag{2.25}$$

where L_x is the length of the reach, τ_L is reach travel time, $C_{w,0}$ is the nutrient concentration at the upstream cross section (i.e., in $x = 0$) and $\kappa = k_{sed}/(S/S_s + k_{sed}/\alpha)$ is a parameter quantifying the decay of nutrient concentration along the stream. Hence, the related nutrient delivery ratio (NDR) can be expressed as

$$NDR = \frac{qC_w(x = L_x)}{qC_{w,0}} = e^{-\kappa \tau_L} \tag{2.26}$$

According to the definition of k_{eff} and its relation with the NDR, from equation (**??**) the effective removal rate constant can be finally expressed as

$$k_{eff} = \kappa = \frac{k_{sed}}{(\beta + k_{sed}/\alpha)} \tag{2.27}$$

Note that in equation (**??**) $\beta = S/S_s$ represents the ratio of the volumes of advective and reactive zones per unit stream length, while the term $1/\alpha$ represents the mass transfer time constant at the

sediment-water interface. Thus, k_{eff} observed in a given system is determined by the biogeochemical factors (k_{sed}), which is moderated by two hydrologic factors, the dilution effect (β) and the mass transfer effect (α).

It is now possible to explicitly consider all of the hydrologic controls (i.e., h-dependency) on various parameters involved in equation (**??**). If we assume hyporheic exchange within the stream bed to be the dominant transfer mechanism with the transient storage zones, the mass transfer coefficient can be expressed as a function of the average flow rate into the sediments per unit bed area q_B $[LT^{-1}]$ and the flow depth as $\alpha = q_B/h$ [*Marion et al.*, 2008; *Wörman et al.*, 2002; *Packman and Bencala*, 2000]. The mass transfer velocity q_B has been shown to be weakly variable within a narrow range (say, between 5 to 15 $[cmd^{-1}]$, [see, e.g., *Birgand et al.*, 2007]. For what concerns the dependence of β on h, we will refer to a simplified scheme employing the basic scales derived from an equivalent rectangular cross sections. S is then simply the product between channel width, w, and the stage, h: $S = wh$. The hyporheic zone cross-sectional area S_s (usually measured indirectly in field studies by using stream tracers [*Wondzell*, 2006]) can be linked to effective depth, d_s, width w_s and porosity of the channel sediments, σ: $S_s = d_s \sigma w_s$. While σ and d_s, which describe key physical properties of the bed, can be safely assumed to be constant within a given reach, both the width of the stream and the width of the hyporheic zone change along with stage. Our hypothesis, however, is that the ratio $r = w/w_s$ is mildly dependent on the stage h and remains relatively constant in time [Battin et al., 2009].

Equation (**??**) can be thus rewritten evidencing the dependencies on h as follows:

$$k_{eff} = \frac{k_{sed}}{h\left(\frac{r}{\sigma d_s} + \frac{k_{sed}}{q_B}\right)} \tag{2.28}$$

While exploring annual or seasonal temporal patterns in instream nutrient losses, we assume the parameters k_{sed} and q_B, which are biogeochemical and physical controls on k_{eff}, to be essentially constant in time at a given location. This is justified by the following considerations. For denitrification, k_{sed} represents the biogeochemical control and is a function of the carbon-normalized, intrinsic, denitrification rate constant k_N $[M^{-1}L^3T^{-1}]$, the dissolved organic carbon concentration, DOC $[ML^{-3}]$, and the degree of anoxia. In laboratory incubation studies conducted under anoxic conditions, k_N was found to be nearly constant (≈ 0.15 $[mg^{-1}DOCLd^{-1}]$) for several mineral and organic soils, while DOC ranged from about 100 to 500 $[mg/L]$ in mineral soils [*Reddy et al.*, 1982]. DOC concentrations in streams and rivers have been reported to range between $1 - 10$ mg/L [*McKnight et al.*, 2002; *Raymond and Oh*, 2007; *Warner et al.*, 2009].

Note that temperature gradients effects on k_{sed} are also neglected. *Bohlke et al.* [2008] modeled denitrification losses in streams by considering the effects of a ten-degree temperature variation over the year, and assumed a Q_{10} of 2. Simulated patterns in N removal illustrated the dominant role of stage and a minor role of temperature effect. Under, under the above simplifying assumptions, the temporal variability of the effective rate constant k_{eff} can be attributed to the variability of h as [*Botter et al.* 2010b]

$$k_{eff}(t) = \left(\frac{k_{sed}}{\frac{r}{\sigma d_s} + \frac{k_{sed}}{q_B}}\right)\frac{1}{h(t)} = \frac{v_f}{h(t)}, \tag{2.29}$$

where v_f, defined as the product of removal rate constant and the river stage, is the so-called uptake velocity. Equation **??** expresses in a quantitative manner the controls exerted by the stream stage on nutrient losses within a given stream reach.

2.4.2 Probability Distribution of the Effective Removal Rate Constant

The rationale for the use of the stochastic model of streamflows is to examine the effect of flow/stage variability on the fluctuations imposed to in-stream processes. Under the assumptions made, the intra-annual stage variability can be described by means of a sequence of uncorrelated steady states for each of which equation (**??**) applies. The approach pursued herein is related to that proposed by *Doyle* [2005], with the important difference, which qualifies the entire approach proposed here, that the pdf's of streamflows used to infer removal rates are not assumed and fitted but rather derived from a full-fledged theoretical ecohydrological model.
Whenever the biogeochemical and physical parameters can be assumed constant in time the pdf of k_{eff}, $p_k(k_{eff})$, can be thus derived from the pdf of the stage (following equations (**??**) and (**??**)) as [*Botter et al.*, 2010b]

$$p_k(k_{eff}) = p_h(v_f/k_{eff}) \left| \frac{dh}{dk_{eff}} \right| = \frac{\Omega}{b\Gamma(\lambda/k)} (\Omega k_{eff})^{-\frac{\lambda}{kb}-1} exp[-(\Omega k_{eff})^{-1/b}], \tag{2.30}$$

where $\Omega = 1/(\theta v_f)$ is the inverse of the value of k_{eff} corresponding to a value of Q equal to the mean streamflow jump $1/\gamma$. The pdf of the effective nutrient loss rate constant (equation (**??**)) is a generalized Gamma distribution with shape parameters λ/k and $-1/b$, and scale parameter Ω. Such pdf embeds the effect of the deterministic increase of k_{eff} during the recessions, and the stochastic (negative) jumps in correspondence of streamflow producing events.
The dependence of the nutrient loss rate constant pdf, $p_k(k_{eff})$, on the channel morphology shape factor, b, for different values of the climate-landscape interaction parameter, λ/k, is explored in Figures **??**e ($\lambda/k = 0.5$) and **??**f ($\lambda/k = 2$). Because when $\lambda/k < 1$ some values of the shape factor imply that the mean of the distribution does not exist, in Figure **??**e the nutrient loss rate constant pdf's are normalized with respect to the median of the distribution, $\tilde{k_{eff}}$. The graph highlights that in this case $p_k(k_{eff})$ is bell-shaped over the entire range of channel morphologies defined by the parameter b. Indeed, the behavior of $p_k(ke)$ for the lowest values of k_{eff} is determined by the exponential part of the pdf, and $lim_{x\to 0+} p_k(x) = 0$, independently on the value of b (Figures **??**e and **??**f). The graph also emphasizes that the mode of the pdf approaches zero as λ/k decreases and for values of b relatively large (Figures **??**e and **??**f). Moreover, in the dry streamflow regime ($\lambda/k < 1$) the distribution of k_{eff} is relatively more asymmetric than the distribution of h (i.e., the skewness of the distribution of k_{eff} is larger than that of the stage pdf). The tail of the distribution, in particular, grows as b increases. This feature of $p_k(k_{eff})$ originates from the fact that, according to equation (**??**), the removal rate constant k_{eff} increases without bounds when the stage tends to zero. Thus k_{eff} is more variable in the dry regimes. As a result, temporal variations in nutrient losses in stream networks in dry domains are expected to be greater compared to those observed in wet domains.
The above framework explicitly links climate, landscape, geomorphologic, and biogeochemical factors to instream nutrient processing. It allows us to study the variation induced by geomorphologic,

climatic, and ecohydrological parameters on the moments of the pdf of the stage and of the effective nutrient-removal rate-constant.

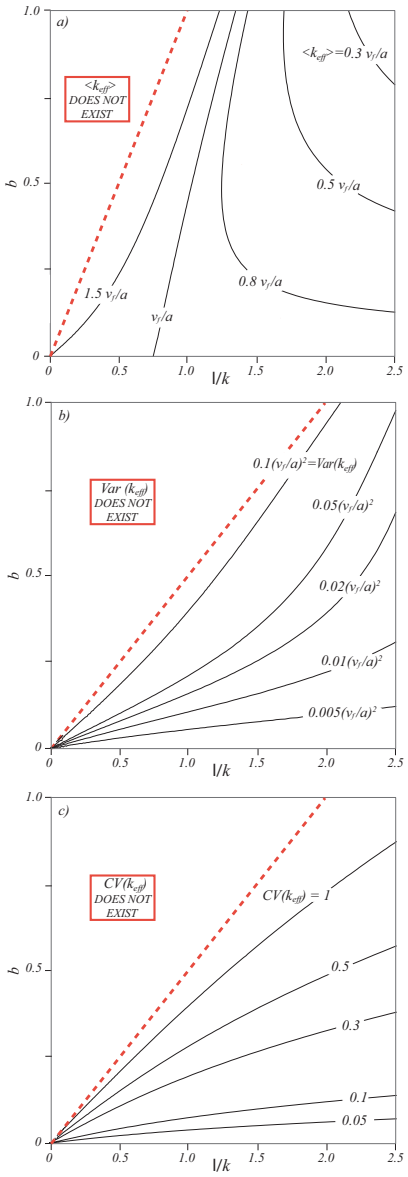

Figure 2.12: Mean, variance and coefficient of variation of the in-stream denitrification constant k_{eff} as a function of the dimensionless parameters λ/k and b. γ is assumed to be constant with λ/k and equal to 0.35 $[s\,m^{-3}]$. The dashed lines bound the domains of each function.

2.4.3 Moments of $p_k(k_{eff})$

The climate, landscape, stream morphology and biogeochemical controls on the pdf of the nutrient removal rate constant can be analyzed deriving the analytical expressions of the moments of $p_k(k_{eff})$ as a function of the model parameters from equation (**??**):

$$\langle k_{eff} \rangle = \frac{\Gamma(\lambda/k - b)}{\Omega\Gamma(\lambda/k)} \tag{2.31}$$

$$Var(k_{eff}) = \langle k_{eff}^2 \rangle - \langle k_{eff} \rangle^2 = \frac{\Gamma(\lambda/k - 2b)\Gamma(\lambda/k) - [\Gamma(\lambda/k - b)]^2}{\Omega^2[\Gamma(\lambda/k)]^2}. \tag{2.32}$$

Note that, in the above equation, the variance of k_{eff}, $Var(k_{eff})$, is finite only when $\lambda/(kb) > 2$, while the mean of k_{eff}, $\langle k_{eff} \rangle$, is finite only when $\lambda/(kb) > 1$. In other words, when the pdf of the stage is monotonically decreasing and the largest probability densities are associated with the smallest stages ($\lambda/(kb) < 1$), $\langle k_{eff} \rangle$ diverges. This is inherent in the proposed relationship between k_{eff} and h (equation (**??**)), according to which k_{eff} tends to infinity when h approaches 0. Such a singularity can be avoided by considering a different relationship between k_{eff} and h. *Fehlman* [1985] showed that for small values of h (say, roughly $h \leq 15$ cm) the exchange coefficient α is inversely proportional to the stage h ($\alpha \propto h^{-1.5}$). Modifying equation (**??**) in such a way would lead to a new expression for $k_{eff}(h)$, according to which $k_{eff} \to 0$ for h approaching 0. Conversely, when $\lambda/(kb) > 1$, equation (**??**) provides a reference value for k_{eff} as a function of a few hydrologic and biogeochemical parameters.

The moments of the distributions of k_{eff} depend on all six parameters controlling the moments of h, plus the parameter embedding physical and biogeochemical attributes, v_f. Again, the intertwined variability of θ, λ, k and b (and maybe even of v_f) along different climatic and geomorphic gradients, makes rather difficult to explore all the geomorphic, hydrologic, biogeochemical and climatic controls on $\langle k_{eff} \rangle$ and $Var(k_{eff})$. In analogy to the analysis carried out for the stage, we recognize the parameters α and v_f to be simply scaling factors for p_k, thus allowing us to focus on the dependence of the moments of the pdf of the removal rate constant on the cross section shape, b, and on the ratio λ/k (which embeds rainfall and landscape features), by assuming γ to be constant. The behaviors of the mean, the variance, and the coefficient of variation (CV) of k_{eff} are shown in Figures **??**a, **??**b, and **??**c, respectively. As stated earlier, the mean of k_{eff} does not exist for $\lambda/(kb) < 1$. $\langle k_{eff} \rangle$ decreases for increasing values of λ/k with increasing rates for progressively drier regimes.

The mean value of k_{eff} increases with b for $\lambda/k < 1$, while it shows the opposite trend for $\lambda/k > 1.5$. The variance and CV of k_{eff} exist only for $\lambda/(kb) > 2$, decrease with increasing λ/k, and increase with b. Similar to the observations noted for the stream stage, we find that as b approaches 0, the sensitivity of the mean, variance and CV of k_{eff} to the ratio λ/k decreases. The overall conclusions are similar (but opposite) to those derived for stage because wet domains have a smaller $\langle k_{eff} \rangle$ and more stable values of k_{eff} over time compared to dry streamflow regimes. Moreover, larger values of b lead to nutrient removal rate constant k_{eff} more stable over time (low CV) but with larger or smaller mean depending on the underlying streamflow regimes.

Finally, it is interesting to to investigate how the variability of h translates into the variability of k_{eff} in different systems. To this end we plot the ratio between the CV of k_{eff} and the CV of h as a

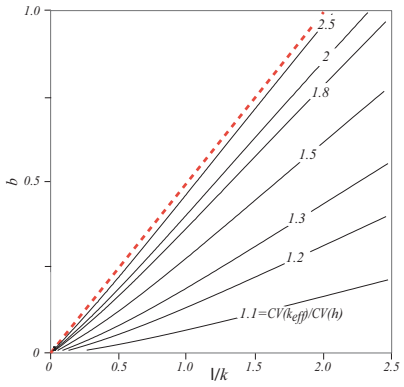

Figure 2.13: Ratio between the coefficient of variation of k_{eff}, $CV(k_{eff})$, and the coefficient of variation of h, $CV(h)$, as a function of λ/k and b.

function of λ/k b (Figure **??**). Note that lower values of the CV ratio characterize streams in which the variability of k_{eff} is close to that of the stage. In contrast, higher CV ratios are representative of systems in which the variability in k_{eff} is amplified with respect to variability of h. For a constant value of b, an increasing of λ/k (implying increasing wetness of the streamflow regime) produces a decrease in the CV ratio, indicative of buffering expected in wet regimes. When instead we consider a constant λ/k, an increase in the shape factor b is noted to amplify k_{eff} variability. Finally, it can be noticed that sensitivity of the CV ratio is greater in dry regimes, and for smaller b values.

2.5 Long-term Variability of Vegetation Water Use

The analysis carried out so far, is based on the probabilistic characterization of daily streamflow. In this section, the effect of the intra-annual variability of the interactions between rainfall, soil moisture, and soil water-losses, on the inter-annual (between years) variability of water balance is investigated. In particular it is examined how rainfall daily fluctuation affects the annual vegetation water use.

Debate over controls on inter-annual variability of water balance, and on the role of vegetation, was recently rekindled by *Troch et al.* [2009], who re-examined Robert E. Horton's discussion of inter-annual variability in the Delaware River [*Horton*, 1933]. Horton's classic work focused on the role of vegetation in controlling the capacity of the soil to store infiltrated water and to evaporate it in return. In particular, the ratio of actual evapotranspiration (precipitation minus total streamflow) to catchment wetting (precipitation minus quick runoff) during the growing season was analyzed. Horton showed that this ratio is very stable from year to year, despite the large inter-annual variability of the seasonal precipitation. On the basis of this evidence Horton hypothesized that the natural vegetation of a region tends to develop to such an extent that it can utilize the largest possible proportion of the available soil moisture supplied by infiltration (*Horton*, 1933, p. 456).

In their recent work *Troch et al.* [2009] re-examined this ratio, which they called the Horton index, along with analyses of vegetation water use efficiency, for about 100 catchments across the United States. They too found a low inter-annual variability of the Horton index exhibited in these 100 catchments, and concurred with Horton that the relative constancy of the Horton index may be a signature of the adaptation of vegetation to variations in water availability.

In this section, it is developed a stochastic model of the annual partitioning of plant available water into vaporization and subsurface runoff. In particular, the model analytically integrates the daily variability of catchment water partitioning to the annual scale, in order to explore the effect of the short-term climatic forcing variability on the long-term catchment response.

This simple modeling approach is used within a top-down framework [*Klemes*, 1983; *Sivapalan et al.*, 2003] to highlight the main physical controls on the inter-annual variability of catchment water balance, i.e., climate (i.e. rainfall and potential evapotranspiration) and soil properties (i.e. soil storage capacity), and through comparisons with observed catchment responses to isolate possible effects of seasonality and associated vegetation adaptations. In this sense, the role of vegetation in the model is minimized in order to keep physical processes separated from biological processes. The only source of intra-annual variability in the model is the stochastic nature of daily rainfall and no seasonal variation in the drivers (e.g., radiation, temperature, leaf area index) is considered. Model predictions are compared with observed data in 431 catchments across the continental US. Through a sensitivity analysis with respect to the physical controls and by analyzing the residuals between model results and observed data, the following hypotheses are to be tested: 1) climate is the main control on the inter-annual variability of water balance whereas landscape constitutes a minor control; 2) the apparently damped variability in the Horton index between years is mainly attributable to physical filtering processes; 3) daily variability of catchment wetting is sufficient to explain inter-annual variability of catchment water balance. While the first hypothesis aims to assess the relative importance of climate and physical controls in different catchments, the second and third represent broader questions. In particular, in those sites where the second hypothesis is rejected the observed damping effect may be due to biological processes or other physical processes that are not considered by the model. On the other hand, when the third hypothesis is rejected other sources of variability need to be taken into account, such as, for example, relative seasonality of rainfall and evapotranspiration.

Within this top-down framework, inadequate model predictions, when they occur, are not to be considered as failures of the model, but rather as indicators of the strength of other controls that are left out. In other words, the main question is not '*how well the inter-annual variability of catchment water balance can be predicted?*' But rather '*what is it that controls the inter-annual variability of catchment water balance?*' And, '*how do these controls change across different catchments?*' Answering these questions in the context of a large number of catchments across continental US will eventually lead to improved and parsimonious models of catchment response to long-term climate variability and change.

2.5.1 Probability Distribution of the Horton Index

The conceptual framework used in this paper is based on the definition of the Horton index given by *Troch et al.*, [2009], and expressed as follows:

$$H = \frac{V}{V+U}. \tag{2.33}$$

where V is water vaporization through soil evaporation, interception and plant transpiration, and U is slow flow (or baseflow), $V + U = W$ is known as catchment wetting, which represents the water potentially available for vaporization. At the catchment scale, V and W can be estimated from measured annual precipitation (P) and streamflow (R). In order to compute the catchment wetting the streamflow needs to be separated into rapid runoff (S) and baseflow (U) using a baseflow separation algorithm *Troch et al.* [2009].

Vaporization and baseflow production mechanisms at the catchment scale are mostly controlled by soil moisture dynamics and driven by the temporal variability of rainfall processes, which affect the water balance in the active topsoil layer. In order to achieve a steady-state probabilistic characterization of the Horton index we first derive an analytical expression for the variability of U.

To model rainfall partitioning at the daily scale, the framework introduced in Section **??** is followed [*Botter et al.*, 2007]. Such approach, in order to achieve an exact mathematical solution, neglects the fraction of daily effective rainfall propagating as surface runoff, focusing on deep infiltration dynamics. This, in other words, implies that the occasional surface runoff events triggered by saturation excess, are still considered as part of the wetting by the model, however, Monte Carlo simulations show that the mean daily wetting depth may be well approximated by the mean daily rainfall depth. On this basis, daily wetting is modeled as a Poisson process with rate λ_p and wetting depths are assumed to be exponentially distributed with parameter γ_p. Effective rainfall, or drainage, is still assumed to be a Poisson process with rate λ and depths exponentially distributed with parameter γ_p.

The Horton index is the ratio of an integrated (in time) vaporization amount to an integrated soil wetting amount (i.e. the sum of vaporization and baseflow). Since the aim of this work is to analyze the inter-annual variability of the annual Horton index, it is necessary to advance from the daily time-scale, at which the soil moisture dynamics as well as the drainage production are described, to the annual time-scale.

Let us first compute the distribution of the annual baseflow, U, from the distribution of daily effective rainfall, Y, which by hypothesis is exponential: $p_Y(Y) = \gamma_p exp[-\gamma_p Y]$. In analogy with the work done by *Thompson* [1984] on monthly rainfall totals, given a fixed total, μ, of effective rainfall events occurring in a year, the conditional probability density function of the yearly baseflow is given by the μ^{th} convolution of $p_Y(Y)$:

$$p_U(U|\mu) = \frac{U^{\mu-1}\left(\frac{1}{\gamma_p}\right)^{-\mu} e^{-U\gamma_p}}{\Gamma(\mu)}. \tag{2.34}$$

The probability of yearly baseflow totals is then obtained by multiplying the conditional probability, $p_U(U|\mu)$, by the probability of μ events occurring in the time period L, and summing the product

from $\mu = 0$ to $\mu = \infty$. Because the drainage events are assumed to be Poissonian, the distribution of the number of events in a year is Poissonian with rate $L\lambda$.

$$p_U(U) = \sum_{\mu=1}^{\infty} p_U(U|\mu) \cdot P_\lambda(\mu) = \frac{\sqrt{L\lambda\gamma_p} e^{-L\lambda - U\gamma_p} I_1\left(2\sqrt{U\gamma_p L\lambda}\right)}{\sqrt{U}} + e^{-\lambda L}\delta(U), \tag{2.35}$$

where, by definition, $P_\lambda(\mu)$ is the Poisson distribution of rate λ, L is the temporal interval in which we are computing the total baseflow (i.e. 365 days), $\delta(\cdot)$ is the Dirac delta function, and I_1 is the modified Bessel function of the first kind. The delta function accounts for the case where baseflow is zero.

In order to derive a full probabilistic model of the Horton index (eq. **??**), it would be necessary to take into account the variability in the vaporization V, including its probable co-variance with U. However doing so poses serious mathematical difficulties. We will therefore assume that the annual vaporization at a catchment scale does not change from year to year. This assumption postulates that annual vaporization is a second order control on the inter-annual variability of the Horton index, relative to the annual baseflow, which is assumed to be the first order control. In this way we neglect the effect of long term vegetation variability on the annual water balance variability. This assumption is consistent with *Oishi et al.* [2010], who also provide an explanation for the observed conservation of annual vaporization.

On the basis of the conceptual framework proposed by *Rodriguez-Iturbe et al.* [1999], *Porporato et al.* [2004] provides an analytical expression of the mean daily evapotranspiration rate, $< ET >$, which is a function of the soil moisture dynamics and the rainfall process:

$$< ET >= PET \frac{1}{\eta\gamma_s}(\lambda_p - Ne^{-\gamma_s}), \tag{2.36}$$

where

$$N = \frac{\eta\gamma_s^{\frac{\lambda_p}{\eta}}}{\Gamma(\lambda_p/\eta) - \Gamma(\lambda_p/\eta, \gamma_s)}, \tag{2.37}$$

where $\gamma_s = nZ_r(s_1 - s_w)$ is the so called storage index and $\eta = PET/(nZr(s_1 - s_w))$ is the normalized maximum evapotranspiration rate. Mean annual vaporization is then computed as follows:

$$V = L < ET > . \tag{2.38}$$

The pdf of the Horton index, $p_{HI}(H)$ can now be derived from the pdf of the annual baseflow, $p_U(U)$:

$$p_{HI}(H) = p_U(U(H)) \left|\frac{dU}{dH}\right|, \tag{2.39}$$

where, from equation **??**, $U(H) = (V - VH)/H$. Given equation **??**, the pdf of the Horton index is expressed as follows [*Zanardo et al.*, 2011a, *in review*]:

$$p_{HI}(H) = \frac{V}{H^2}\left(e^{-L\lambda}\delta\left(\left(H-1\right)V\right) + \frac{\sqrt{L\lambda\gamma_p}e^{\frac{(H-1)V\gamma_p}{H}-L\lambda}I_1\left(2\sqrt{L\lambda\gamma_p}\sqrt{\left(\frac{1}{H}-1\right)V}\right)}{\sqrt{\left(\frac{1}{H}-1\right)V}}\right), \quad (2.40)$$

where V is given by equation **??**.

2.5.2 Moments of the Horton Index

An exact analytical expression for the moments of H could not be found, however it was possible to derive approximate analytical expressions using the Taylor series. It will be shown later in the section that this approximation is very accurate for the physical domain under consideration.
The moments of H are here obtained by means of a Taylor series expansion of the function $H(U)$ (Eq. **??**) around the mean of U, and the moments of U, which can be derived analytically from our conceptualization. The approximated mean, $\widetilde{H}$, and variance, $\widetilde{Var}(H)$, of H are then given by the following equations:

$$\widetilde{H} = H(\overline{U}) + \frac{Var(U)}{2}\left(\frac{d^2H}{dU^2}\right)\Bigg|_{\overline{U}}, \quad (2.41)$$

$$\widetilde{Var}(H) = Var(U)\left(\frac{dH}{dU}\right)^2\Bigg|_{\overline{U}}; \quad (2.42)$$

where $\overline{U}$ and $Var(U)$ are, respectively, the analytical mean and the analytical variance of baseflow, which may be expressed as follows:

$$\overline{U} = \frac{L\lambda}{\gamma_p}, \quad (2.43)$$

$$Var(U) = \frac{L\lambda\left(4 - e^{-L\lambda}L\lambda\right)}{2\gamma_p^2}. \quad (2.44)$$

The approximated mean and variance of H computed from Eq. (**??**) and (**??**)) are then [*Zanardo et al.*, 2011a, *in review*]:

$$\widetilde{H} = \frac{V}{V + \frac{L\lambda}{\gamma_p}} + \frac{L\lambda\left(4 - e^{-L\lambda}L\lambda\right)V}{2\gamma_p^2\left(V + \frac{L\lambda}{\gamma_p}\right)^3}, \quad (2.45)$$

$$\widetilde{Var}(H) = \frac{LV^2\lambda\left(4 - e^{-L\lambda}L\lambda\right)}{2\gamma_p^2\left(V + \frac{L\lambda}{\gamma_p}\right)^4}. \quad (2.46)$$

In order to evaluate the accuracy of this approximation we express the approximated mean and variance and the pdf of H in terms of two, dimensionless variables: 1) $\Sigma' = L\lambda$ and 2) $\psi = L\left\langle ET\right\rangle\gamma_p$. The former represents the mean number of drainage events during the year, and the

latter is the ratio of the mean actual evapotranspiration rate to the mean daily rainfall, multiplied by L. Σ' is limited by 0 and the mean number of rainfall events, $L\lambda_p$, whereas ψ is limited by 0 and 365 since the actual evapotranspiration cannot be larger than precipitation. Such ranges define the domain in which the accuracy of the Taylor series approximation has to be verified.
The relative error on the mean of H is defined as the absolute value of the difference between the approximate mean and the exact mean (obtained via numerical integration of the pdf of H), divided by the exact mean. The relative error on the variance of H is calculated in a similar way. Figure **??** shows the relative errors of the approximation on the mean (**??***a*) and on the variance (**??***b*) of H in the domain of interest. The approximation is indeed very good suggesting that the mean and the variance of H defined by equations **??** and **??** can be used instead of the exact analytical expressions.

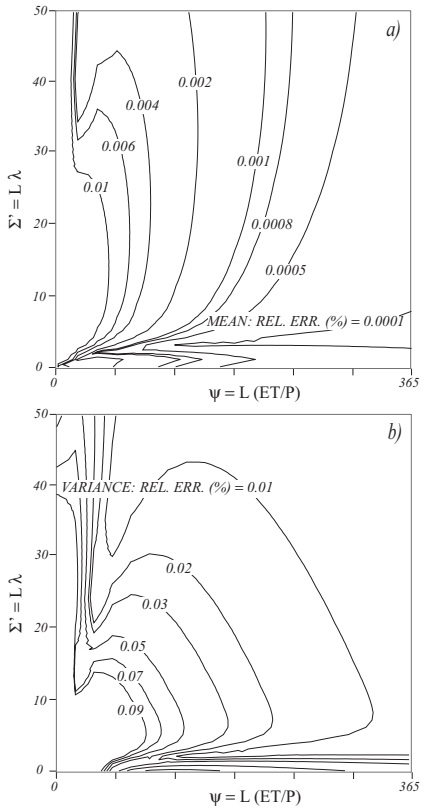

Figure 2.14: Relative errors of the approximated mean (a) and variance (b) of H computed with the the Taylor approximation.

The mean and variance of H may be expressed as functions of three dimensionless variables: 1) the humidity index, ϕ, defined as the ratio of precipitation to potential evapotranspiration; 2) the storage index, γ_s, defined as the ratio of the storage capacity ($nZ_r(s_1 - s_w)$) of the soil to the mean

precipitation; 3) the mean amount of storm events in the time period of interest, Σ ($= \lambda_p L$):

$$\widetilde{H} = \frac{1}{2N_1\gamma_s\Sigma}e^{-\gamma_s}\left(1-\frac{e^{-\gamma_s}N_2}{N_1}\right)\left(\left(4-\frac{e^{-\gamma_s-\frac{e^{-\gamma_s}N_2\Sigma}{N_1}}N_2\Sigma}{N_1}\right)\gamma_s^{\gamma_s\phi}+2e^{\gamma_s}N_1\Sigma\gamma_s\right); \tag{2.47}$$

$$\widetilde{Var}(H) = \frac{1}{2N_1^4\Sigma}e^{-4\gamma_s-\frac{e^{-\gamma_s}N_2\Sigma}{N_1}}\gamma_s^{\gamma_s\phi-4}\left(\gamma_s^{\gamma_s\phi}-e^{\gamma_s}N_1\gamma_s\right)^2\left(\gamma_s^{\gamma_s\phi}\Sigma-4e^{\gamma_s+\frac{e^{-\gamma_s}N_2\Sigma}{N_1}}N_1\gamma_s\right), \tag{2.48}$$

where

$$N_1 = \phi(\Gamma(\gamma_s\phi)-\Gamma(\gamma_s\phi,\gamma_s)), \tag{2.49}$$

$$N_2 = \gamma_s^{\gamma_s\phi-1}. \tag{2.50}$$

Let us notice that ϕ and Σ are pure climate indicators, representing the competition between energy and water availability and the frequency of storms event respectively, whereas the capacity ratio embeds a landscape as well as climate component.
In Figure **??** we show how mean (a) and standard deviation (b) of the Horton index vary with ϕ and γ_s whereas in Figure **??** the control of ϕ and Σ on the mean (a) and the standard deviation (b) is explored. Figure **??** is drawn assuming $\Sigma = 20$, whereas in figure **??** we assume $\gamma_s = 7$.
Figures **??***a* and **??***a* show that the major control on mean H is the humidity index, which is in agreement with the previous analysis on actual data made by *Troch et al.* [2009]. It may also be observed that the dependence of mean H on the storage index γ_s decreases with the humidity of the site; in other words, the capacity of the catchment to store water has more impact on the water balance in water limited climates than in energy limited climates. In particular, when the soil water storage is small, the annual water balance in both arid and humid sites reflects the behavior of energy limited systems. Nevertheless, soil water capacity has a relevant effect only for small values of the storage index ($\sim \gamma_s < 3$). The opposite behavior is observed in Figure **??***a*, relatively to the number of storm events, as its control on mean H increases with the humidity index and, in particular, the mean of H decreases with Σ increasing. As a matter of fact, even though high values of humidity index usually characterize humid sites, when the total rainfall is confined to a small number of events the environment is water limited and the Horton index tends to one. However, this effect is limited to very small values of Σ ($\sim \Sigma < 3$) and for greater values H does not depend on this parameter.
Figure **??***b* and **??***b* give some insight into the variability of the Horton index, showing its standard deviation as a function of ϕ, γ_s and Σ. Interestingly, as opposed to the mean plot, the standard deviation plot is not monotonic but there is a maximum line that divides the region of interest into two zones. Moving from the left side of the plot and gradually increasing the humidity index produces a relatively steep increase in the variability of H until the maximum is reached, after that point the variability slightly decreases. Let us focus for a moment on the region of the graph where γ_s is greater than $2-2.5$, we observe that the line of maximum variability approximately lays over the $\phi = 1$ line. This suggests that those situations in which the water availability approximately equals the atmospheric demand represent a sort of critical point for the water balance, which produces the highest variability in the vegetation water use. This conclusion is in agreement with other

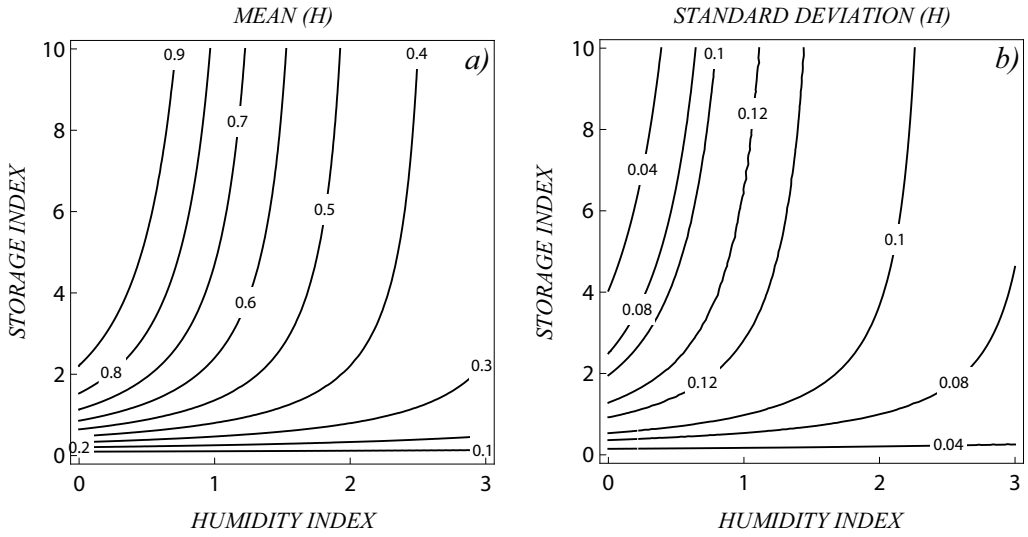

Figure 2.15: Sensitivity analysis on the climate and the physical controls on the Horton index. Mean (a) and standard deviation (b) of the Horton index as functions of humidity index ($\phi = P/(L\,PET)$) and storage index ($\gamma_s = \gamma_p n Z_r (s_1 - s_w)$).

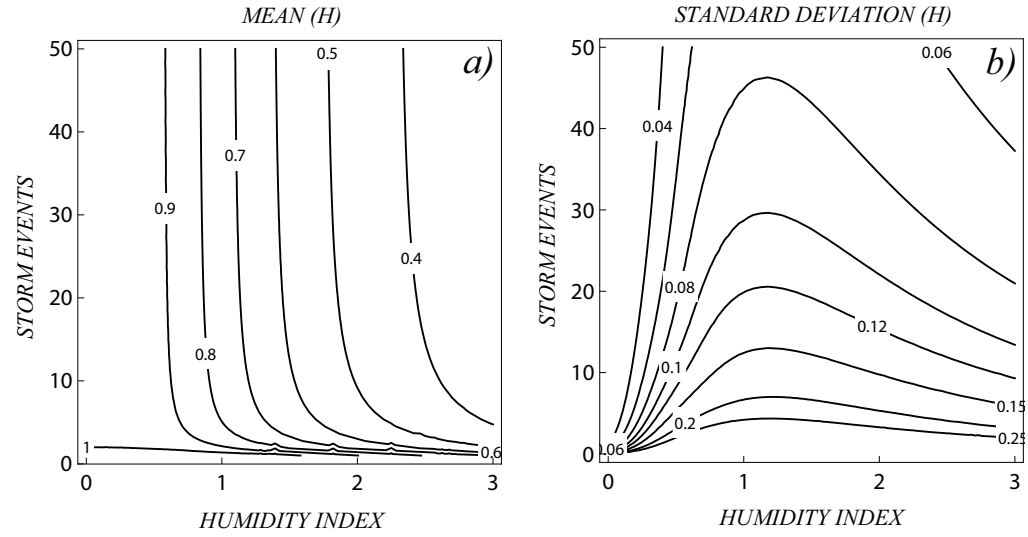

Figure 2.16: Sensitivity analysis on the climate and the physical controls on the Horton index. sensitivity analysis. Mean (a) and standard deviation (b) of the Horton index as functions of humidity index ($\phi = P/(L\,PET)$) and mean number of storm events ($\Sigma = \lambda_p L$).

researchers who have found that stochastic soil moisture dynamics show high levels of variability in intermediate climates, producing intriguing behavior such as temporal clustering of macro-pore initiation [*McGrath et al.*, 2007] and unconstrained optimal rooting depths [*Guswa*, 2008]. As γ_s increases the maximum of variability moves towards slightly higher values of ϕ. Let us now consider the lower part of the graph, as γ_s decreases the maximum variability line bends away from the $\phi = 1$ vertical intercept, towards the $\gamma_s = 1$ horizontal intercept. As with the mean, when humidity is low the main control on the variability of H is the storage index. The maximum variability occurs along the critical line $\gamma_s = 1$, implying that, as the atmospheric demand becomes larger than the water availability, the variability of vegetation water-use reaches a maximum when the soil storage capacity equals the mean rainfall depth. These observations suggest that the values $\phi = 1$ and $\gamma_s = 1$ constitute critical translations in the competition between process controls on inter-annual variability of water balance.

Figure **??***b* represents the dependence of standard deviation of H on Σ and ϕ, assuming $\gamma_s = 7$. The graph shows that in arid sites the variability of H is driven by ϕ unless the number of events is very small (< 10). As ϕ increases the number of rainfall events becomes a more important factor for the variability of H. Overall, high frequency precipitations produce stability in the annual water balance, even though for each value of Σ the water balance may be more or less variable depending on the mutual relationship between ϕ and γ_s.

Overall, Figure **??** and **??** are in agreement with the previous findings of *Troch et al.* [2009] and *Huxman et al.* [2004], as (1) the Horton index increases as water availability decreases, whereas (2) its inter-annual variability decreases and (3) the catchment-scale vegetation water use efficiency converges to a maximum value. To these findings, the present analysis also adds that rainfall frequency does not have a relevant effect on the annual vegetation water-use whereas the storage capacity does have an effect on both mean annual vegetation water use and its inter-annual variability in water limited climates. Inter-annual variability, however, is mainly driven by rainfall frequency and humidity. Figure **??**, is also consistent with one of the results in *Milly* [1993], whose case study showed that an increase in the soil storage capacity yields a smaller change in the water balance than does an equal decrease. Our analysis actually suggests that an increase in γ_s yields a smaller change in the annual water balance and its inter-annual variability, than does an equal decrease. In fact, as γ_s increases, the annual water balance and its inter-annual variability tend to a constant value that is solely driven by climate variability.

2.5.3 Case Study

The theoretical derivations and analysis presented thus far provide a framework for understanding the controls on inter-annual variability of the Horton Index.

The model is now applied to data from the Mopex database (http://www.nws.noaa.gov/oh/mopex, see Figure **??**) of catchments across the United States in order to A) test the validity of the model and B) use it to understand the controls on inter-annual variability of water balance and the damping thereof. The dataset includes approximately 54 years of rainfall and streamflow records, as well as estimates of soil properties (i.e. porosity, field capacity and wilting point), for 431 catchments located across continental USA, belonging to a variety of eco-regions (Figure **??**). The climatic humidity index (i.e. the ratio of precipitation to potential evapotranspiration) spans from

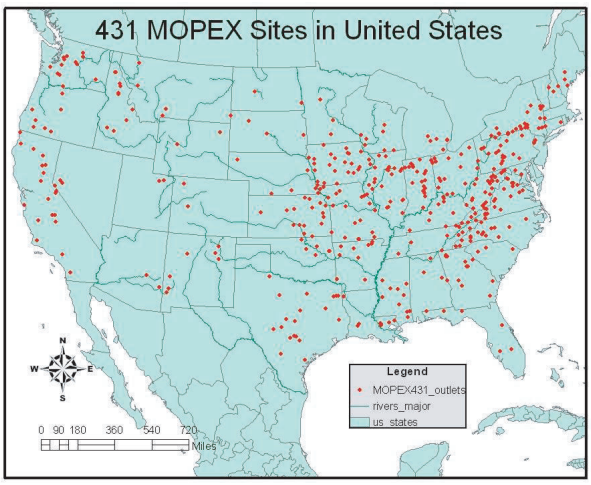

Figure 2.17: Locations of the Mopex sites across the United States.

0.5 to 5 and the drainage areas vary from 66 to 10329 km^2. Potential evaporation climatology for these catchments is available from NOAA's free water evaporation atlas (*Farnsworth et al.*, 1982). Figure **??** represents the mean Horton index for each of the Mopex sites as a function of the humidity index; as it was already observed by *Troch et al.* [2009], the H consistently tends to 1 as the humidity of the sites decreases, whereas H decreases and its variability among sites increases as the humidity increases.

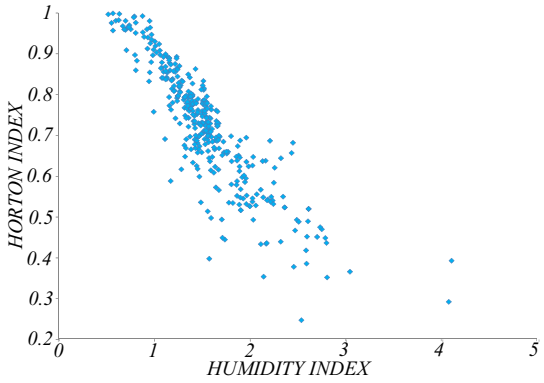

Figure 2.18: Mean Horton index for each of the Mopex sites as a function of the humidity index of each site.

The model is applied to the Mopex database with no calibration in order to test whether it is able to reproduce observed variations in the mean and variance of the annual Horton Index. For each year of record and for all the 431 sites the annual Horton index was calculated, allowing for the derivation of the inter-annual distribution as well as the mean and the variance of observed H

for each catchment. The parameters used in the model were estimated from the Mopex dataset. The mean frequency, λ_p, and the mean depth, $1/\gamma_p$, of rainfall events are directly computed from the daily rainfall records; the potential evapotranspiration, PET, is obtained from NOAA's free water evaporation atlas; the soil properties are all available within the Mopex dataset except for the catchment average rooting depth, Z_r. In order to estimate the rooting depth we used the model proposed by *Schenk et al.* [2008], that relates the spatial distribution of rooting depths to long term precipitation and evapotranspiration measurements as well as to soil textures. We computed the distribution of rooting depths for all the Mopex catchments and used, as an effective value for our model, the depths containing 95% (D_{95}) of all roots in the profiles.
As an example, Figure **??**, shows a comparison between the analytical pdf of H derived with the model and the distribution of H computed from the dataset. The red plots represent an arid site whereas the blue ones represent a humid site. A better evaluation of the accuracy of the model can be addressed comparing the observed means and standard deviations of H for all the Mopex sites to the ones calculated with the model (Figure **??**). Observed means of H range approximately from 0.2 to 1, whereas observed standard deviations range from 0.01 to 0.1. As *Horton* [1933] and *Troch et al.* [2009] have already noted with other datasets, the inter-annual variability of H is indeed very low across the MOPEX catchments.

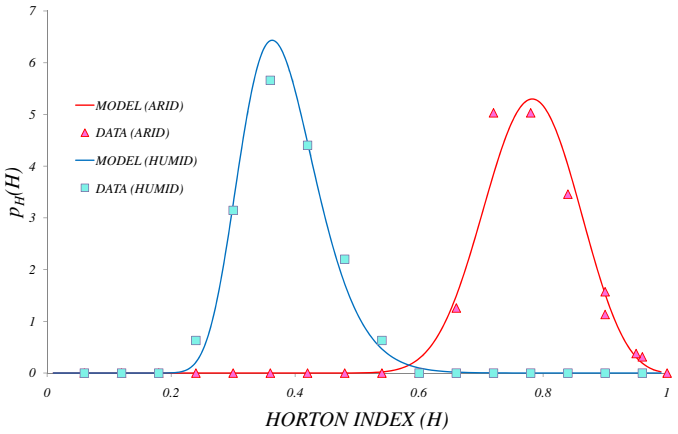

Figure 2.19: Comparison between the probability distribution of the Horton index observed in two sites (arid and humid) of the MOPEX dataset and the respective analytical probability density function (solid line). The humid site is in blue, the arid site is in red.

Figure **??***a* shows a good agreement between data and model output, especially for higher values of mean H, the mean absolute error is 0.09. Figure **??***b* shows that the model predicts the appropriate range of values for the inter-annual variability when the ensemble of catchments is considered, but does a relatively poor job at predicting the standard deviation of a particular catchment; the mean absolute error for the standard deviations is 0.02. We also noticed that there exists a very weak correlation between the errors in predicting the mean of H and the errors in predicting the standard deviation as the coefficient of correlation is +0.32.

A correlation analysis was conducted to find a relation between the magnitude of errors and the physical parameters used. The errors correlated most strongly with the frequency of rainfall (i.e., -0.34 for the means and -0.16 for the standard deviations) and rooting depth (i.e., 0.37 for the means and 0.24 for the standard deviations). This could arise from systematic deviations from the assumed Poissonian nature of the drainage process. In fact, numerical simulations by *Botter et al., [2007]* have shown that when the interarrival time between drainage events is small, the drainage process is more Poissonian. Therefore, the smaller the frequency of rainfall events, the smaller is the frequency of drainage events and the larger are the errors; similarly the larger the storage capacity, the smaller is the frequency of drainage events and the larger the errors. Such values of correlation are probably too weak to provide a satisfying explanation of the observed errors, a broader discussion on model inaccuracies is given later in the chapter.

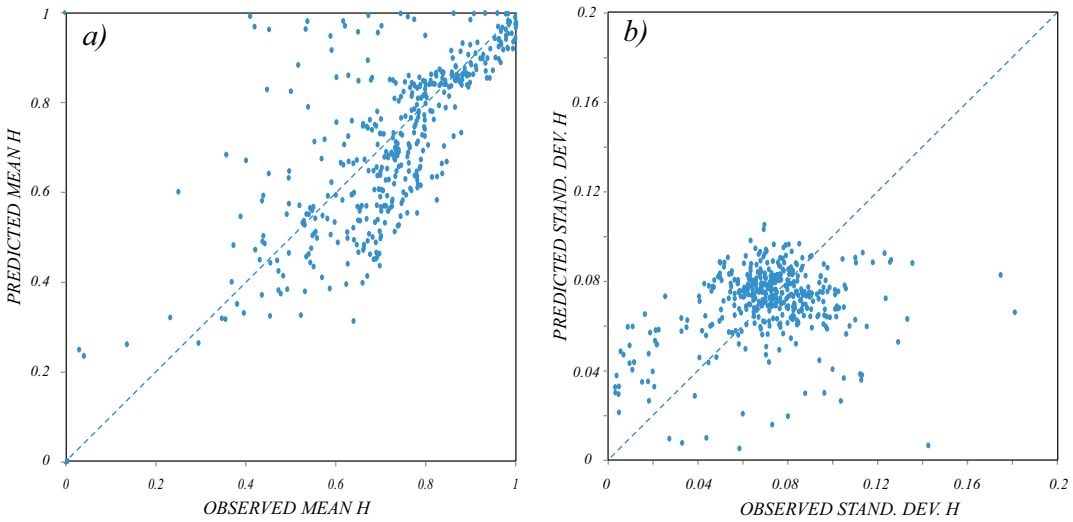

Figure 2.20: Comparison between observed and predicted means (a) of H and observed and predicted standard deviations (b) of H for all the Mopesx sites.

Damping of Variability across Climates

One of the main results presented by *Horton* [1933] is that the inter-annual variability of the Horton index is much smaller than the variability of rainfall, suggesting a damping in the translation of the signal from the forcing precipitation to vegetation water use. *Troch et al.* [2009] show that this damping effect is larger in the driest climates implying that vegetation uses water more efficiently during dry periods.

To explore this damping effect we define the damping index, D_{PH}, as the ratio between the coefficient of variation of the annual precipitation, $CV(P)$, and the coefficient of variation of the Horton index, $CV(H)$. In Figure **??** we plot the damping indexes observed for the Mopex catchments.

The trend confirms the observations made by the previous authors as the damping ratios clearly decrease moving from water-limited climates to energy limited climates. Additionally, a discontinuity between higher and lower values of D_{PH} is observed when the humidity index is equal to 1, suggesting that such value represents a sort of threshold for the damping process between precipitation and vegetation water use.
Here the buffering effect from rainfall to vegetation water use is investigated by means of the analytical model. Assuming that daily rainfall is a marked Poisson process with rainfall depths distributed exponentially, the mean and the variance of the annual precipitation may be expressed as follows:

$$< P >= \frac{\lambda_p L}{\gamma_p} \tag{2.51}$$

$$< P^2 > - < P >^2 = \frac{\lambda_p L(4 - e^{-\lambda_p L}\lambda_p L)}{2\gamma_p^2}, \tag{2.52}$$

where $\lambda_p L$ is the number of storm event in a year, Σ. The coefficient of variation of rainfall is then

$$CV(P) = \frac{\sqrt{\Sigma\,(4 - e^{-\Sigma}\Sigma)}}{\Sigma\sqrt{2}}, \tag{2.53}$$

Note that the expressions for the mean and the standard deviation of annual rainfall (Equations **??**-**??**) are identical to those for the annual drainage except that the drainage frequency, λ, is replaced with the rainfall frequency λ_p. This is because both daily rainfall and daily drainage are assumed to be Poisson processes with exponentially distributed depths, and because losses from evapotranspiration are linearly related to soil moisture.

The damping ratio is obtained from equations **??**-**??** and **??**-**??**, (but is not expressed here for brevity) and can again be expressed as a function of the three dimensionless numbers, ϕ, γ_s, and Σ, considered in the previous section. However, the coefficient of variation of rainfall is just a function of Σ, thus only the frequency of storm events determines the contribution of rainfall variability to the damping ratio.
Figure **??** shows the damping ratio as a function of Σ and γ_s. Figure **??***a*, uses a humidity index equal to 0.5 and Figure **??***b* uses a humidity index equal to 2. Figure **??***a* shows that, in arid sites, the main control on the buffering from precipitation variability to vegetation water-use is the storage index: for $\phi = 0.5$ the variability of annual precipitation can be up to 5 times larger than the variability of H. When γ_s and Σ are small the variability of rainfall is nearly equal to the variability of the Horton index. As humidity increases (Figre **??***b*) the damping ratio decreases considerably and its dependence on both γ_s and Σ decreases.
In conclusion, this analysis suggests that in arid ecosystems the variability of vegetation water-use is more buffered with respect to the variability of precipitation where the active soil depth is deeper. As the humidity of the ecosystem increases the damping effect decreases and the variability of annual vegetation water-use gets closer to the variability of precipitation.

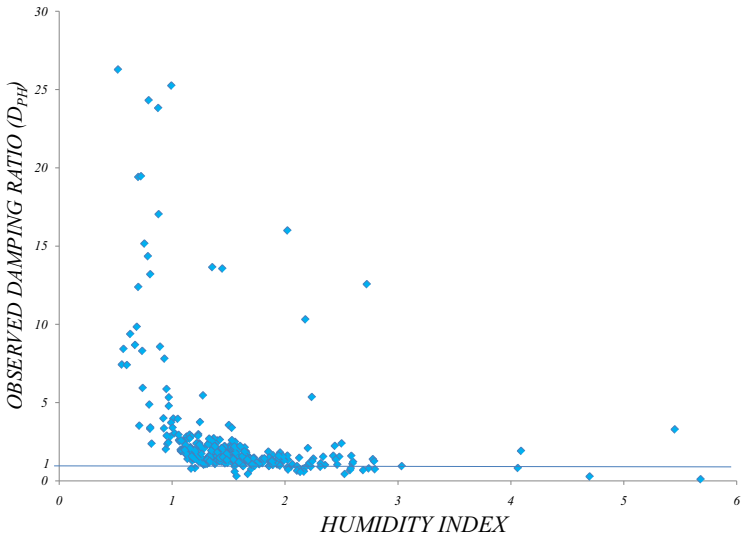

Figure 2.21: Observed damping indexes, D_{PH}, for the Mopex catchments as functions of the humidity index.

Regional Patterns in the Active Soil Layer

Generally, it is very difficult to evaluate a spatial average, or effective, value for all the soil properties, yet such quantities represent necessary parameters for several ecohydrological models (e.g. *Porporato et al.*, [2004], *Botter et al.*, [2008]). In such works, as well as in this paper, all the soil properties are usually embedded in the soil storage capacity, $w_0 = Z_r n(s_1 - s_w)$.
When the mean Horton index is known, we can obtain an estimate of w_0 if we treat it as a calibration parameter for the Horton index model and tune it in order to minimize the deviation of the modeled mean annual H (Eq. **??**) from the observed one.
Figure **??***a* shows that the model, after the calibration of this one parameter, is able to exactly reproduce the observed mean annual H for most cases. For 15 % of the catchments the model is unable to simulate accurately the observed value of H for any storage capacity. These cases have an effectively infinite storage capacity.
The spatial distribution of calibrated w_0's across the U.S. (Figure **??***b*) shows a clear regional pattern. The largest soil capacities are located in the south-eastern part of the U.S., from the Appalachians to Florida. The Midwest and in general the Mississippi river basin show a wide variety of capacity sizes, from $10^{1.5}$ to 10^3 mm, whereas the smallest soil capacities are found in the western part of the country. The black circles represent those catchments where the calibration procedure does not converge to a finite soil storage capacity. Curiously, these catchments are all located in the same region, around the Appalachian chain, where the analysis presented in the previous section showed a consistent underestimation of the mean of H in the model predictions.
Let us recognize that the soil storage capacity that has been calibrated is actually the depth of the 'bucket' that exemplifies the catchment in our conceptualization. It represents an effective, active

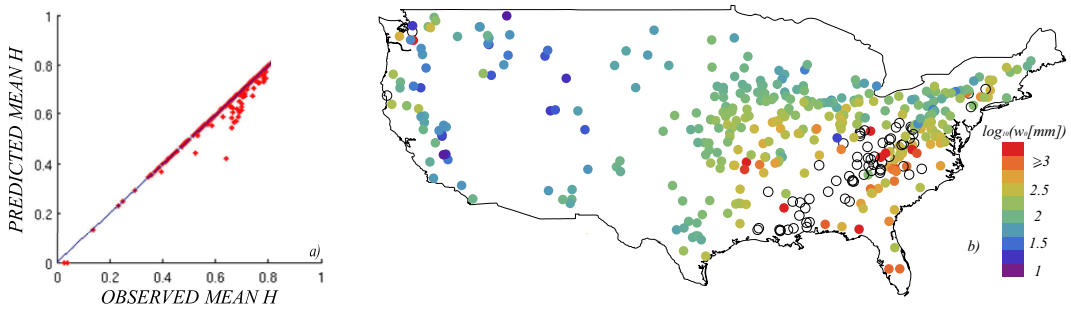

Figure 2.22: Calibration of the soil storage capacity. a) shows the comparison between mean Horton indexes observed at the MOPEX sites and mean Horton indexes predicted after calibrating the soil storage capacity; b) shows the the mean soil storage capacities calibrated in order for the model to reproduce the mean observed Horton indexes. The black circles represent the sites where the calibration procedure did not converge.

soil layer rather than the soil layer actually limited by the average rooting depth, yet the pattern shown in Figure **??***b* suggests that it has a phenomenological (if not physical) basis.
Since it was shown that the Horton index is generally characterized by a very low variability [*Troch et al.*, 2009], few years of annual baseflow and rainfall measurements may be enough to estimate the mean H. Once such estimation is provided the calibration procedure of the model can serve as a tool to estimate the soil storage capacity on the basis of the catchment scale vegetation water-use. This value can be readily used as an input parameter for more detailed models, such as the probabilistic characterization of daily runoffs (*Botter et al.* 2007).
Clearly, this estimate is very rough, as it is based on data averaged over several years (e.g. mean daily rainfall, mean rainfall frequency etc.), which are also subject to uncertainty. Additionally, this value is representative of a whole catchment and necessarily neglects the high geographic variability that may characterize both soil and vegetation. For these reasons such estimates are to be taken as a first order representation of an *'effective'* soil storage capacity that allows to reproduce the long-term vegetation water use.

2.5.4 On the Structure of Residuals between Model Predictions and Data

As pointed out in Section **??**, for some of the catchments the model does not provide accurate predictions for the mean Horton index and for many it poorly predicts its standard deviation. In this section we show that, in many cases, model errors show a spatial or climatic pattern, suggesting that in certain regions (or climates) the model conceptualization well describes the system, whereas in other regions, there exist other controls that need to be taken into account. As the model analytically integrates the daily water partitioning to the annual time-scale, in order to derive the pdf of the annual Horton index, the only source of variability considered is the daily rainfall fluctuation. Therefore, in those sites where the model fails to predict the statistics of the Horton index, there may be other sources of variability that either amplify or damp the variability produced by rainfall.

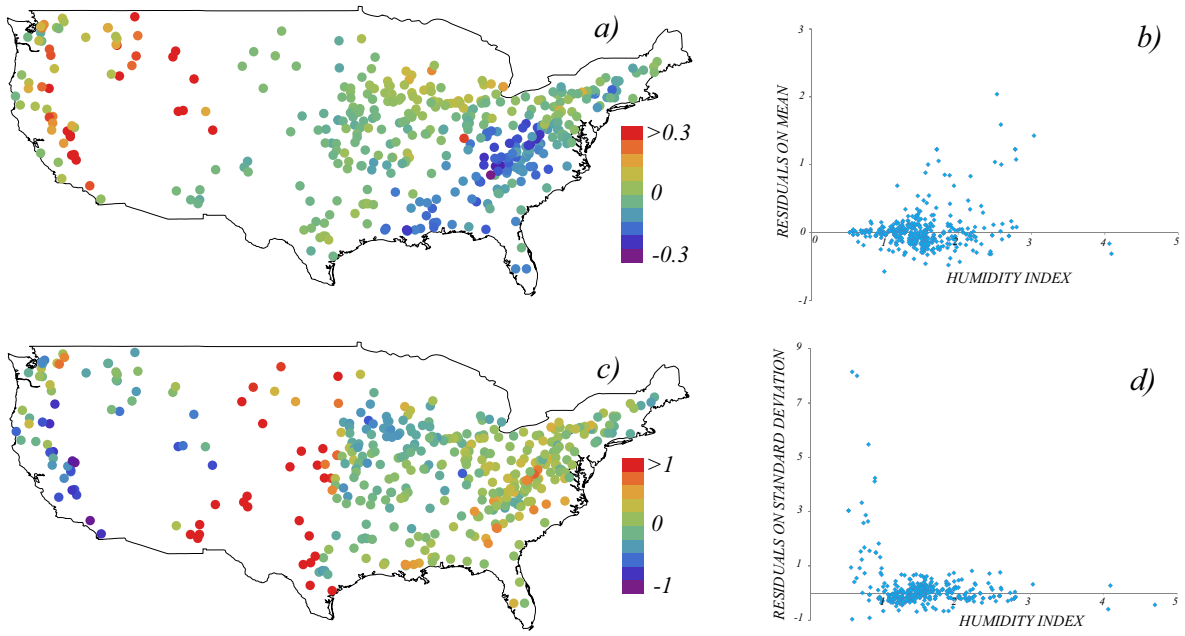

Figure 2.23: Panels a and c show the map of residuals between predicted and observed mean of H (a) and standard deviation of H (c) for the Mopex catchments. In c values are normalized by the observed data. Panel b and d show the residuals between the predicted and observed mean of H (b) and standard deviation of H (d) as functions of the humidity index for the Mopex sites. Positive values ('warm' colors in the maps) characterize predictions higher the measured values. higher than observations.

Figures **??***a* and **??***c* represent the residuals between observed and predicted means and standard deviations of the Horton index, respectively. Since standard deviations are generally very small, we normalize the residuals by observed standard deviation. Positive values of the residuals (*warm* colors) represent an overestimation of the model predictions with respect to the observed data. A clear pattern can be observed in the residuals of the means. In the Eastern parts of the United States, in correspondence to the Appalachian chain, the means of H are overestimated, whereas an overall underestimation is observed in the Western part of United States. Therefore in these regions, the long-term water balance seems to be controlled by factors other than the daily hydrologic partitioning. For example, in the Western United States the El Nino Southern Oscillation (ENSO, *Cayan and Webb*, 1992) is known to play a significant role in the climate of this area. ENSO has a return time of 4-7 years, and wet and dry phases that last from 6 to 18 months (*Barry and Chorley*, 1998), thus constituting a source of variability that is not captured by the model.
The map of standard deviations is more scattered, however some clustering can still be observed. In dry regions, such as Arizona, New Mexico and Texas, an overall over-estimation of the variability of H is observed, suggesting that the damped variability of vegetation water-use in these regions is not attributable to short-term variability. At the other end, two clusters of variability amplification are

observed in the Western U.S. and in parts of the Midwest (i.e., Iowa, Missouri and Illinois). In the Midwest, the analysis may be affected by intensive agricultural managements that have taken place and that obviously is not taken into account by the model. On the other hand, in the Western U.S., this result is unclear and needs further investigation, considering that global sources of inter-annual variability (such as El Nino) are known to play a significant role in this area. In the Eastern part of U.S. the variability of H is generally well predicted, suggesting that in those regions the within year variability of water partitioning is the most important control on the inter-annual variability of water balance.

Figures **??**b and **??**d represent the residuals for the mean and the standard deviation of H (normalized by the observed values) as a function of the humidity index, ϕ. Figure **??**d shows that in water-limited environments the variability of H is over-predicted, whereas, in energy limited sites, the model is generally able to capture the observed values and the accuracy of predictions is more homogeneous (i.e. over- and under-predictions more or less balance each other). Conversely Figure **??**c shows that the mean is well predicted in water limited environments and the magnitude of the errors increases with the humidity of the site. Moreover, residuals on the mean show both negative and positive values implying that, regardless of the humidity of the site, the model may under- or over-estimate the mean of the Horton index.

Overall this suggests that, in water-limited environments, short-term rainfall variability does not constitute the main control on the inter-annual variability of water balance, or, at least it is, smoothed down by other, equally important controls. Therefore, the causes of this damping effect are to be sought among other aspects of the annual water balance. For example, following *Huxman et al.* [2004], this effect may be produced by a long-term selection pressure on vegetation, arising from different ability of species to acclimate to resource variability in water-limited environments. This is also analogous to what is shown in Figure **??**, where data suggest that in arid sites the variability of vegetation water use is much smaller than the variability in annual precipitation and therefore the damping effect is very strong only in water limited environments. When it comes to the mean of H, mean values of climatic variables are good descriptors of the system in water limited environments whereas as the humidity increases their ability to characterize the system decreases. This, in turn, is analogous to Figure **??**, where data show that as the humidity index tends to zero all the catchments' H's tend to one, whereas when the humidity increases the variability of H among the sites increases and, possibly, the humidity index is no longer the most important control for the mean of H.

Chapter 3

Age of Runoff: Inferences from Catchment-scale Studies

This Chapter reports a field experiment on solutes transport where point and non-point source tracers are used: nitrates (NO_3^-) from diffuse agricultural sources and lithium (Li^+) from a point injection. Owing to their chemical and physical properties, nitrates constitute a relatively conservative tracer which travels mostly dissolved in soil moisture and mobile soil water. Nitrate transport may build up remarkably high concentrations of nitrogen in soils and in streamflows, especially in catchments where agricultural practices are significant [e.g., *Botter et al.*, 2006; *Darracq et al.*, 2005; *Darracq and Destouni*, 2007]. Nitrate concentrations in runoff (i.e., streamflow) are generally considered a relevant indicator of water quality in riverine systems for the number of impacts that may be generated [e.g., *Darracq and Destouni*, 2007] and consequently nitrate leaching through runoff has received growing attention from hydrologists and ecologists, leading to a number of coupled experimental and modeling studies [e.g., *Creed et al.*, 1996; *Creed and Band*, 1998a,b; *Evans and Davies*, 1998; *Gupta and Cvetkovic*, 2000, 2002; *Porporato et al.*, 2003; *Lindgren et al.*, 2007; *Darracq et al.*, 2005; *Rinaldo et al.*, 2006b; *Weiler and McDonnell*, 2006; *Botter et al.*, 2006, 2008b; *Darracq and Destouni*, 2007; *Bosch*, 2008]. Nitrate dynamics at the watershed scale is a complex issue, however, and a satisfactory closure is still lacking for several questions like, e.g., the hysteretic nature of dischargeconcentration relationships; the impact of point or non-point source distributions in space and time; the role of catchment topography and geomorphology; the effect of large-scale in-stream denitrification processes [e.g., *Brusseau and Rao*, 1990; *Alexander et al.*, 2000; *Mulholland et al.*, 2008]; and the upscaling of the main biogeochemical and hydrologic processes that control the storage and transport of nutrients, to name a few.

Lithium is a weakly sorbing solute widely employed in tracer studies for its chemical features [e.g., *Packman et al.*, 2000; *Botter et al.*, 2008b]. Its high measurability and the negligible impact on the environment suggest its use in many contexts, particularly in fragile ecosystems. Moreover, transport through heterogeneous soils characterized by relatively small clay contents is only weakly affected by sorption phenomena onto mineral soil components [*Anghel et al.*, 2002]. As the percentage of clay in the experimental catchment does not exceed a few percents, lithium may be safely considered a conservative tracer. One may thus reasonably assume that dispersion is largely

controlled by hydrological processes [*Botter et al.*, 2008b].
During rainfall events, part of the solutes stored in immobile soil moisture mixes with rainfall infiltrating into the soil matrix (the mobile phase) and is eventually transferred to the control section of the transport volumes during runoff events. At catchment scales, a stream network may be seen as a chain of such transport volumes where solutes are mobilized by leaching through runoff. The above processes will be modeled by means of a Mass Response Function (MRF) approach [*Rinaldo and Marani*, 1987; *Rinaldo et al.*, 1989; *Botter et al.*, 2005; *Rinaldo et al.*, 2006a,b; *Botter et al.*, 2006], which is presented in the next section. The main idea underlying the MRF model is that the solute release from hydrologic units comprising soil is largely controlled by the time allowed for the exchange between immobile and mobile phases. This, in turn, is the residence time distribution of water within soil states embedding the individual trajectories of the water particles traveling and exchanging mass [*Rinaldo and Marani*, 1987].
According to the scheme adopted, the various water pulses entering the control volume as rainfall (and, of course, the pre-event water already contained in the control volume at the beginning of the precipitation event) are assumed to be characterized by a different solute concentration, in relation to their different residence time in soil. The mixing between old (pre-event) water, usually characterized by local equilibrium solute concentrations because of residence times much larger than any reaction or mixing time-scales, and new water (i.e., event water pulses infiltrated into soil during the considered precipitation event) may induce dilution of the chemicals stored in soil moisture, or of the solute particles initially contained in precipitation, depending on the boundary conditions of the problem. The overall mixing/dilution effect induced by the interaction between old and new water during runoff events (which proves crucial to determine the chemical response of a catchment) is assumed to result from the interplay of the following two mechanisms:

- the local mixing between pre-event and event water occurring within the control volume. This process is modeled as a reversible mass transfer process controlled by the residence time of water (seen as the contact time between the mobile and immobile phases) and by the difference between the solute concentration in the two phases. The dilution process is affected also by the temporal evolution of the infiltration rate, which determines the mass transfer dynamics;

- the combination/blending among event water particles characterized by different ages. This process takes place when runoff events are produced and originates from the fact that, at any given time, runoff is constituted by a collection of water particles characterized by different ages (i.e., the outflowing water particles have entered the control volume at different times, according to a suitably defined age-distribution. The latter 'blending' process is assumed to be activated by soil moisture contents exceeding field capacity, and embeds in a simplified manner the underlying heterogeneity of velocities and flow paths.

Needless to say, the above schemes of the mixing/dilution between old and new water is a drastic simplification of complex, possibly highly nonlinear dispersion processes. However, theoretical and computational results have suggested that owing to the spatial and temporal scales involved in runoff-driven transport, the simplified scheme depicted above allows to capture the essence of

dilution, mixing and mass transfer processes shaping the residence time distribution of solutes in soils [*Botter et al.*, 2005].

3.1 Hydrological and Biogeochemical Models

The main idea underlying the transport model used is that the evolution of the solute concentration of pre-event water depends only on time t, while the evolution of the event water solute concentration, C, is largely controlled by the residence time of water within soil states (which defines the time available for the mixing between event and pre event water) [*Rinaldo and Marani*, 1987; *Rinaldo et al.*, 1989]. Accordingly, the various water pulses entering the control volume as rainfall are assumed to be characterized by a different solute concentration, in relation to their different residence time in soil (and, possibly, to different initial concentrations in mobile phases $C(0,t)$). As a result, the solute concentration of the infiltrating water moving in the soil $C(\tau,t')$ depends explicitly on two different timescales: the time t' at which the water pulse enters the soil and the residence time τ, which serves as driver of mass exchange through contact between mobile and immobile waters. Note that at any given current time t we have $\tau = t - t'$.
As the pre-event water is seen as an immobile phase, water particles which entered the system during previous rainfall events cannot be mobilized by the rainfall event under consideration. However, in our scheme solute mass contained in the immobile water can be released to mobile waters according to a suitable mass transfer process. In particular, the mixing between 'pre-event' and 'event' waters infiltrating into soil during a precipitation event is assumed to follow a linear (reversible) first-order kinetic controlled solely by the contact time between the mobile and immobile phases $\tau = t - t'$ and the difference between the solute concentration in the two phases [*Botter et al.*, 2005; *Rinaldo et al.*, 2006a]:

$$\frac{\partial C(\tau,t')}{\partial \tau} = k_e[N(\tau + t') - C(\tau,t')] \tag{3.1}$$

where k_e is an effective mass transfer rate between the mobile and the immobile phases. Should the inverse of such rate be small with respect to mean residence time, one would obtain the local equilibrium assumption commonly used in subsurface transport (*Rinaldo and Marani*, 1987). $N(t)$ is updated in the simulations consistently with the solute mass exchanged with the water pulses present in the system. The initial conditions for the mass transfer Eq. (**??**) are specified by the solute concentration in the soilwater system at the beginning of the rainfall event, $N(t = 0)$, and by the initial solute concentration of rainfall pulses, $C(0,t)$. Note that the use of a well mixed immobile concentration $N(t)$ - instead of the corresponding spatially distributed field $N(x,t)$ - proves meaningful when considering transport in heterogeneous environments, particularly in the case of relatively slow mass transfer processes and non-point injections [*Botter et al.*, 2005]. The approximation may be thought of as corresponding to adopting Eq. (**??**) with ensemble (or spatial, under the ergodic assumption) averages of C and N and an effective rate transfer coefficient k_e.
During rainfall events producing runoff, part of the solutes stored in the mobile phase is eventually transferred to the stream network by leaching processes. In order to define the solute mass flux produced by a given runoff event, we need to define a suitable rainfallrunoff model (which defines the streamflows produced at the outlet, $Q(t)$) and the evolution of the resident concentration $C(t',\tau)$

describing the mixing between mobile and immobile water. Both the above ingredients are crucially linked to the underlying residence time distribution, seen as the driver for contact times for mass exchange between mobile and immobile waters.
The hydrological model adopted is a standard one that derives the net rainfall through a mass balance which includes Hortonian and Dunnian infiltration mechanisms and evapotranspiration terms (FAO-Pennman Monteith equation) [*Nicotina et al.*, 2008; *Botter et al.*, 2008a]. Then, following a framework widely employed in the hydrological literature, the outflow is modeled assuming a linear, time invariant response to the net rainfall. Therefore, the discharge at the outlet can be expressed as the integral convolution:

$$Q(t) = A \int_0^t j(t')g(t-t')dt' \tag{3.2}$$

where $j(t)$ is the net rainfall time series, A is the drainage area, and $g(t)$ represents the response of the system to a instantaneous unit input (i.e., the instantaneous unit hydrograph, or IUH). Nonlinearities and time-variant effects induced by the underlying soil moisture dynamics are included into the forcing j, as customary. If all the water particles which exit the system at time t due to a rainfall pulse occurred at time t0 (i.e., $j(t')g(t-t')dt'$) are assumed to have entered the system at time t', they all have the same residence time $\tau = t - t'$. Under the additional assumption that no mixing occurs of waters of different ages, the mass flux at the outlet, $\phi(t)$, can be straightforwardly derived from Eq. (**??**) as:

$$\phi(t) = A \int_0^t j(t')g(t-t')C(t-t',t')dt' \tag{3.3}$$

Eq. (**??**) applies if the water particles composing the net rainfall are assumed to exit the control volume delayed according to an invariant residence time distribution, which is equal to the IUH $g(t)$. More realistically, we can assume that the forcing inputs are able to mobilize, by routing them towards the outlet, water particles already contained within the system, i.e., water particles that may have entered the control volume through precipitation at different times. In this case, the water particles which exit the system at time t forced by the rainfall pulse occurred at time t' (i.e., the flux $j(t')g(t-t'dt')$) are assumed to be characterized by a certain distribution of ages $\omega(x,t)$, i.e., the distribution of the times x at which the fraction of water particles $j(x)g(t-x)$ leaving the soil through runoff at time t have entered the control volume through precipitation. Note that $\omega(x,t)$ is the fraction of water particles leaving the control volume at time t having a residence time equal to $t-x$.
The age distribution depends on the mixing processes that involve water particles with different residence times within the system. Under the above general assumption, the mass flux can be expressed as:

$$\phi(t) = A \int_0^t j(t')g(t-t') \left[\int_0^t \omega(x,t)C(t-x,x)dx \right] dt' \tag{3.4}$$

where the solute concentration of the water particles flowing through the outlet at time t is weighted accordingly to their proper residence times $t-x$. According to what stated previously, the lower limit of integration for the age structure ω is the initial time $t_0 = 0$ of each simulation. Notice that while the age distribution is immaterial for the computation of the discharge (Eq. **??**), it could

strongly affect the mass flux because the residence time is assumed to be one of the main drivers of mixing processes between event and pre-event water. Also notice that the second integral in Equation **??** can be taken out from the first integral and $\phi(t)$ would simply be expressed as the product of the two. However, as it will be shown later in the section, there are cases in which the two integrals cannot be uncoupled, therefore, for consistency, a 'nested' form is used in Equation **??**.

A physically-based Green-Ampt infiltration model is adopted, suitably accounting for evapotranspiration computed through a PenmanMonteith approach [e.g., *Brutsaert*, 2005] into a general soil moisture balance scheme. These schemes allow to identify four different components of streamflow on the basis of the soilwater balance: surface runoff in vegetated soils, $Q_{sur}(t)$ (triggered when the soil becomes saturated or when the precipitation rate exceeds the actual soil infiltration capacity); overland flow in impermeable areas, $Q_{imp}(t)$; interflow, $Q_{int}(t)$, and subsurface flow, $Q_{sub}(t)$, which originate from field capacity exceedance. We shall indicate the effective rainfall series corresponding to the above runoff components as j_{sur}; j_{imp}; j_{int} and j_{sub}, respectively (where $j = j_{sur} + j_{imp} + j_{int} + j_{sub}$ and j_{imp} is proportional to the overall rainfall according to the relative area covered by impermeable surfaces). The overall water discharge can therefore be expressed as:

$$Q(t) = Q_{sur}(t) + Q_{imp}(t) + Q_{int}(t) + Q_{sub}(t) = A \int_0^t [j_{sur}(t') g_{sur}(t-t') + j_{imp}(t') g_{imp}(t-t') + \\ + j_{int}(t') g_{int}(t-t') + j_{sub}(t') g_{sur}(t-t')] dt' \quad (3.5)$$

where the functions g_{sur}, g_{imp}, g_{int}, and g_{sub} are namely the instantaneous unit hydrograph of the surface runoff in permeable vegetated soils, of the overland flow in impermeable areas, of the interflow and of the subsurface flow. For the sake of simplicity we make the additional assumption that all the above IUHs are exponential (and thus defined by a single parameter). Although this hypothesis does not rely on general grounds, we recall that this assumption is often made in studies of subsurface environments [e.g., *Stewart and McDonnell*, 1991; *Brutsaert*, 2005; *Rinaldo et al.*, 2006a,b; *Botter et al.*, 2008a,b; *McGuire et al.*, 2007]. Finally, the overall mass flux at the outlet is modeled as:

$$\phi(t) = \phi_{sur}(t) + \phi_{imp}(t) + \phi_{int}(t) + \phi_{sub}(t) = A \int_0^t [j_{sur}(t') g_{sur}(t-t') C(t-t', t') + \\ + j_{imp}(t') g_{imp}(t-t') \left[\int_0^t \omega(x,t) C(t-x, x) dx \right] + \\ + j_{int}(t') g_{int}(t-t') \left(\int_0^{t'} \omega(x,t) C(t'-x, x) dx \right)] dt' \quad (3.6)$$

Notice that in Eq. (**??**) we assume negligible solute mass exchange between overland flows from impervious areas and the surrounding environment. The latter assumption may be reasonably applied to the chemical species like nitrates, lithium but may be straightforwardly relaxed if at all needed (e.g., when modeling the transport of hydrocarbons from paved surfaces). Moreover we neglect mass exchange processes in the subsurface layer. Indeed, in the last term of Eq. (**??**) the concentration C is evaluated only for $t \leq t'$. In fact, when a subsurface pulse is produced an equal

amount of water is assumed to be instantaneously released from the hydrologically active top soil layer where mass exchange processes are assumed to occur. Therefore, mass exchange processes are supposed to stop when the water flows through the subsurface layer. Finally the residence time distribution of the surface flow is assumed to coincide with the instantaneous unit hydrograph (see the second term of **??**) because blending processes and the soil moisture dynamics that can delay water particles mobilization in this layer are negligible.

3.2 Test Catchment and Experimental Setting

The Piovega Tre Comuni is a small tributary of the Dese catchment, a complex River/drainage system discharging into the Venice Lagoon, north-east Italy (Fig. 1a). The site selected has been already described in several recent hydrologic studies (*Rinaldo et al.*, 2006a,b; *Botter et al.*, 2006, 2007a), where a detailed characterization of the site is provided. The Piovega Tre Comuni watershed

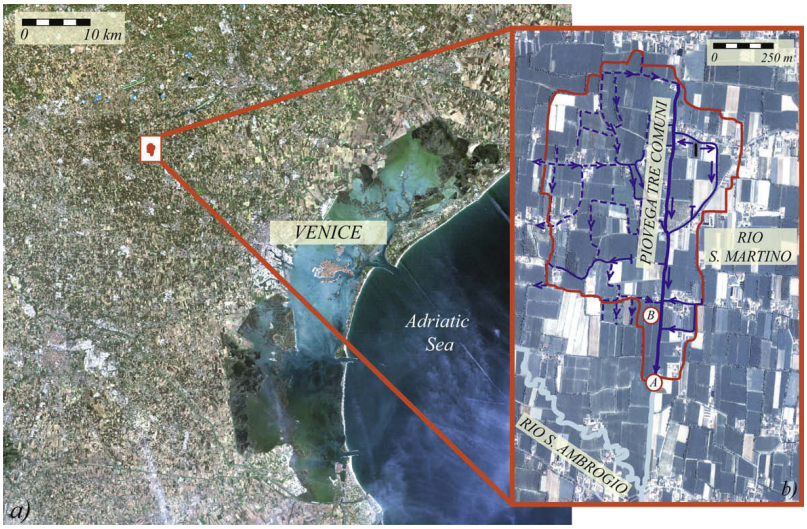

Figure 3.1: Morphologic description of the Piovega Tre Comuni catchment, which is a tributary of the Dese river basin (a flat basin discharging into the lagoon of Venice, North-Eastern Italy (a)). The overall catchment area is about 1 km^2 (b). Land use is rather homogeneous as surfaces are mainly devoted to agricultural uses. The control section selected for the tracer experiment has been chosen at a drop in bottom elevations in the main channel, located approximately 300 meters upstream of the confluence with the Rio S. Ambrogio stream. The drainage area at the chosen outlet is 0.7 km^2.

is mainly devoted to agricultural uses (e.g., wheat, maize and alfalfa), and is characterized by a moderate (10%) presence of urban, impermeable areas (chiefly houses, roads and farms) (Fig. **??**b). The drainage network is composed of a main straight channel and several smaller channels, partially dry during the dry season (Fig. **??**b). The control section selected corresponds to a drop in bottom elevation located along the main channel, 300 m upstream of the confluence of the Piovega Tre

Comuni with the Rio S. Ambrogio stream (Section A in Fig. **??**b). The drainage area at the selected outlet is 0.7 km^2. An important flow component is represented by the flow component resulting from the interception of deep groundwater operated by the farmers (thus poorly related to the soilwater dynamics occurring in the upper soil layer). This will be denoted in what follows as baseflow, Q_b, even though in the literature the latter term usually refers to the slow components of the hydrologic response. Q_b shows a moderate seasonal and inter-annual variability (at least at the temporal scales investigated) with values weakly fluctuating around 85 L/s.

Due to extensive agricultural and farming activities, high levels of dissolved nutrients (e.g., nitrates, ammonia and phosphates) have been detected in the drainage waters since the seventies. As a consequence, enhanced eutrophication and algal blooms are frequently observed, especially during spring and late summer (e.g., *Botter et al.*, 2006).

The point injection of lithium chloride was conducted within a small hillslope (about 1 ha) directly drained by the main channel of the Piovega Tre Comuni (area B in Fig. **??**b). The site is a private crop field where, e.g., alfalfa and radicchio (Chicorium intybus) is grown, and is characterized by a gentle slope (3°) toward the main drainage channel (see Fig. **??**b). The channel banks are vegetated and quite steep, with average slope of 45°.

A rough geo-pedological characterization of the site was achieved by means of several soil cores, which were sampled and analyzed. The stratigraphy was found to be weakly variable in space (i.e., from drill to drill), with a superficial horizon of unconsolidated loam (0-70 cm), and a deep horizon of consolidated silty loam (70-200 cm). Negligible fractions of clay were detected in all the soil samples examined.

The free surface of the water table in hydraulic contact with the main drainage channel was found at an average depth of about 200 cm. Hence, the upper water table is mostly comprised within the deeper soil horizon.

A continuous tracer experiment was performed in the Piovega Tre Comuni catchment between 01/16 and 02/10, 2008. During the above time window, two subsequent rainfall events has been recorded in the area. A lithium mass of 165 g (M_{inj}) was injected as pre-diluted $LiCl$ within a small area of about 5×4 m^2 located at a distance of about 4 m from the Piovega Tre Comuni main stream (Fig. **??**a) between 3:00 and 4:00 p.m. on January, 16, 2008. The injection was carried out during the first of the two rainfall events recorded. At the moment of the injection, the soil was extremely wet, and in the subsequent hours a series of intense rainfall pulses (leading to an overall depth of 57.6 mm in 48 h) have been recorded.

Stream water was sampled at the outlet (Section A in Fig. **??**b) at variable time steps for 25 days, yielding a total of 206 water samples. Li^+ concentrations were measured through coupled plasma spectrometry (ICP-MS). Each water sample was mixed with argon and heated within a plasma, allowing the ionization of the various elements contained in the water sample (for further details, see *Botter et al.* [2008b]). The relative abundance of each species was then estimated on the basis of the intensity of the micro-currents originating from the ionized elements. The background natural concentration of Li^+, measured before the injection, was $C_b^L = 0.76 \pm 0.03$ $\mu g/L$, whereas the peak concentration observed during the first event was 3.2 $\mu g/L$. The second rainfall event, instead, did not produce a clear response in terms of lithium mass flux, with recorded output concentrations relatively close to the initial background noise. This is probably due to the fact that a large part of

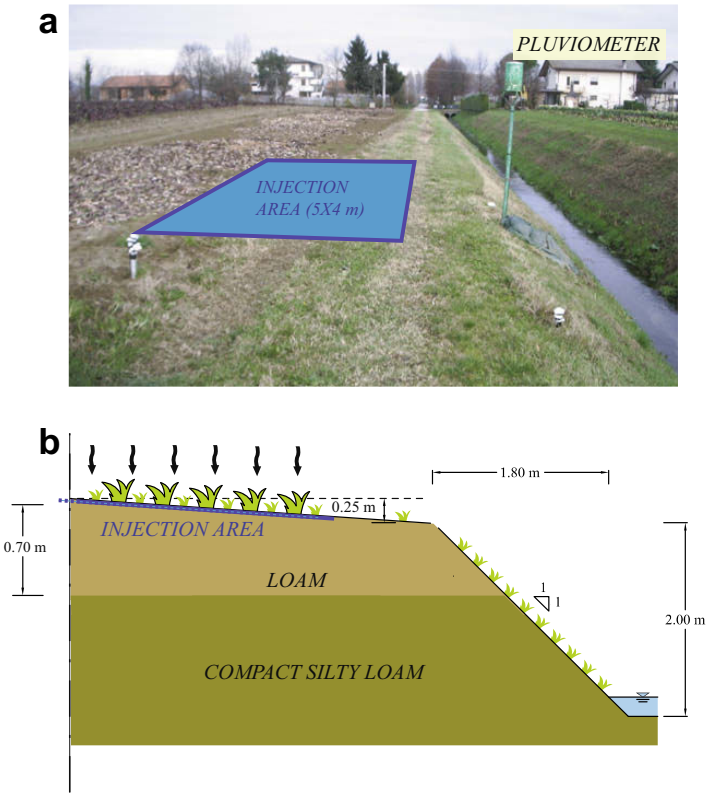

Figure 3.2: Sketch of the experimental unchanneled area chosen for the tracer injection at the Piovega Tre Comuni catchment. The stratigraphy of the soil is roughly sketched in Figure (b).

the lithium mass injected has been effectively leached during the first (and more intense) rainfall event.

Nitrate concentrations in the stream waters was also determined at the same control section in the experiment period by means of spectrophotometry. The samples were refrigerated to 4 $°C$ and then analyzed by means of a copper-coated cadmium column capable of reducing nitrate ion to nitrite. The relative abundance of nitrite ions was then estimated by means of a suitable colorimetric method.

Owing to the widespread and delocalized presence of agricultural activities in the area (see *Botter et al.*, 2008b and Fig. **??**b), nitrates transported through runoff waters can be considered as the product of non-point leaching processes. Observational evidences suggest the presence of high NO_3^- background concentrations in stream waters, with average concentrations of the order of $C_b^N = 12$ mg/L in the period preceding the two events. High nitrate concentrations recorded in stream waters are likely related to continuous, direct nitrogen inputs deriving from fertilizations and/or other farming practices. Rainfall NO_3^- concentrations were also measured during the experiment.

Relatively high nitrate concentration of rainfall ($\approx 4 \pm 0.5\ mg/L$) have been observed probably due to wet deposition of gaseous nitrogen. Rainfall was measured near the outlet (Fig. **??**a) at a relatively high temporal resolution ($\Delta t \approx 1\ min$), and the resulting rainfall depths were then aggregated at hourly time steps. Meanwhile, streamflow rates were estimated on the basis of water level measurements at the outlet (one observation every 5 min), where the presence of a control weir allowed the establishment of a reliable discharge rating curve. Further details about the experimental setup, which was employed for previous tracer studies, can be found in *Botter et al.* (2008b).

3.3 Nitrates and Lithium Mobilization

The aim of this study is a coupled description of solute transport processes acting at different spatial scales: the transport of lithium from the point injection (plot scale experiment); and the transport of nitrates from diffuse sources (catchment scale experiment). In fact, while the area through which Li^+ was injected is of the order of a few square meters, nitrates transported through runoff originate from diffuse fertilizer injections throughout the catchment. In both cases the system is modeled as a single hillslope source state drained by a single channel. However, the two systems have different hydrologic and morphologic characteristics, as outlined below. When modeling nitrate transport, the control volume has been assumed to be delimited by a surface of 0.7 km^2, corresponding to the vegetated fraction (90%) of the catchment, while the contribution to the water and solute discharge due to the presence of impermeable surfaces, has been accounted for separately. The different contributions to the overall discharge originating from the above control volume will be denoted by the superscript C, in order to highlight the fact that these contributions must be evaluated at the scale of the whole catchment. Accordingly, the parameters of the instantaneous hydrograph used to compute such contributions should be intended as basin-scale parameters. The nitrate mass fluxes corresponding to the above contributions are denoted by the superscript N. In this context, the contribution to runoff due to impervious areas, $Q^C_{imp}(t)$, has been calculated by converting the whole rainfall insisting over the impermeable areas of the catchment into effective rainfall, and then convolving the net rainfall pulses with an exponential unit hydrograph (see Section **??**) with an average of 1 h. The contribution of the impervious surfaces to the nitrate mass flux has been instead neglected (i.e., $\phi^C_{imp}(t) = 0$, see *Botter et al.* [2008c]). The overall nitrate flux concentration at the outlet, $C_N(t)$, can be thus computed as follows:

$$C_N(t) = \frac{\phi^N_{int} + \phi^N_{sub} + \phi^N_b}{Q^C_{int} + Q^C_{sub} + Q^C_{imp} + Q^C_b} \tag{3.7}$$

where $\phi^N_b = Q_b C^N_b$ is the nitrate mass flux due to the base flow. Note that in all the cases investigated the water mass balance yields $Q^C_{sur} = \phi^N_{sur} = 0$

In the case of lithium transport, instead, the reference control volume consisted of a plot-scale soil column (with a depth of 0.7 m) delimited by a completely vegetated area of 20 m^2 (roughly corresponding to the injection area, see Fig. **??**). The different contribution to runoff (e.g., subsurface, interflow, etc.) originating from the latter control volume have been labeled by the superscript

P (to highlight the fact that these contribution must be evaluated at the plot scale) and the corresponding mass fluxes will be indicated by the superscript L (meaning lithium fluxes). As the control volume is in this case completely vegetated, we also have: $Q^P_{imp} = \phi^L_{imp} = 0$; moreover, the water balance at the surface in the soil unit previously defined resulted into a zero surface runoff $Q^P_{sur} = \phi^L_{sur} = 0$. The hydrologic effect determined by the interaction of the water particles falling directly over the injection area and the runoff originating from the surrounding sites was implicitly included into the unit hydrograph used, which (at the plot scale) has a different timescale than that used for the whole catchment (see Table **??**). Moreover, the export of lithium due to water particles entering the control volume through lateral interflow or subsurface flows is neglected, because their residence time is arguably much smaller than that of the water particles precipitated directly over the injection region. Under the above simplifications, the lithium flux concentration at the outlet can be calculated as:

$$C_L(t) = \frac{\phi^L_{int} + \phi^L_{sub} + \phi^L_b}{Q^C_{int} + Q^C_{sub} + Q^C_{imp} + Q^C_b} \tag{3.8}$$

where $\phi^L_b = Q_b C^L_b$ b is the lithium mass flux due to the base flow. Note that, in order to model the dilution effect exerted by the discharge originating from the catchment portions external to the injection area, in Eq. (**??**) the first two terms at the numerator are fluxes evaluated at the plot scale, whereas the terms appearing at the denominator are evaluated at the scale of the whole catchment.

Finally, one has to choose a criterion to derive the age distribution of the exiting water particles, i.e., the function $\omega(x)$ in Eq. (**??**). Such criteria may be conceptual or physically-based. In this work, four different modeling options for the age function $\omega(x)$, all equally plausible in principle, were analyzed:

- (a) *Old water first* according to this scheme, the first water particles that leave the control volume when runoff is produced are the oldest available (i.e., the particles that have entered the soil at the earliest times). The age structure ω is chosen by ranking residence ages computationally, and attributing to exiting particles the oldest available residence times within the transport volume. This modeling scheme resembles some kind of piston flow where the new water infiltrating into soil pushes out of the control volume the oldest water particles;

- (b) *Age mixture* (1) when a runoff event is produced, the water particles leaving the control volume are assumed to have a mixture of ages, uniformly sampled among all the ages available in the soil system. Thus, according to this scheme age sampling is taken by keeping roughly the same number of water particles for each available age (i.e., ω is nearly a uniform distribution);

- (c) *Age mixture* (2) when a runoff event is produced, the water particles leaving the control volume are randomly sampled among all the water particles available within the control volume, regardless of their age. Hence, the probability of spilling water particles characterized by a given age at given time, is proportional to the relative fraction of water particles characterized by that age still available in the control volume at that time. As the water amount of the different pulses (characterized by different ages) progressively decreases with time as a result of the flushing operated by runoff events, the highest water amounts are in general

spilled from the pulses characterized by the most recent ages. Hence, preferential flows are accounted for, even though in a simplified way;

- (d) New water first according to this scheme, the water particles most recently infiltrated into the soil are the first to leave the control volume as runoff. This scheme computationally selects the rank of ages in inverse order: it emphasizes the effect of macropores and/or preferential flow paths, which may establish a direct, physical linkage between input and output water fluxes.

3.4 Results

3.4.1 Data Interpretation

The complete set of hydrologic and chemical data collected in the experiment period (01/16 - 02/09, 2008), displayed in Fig. **??**, includes rainfall depths, discharge and Li^+/NO_3^- concentrations at the outlet. The recorded cumulative rainfall depth of the first rainfall event was about 81.4 mm, mainly concentrated on January, 16 and 17 (Fig. **??**a). The graphs reported in Fig. **??** highlight the extraordinary intensity of the peakflow produced by the first rainfall event (about 1.6 m^3/s, corresponding to a specific discharge close to 10 mm/h), which also produced a significant increase of Li^+ stream concentrations. The latter peak was observed quite soon after the injection of $LiCl$ leading to a maximum concentration of 3.2 $\mu g/L$ recorded on January, 16 at 5 p.m., about 14 h before the peak of the hydrologic response. It should be noticed, however, that a few hours later the Lithium concentrations showed a rapid and pronounced decrease, in correspondence to the increase of the discharge rate (January, 17 in the morning), followed by a moderate increase during the recession phase of the flood. Three days after injection, stream lithium concentrations decreased to about 0.9 $\mu g/L$, close to the base value observed at the beginning of the experiment. The measured concentration of nitrates originating from catchment-scale non-point sources during the first event exhibits a somewhat different behavior: the peak (38 mg/L) is delayed by about 6 h with respect to the peak of the lithium concentration, and the tail of the breakthrough curve was found to be persistent, with significant releases even 1 week after the rainfall event. Moreover, the collected data suggest that a pronounced decrease of the NO_3^- concentrations was observed during the morning of January, 17 probably due to the dilution effect produced by the peak of the hydrologic response. Note also that during the period from 3 a.m. to 10 a.m. of 01/17, Li^+ and NO_3^- concentrations have not been measured due to a temporary breakdown of the automatic sampler.

A second rainfall event, recorded on 02/02 - 02/09, carried an overall depth of about 45 mm (about 55% of the cumulative rainfall of the first event). The latter event produced a peak flow of about 0.35 m^3/s at the control section corresponding to a specific discharge of about 2 mm/h. In this case a clear response to the observed rainfall event in terms of lithium concentrations was not observed, with measured values fluctuating around those of the base flow. Instead, intense flushing of nitrates originating from catchment-scale sources was measured. A peak concentration of 25.2 mg/L was observed on February, 6 at 9:00 am (with a delay of about 6 h with respect to the peak runoff). Interestingly, the nitrate response showed a second, smoothed peak on February, 5 at 7:00 pm, and

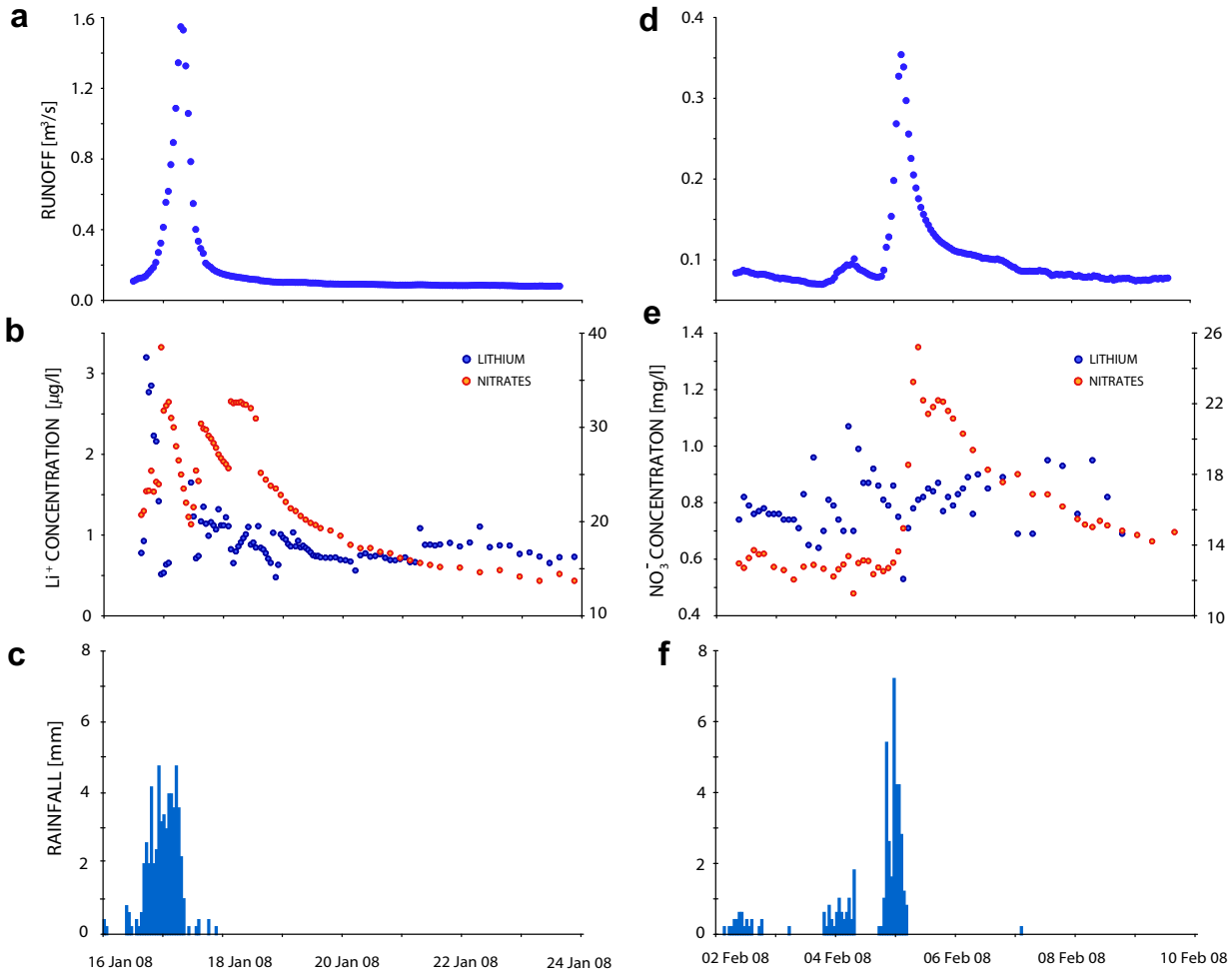

Figure 3.3: Summary of the hydrologic and chemical data recorded during the experiment. The plots on the left side (a-c) focus on the first rainfall event (January 16-24, 2008) while the corresponding right plots (d-f) refer to the second rainfall event (February 2-10, 2008). The graphs show the temporal evolution of streamflows (a) and (d)), lithium and nitrates concentrations at the outlet (b) and (e)) and rainfall depths (c) and (f)).

a persistent tail, with significant releases even 1 week after the rainfall event.
The hydrologic exercise of comparing rainfall intensities with observed and modeled discharges (Fig. **??**) provides insight into the nature of the large peak discharge recorded during the first rainfall event. In particular, for the above event, the actual runoff coefficient resulted to be larger than one. The above fact clearly indicates the presence of runoff sources not explicitly relatable to the rainfall insisting on the source area. These external sources are likely to be represented

by the urban rainwater overflows collected from the nearby village of Scandolara (usually received by the rio Storto channel), which were diverted during the event into the Piovega Tre comuni stream through a by-pass located in the northern part of the catchment. Independent estimates of urban water overflows fluxes proved unreliable and are not reported herein. The same problem was not encountered during the second event, which was less intense and did not activate the by-pass device. Accordingly, the calibration of the hydrologic model during the second event suggests that the performances of the hydrologic model are satisfactory. The magnitude and timing of the main peaks are well captured by the model, which provides estimates of the runoff volumes. The corresponding values of the calibrated parameters (i.e., saturated hydraulic conductivity, porosity, mean residence time for the four runoff components; see Table **??** for a detailed list of all the parameters required by the hydrologic model, which are obtained by calibration) prove rather consistent with those derived independently for a different dataset for the same catchment by *Botter et al.* [2008b].
Conversely, the comparison of the discharges obtained during the first event using the parameters derived by calibration in the second event and the corresponding observed streamflows evidences a marked underestimation of the peak flow and of the runoff volumes during the events. The difference between the curves provides a rough estimate of the runoff contribution diverted from the urban drainage system of the upstream village of Scandolara, $Q_{ext}(t)$. Such external contribution has a measured water volume of 36,000 m^3 and a peak flow of 1.2 m^3/s. As the lithium and nitrate concentration of this contribution are unknown, for simplicity we shall assume a value for the NO_3^- and Li^+ concentration of Q_{ext} respectively equal to the corresponding base flow concentrations. This is tantamount to assuming that during the first event the base flow term Q_b incorporates also the external contribution Q_{ext} and becomes time-variable according to the plot shown in Fig. **??**.
Despite the differences between modeled and observed streamflows during the first event, the results shown in Fig. **??** (and those reported by *Botter et al.* [2008a]) suggest that the calibration performed during the second rainfall event allows for a proper evaluation of the structure of contact times between the mobile and the immobile phase in both the considered events and, in particular, the key timescales of the relevant processes. The calibration of the transport model is relatively simple in this observational context because the hydrologic model is independently calibrated and residence times are seen as contact times between immobile and mobile phases. In particular, when modeling the flushing of NO_3^- , the initial concentration in the rainfall pulses, $C(0,t)$, can be obtained by collecting samples of rainfall during the events. In this case the analysis of the rainfall samples collected suggests that the initial nitrate concentration of the rainfall pulses infiltrating into soil can be assumed to be nearly constant, and roughly equal to 4 mg/L not negligibly small as usually thought of. Hence, three main parameters remain to be calibrated:

- (i) the initial nitrate content in the soil, $N(t = 0)$. The adopted value (Table **??**) suggests that heavy fertilizations occurred in the time period preceding the event. Notice that in long term simulations continuous nitrogen cycling models may serve to update in time the actual soil nitrate content $N(t)$ including biogeochemical processes and the modes of fertilization (e.g., Botter et al., 2006), whereas for event-based simulations one has to treat $N(0)$ as a parameter;

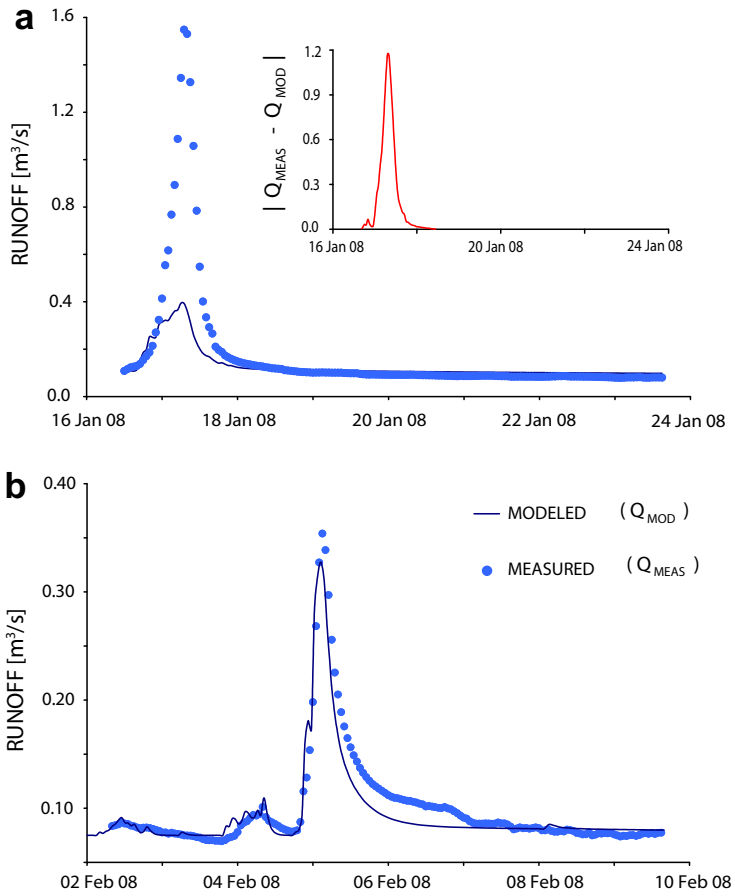

Figure 3.4: Comparison between the computed and measured streamflows during the first (a) and the second (b) period. Also shown is the absolute value of the difference between computed and measured streamflows during the first period.

- (ii) the average mass transfer coefficient, α, which determines the mixing rates between pre-event and event water (see Eq. **??**);

- (iii) the denitrification rate accounting for the conversion of NO_3^- into gaseous nitrogen operated by denitrifying bacteria under anoxic conditions (which are typical of groundwater environments). However, in this case the effects of denitrification processes on the overall nitrate response resulted to be weak and concentrated in the tail of the breakthrough curve.

The whole set of parameters used in the model is reported in Table **??**.

3.4.2 Considerations from the Modeling Exercise

Figure **??** shows the comparison between modeled and observed NO_3^- flux concentrations at the outlet between 01/16 and 01/24 (first rainfall event). The modeled nitrate flux concentration, C_N, is computed through Eq. (**??**) adopting the four different schemes (a)-(d) described in Section **??**. The modeled flux concentration are computed by using modeled mass fluxes and measured discharges. Interestingly, three of the four mixing schemes ((a) - (c)) appear to give quite similar results, provided that the initial concentration of nitrates has been suitably calibrated. The only scheme which does not prove suitable to describe the nitrate response of the considered system is the one assuming that the first water particles leaving the control volume through runoff must be the water pulses most recently infiltrated into the soil (scheme (d)). The latter scheme, indeed, is not able to adequately capture the peak nor the timing of the observed NO_3^- response. For the remaining schemes, the agreement between observed and modeled nitrate flux concentrations is good, with the exception of a slight bias appearing during the morning of January 18, when the measured nitrate concentrations show a sudden increase which cannot be related to rainfall forcing and thus is not captured by the model. Such increase in nitrate concentration is likely to be related to point sources related to farming not explicitly included in our modeling scheme. Overall the model response is able to satisfactorily reproduce both the peak of the chemical response of the catchment and the long tail of the breakthrough curve.

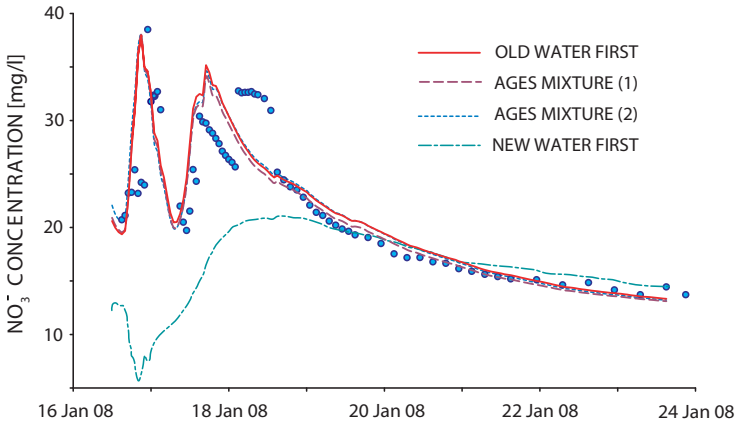

Figure 3.5: Comparison between measured and modeled NO_3^- flux concentrations for the four different ages distribution used (for a complete description see the text). The plot refers to the first rainfall event (January 16-24, 2008). The record of NO_3^- concentration displays two peaks, with a marked minimum located between January 17 and 18. This minimum is correlated to the runoff peak displayed in Fig. **??**a, which is attributed to runoff sources external to the test area, as external sources determine a considerable degree of dilution as emphasized by Eq. **??**. Note that the external sources are only represented by the model implicitly via calibration of the fluxes.

It is worth noticing that, even without a proper calibration of the initial nitrate concentration in the soil system, the three schemes (a) - (c) yield quite similar results, however with simulated peak concentrations that progressively decreases from (a) to (c) (this result has not been shown in Fig.

Table 3.1: Parameters of the hydrologic model used in this study.

Parameters		**Legend**
k_s $[mm/s]$	2.2×10^{-3}	Saturated hydraulic conductivity
nZ_r $[cm]$	36.4	Maximum soil water storage
θ_{FC}	0.2	Initial water content
θ_{WP}	0.2	Soil field capacity
$\theta(0)$	0.15	Wilting point
η	0.3	Fraction of deep infiltration contributing to the interflow response
η'	0.7	Fraction of deep infiltration contributing to the subsurface response
Plot Scale		
T_{imp} $[h]$	0.5	Mean residence time (overland flow)
T_{int} $[h]$	5	Mean residence time (interflow)
T_{sub} $[h]$	80	Mean residence time (subsurface flow)
Plot Scale		
T_{imp} $[h]$	1	Mean residence time (overland flow)
T_{int} $[h]$	6	Mean residence time (interflow)
T_{sub} $[h]$	120	Mean residence time (subsurface flow)

?? for the sake of clarity). This suggests that the specific scheme adopted has a limited impact on the nitrate basin-scale response provided that the scheme adopted allows for runoff to be composed by a sufficiently large amount of old water.

The same considerations can be drawn also by looking at Figure **??**, which shows a comparison between modeled and observed NO_3^- flux concentrations at the outlet for the second recorded event considered in this study (from 02/02 to 02/10, 2008). Also in this case the model reproduces satisfactorily NO_3^- flux concentrations observed at the outlet (cases (a)(c)). Moreover, while after a proper calibration of the initial nitrate concentration the first three schemes provide similar model responses, the last scheme (d) proves once again inadequate to mimic the observed behavior of the flux concentration at the outlet. Note also that the value assumed in these simulations for the nitrate mass stored at the beginning of the event in the soil system is congruent with the simulated value at the end of the simulation of the previous event.

The transport of lithium injected as a tracer during the experiment was modeled using the same model structure adopted for nitrates. Values of model parameters, however, are different to account for the different properties and modes of injection of the two solutes (Table **??**). Qualitatively, the main contribution to the concentration peak is the interflow, while groundwater mainly determines the tail of the breakthrough curve and overland flow does not contribute. Interestingly, the mean temporal response T_{int} of interflow from the point source is not much different than that of non-point sources over the entire the catchment (5 h instead of 6 h), possibly owing to the high drainage density of the catchment.

The simultaneous analysis of the flushing of nitrates and lithium allowed the evaluation of model

Table 3.2: Parameters of the solute transport model for the different rainfall events considered. $N(t=0)$ is the initial nitrate mass stored in the soil system expressed in Kg/ha (the values a, b, c, and d refer to the four mixing schemes examined), α is the mass transfer rate simulating the mixing between event and pre-event water expressed in $1/s$, and M_{inj} (not a calibration parameter) is the lithium mass at the beginning of the different events considered expressed in Kg.

Parameters		16-24 January 08	2-16 February 08	6-15 December 06
Nitrates				
α $[1/s]$		10^{-4}	10^{-4}	10^{-4}
$N(t=0)$ Kg/ha	**a)**	135	48	8.4
	b)	145	53	9.6
	c)	193	96	13
	d)	159	65	7
Lithium				
α $[1/s]$		10^{-4}	10^{-4}	10^{-4}
M_{inj} $[Kg]$		0.165	0.1	0.165

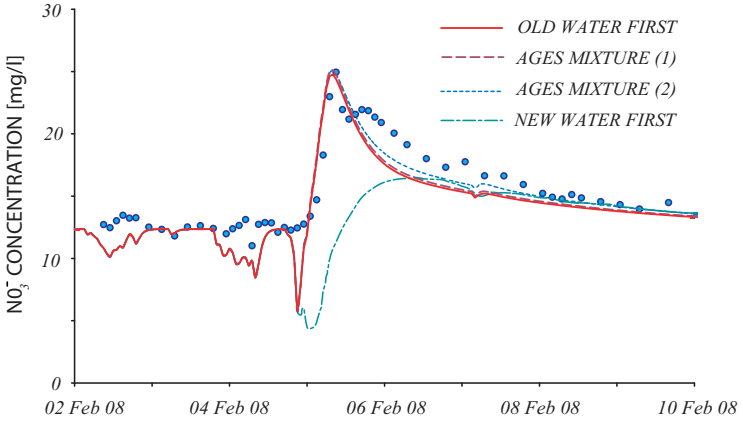

Figure 3.6: Comparison between measured and modeled NO_3^- flux concentrations for the four different ages distribution used (for a complete description see the text). The plot refers to the second rainfall event (February 2-10, 2008).

performance and robustness across different spatial scales. The overall lithium mass introduced into the soil is known (165 g), and it was added to the control volume through the injection of 200 l of aqueous solution of $LiCl$ aspersed over the soil at 3 p.m. of Jan 16. This circumstance has been included in our modeling framework by adding to the observed rainfall sequence a fictitious water pulse at the time of the injection with an overall depth of 200 $l/20$ $m^2 = 10$ mm. The initial lithium concentration of the added pulse is 165 $g/200$ $l = 0.825$ g/l. As we shall see, in this case the initial and boundary conditions are crucial to properly simulate the lithium release from the

plot. Figure **??**a shows the modeled and observed lithium flux responses during the first rainfall event, as inferred from the four age-structure options (a) - (d). The modeled flux concentrations are computed by means of Equation (**??**). The Figure shows that the specific type of age function employed (cases (a) - (d) described before) has a dramatic effect on the lithium concentration in the streamflow at the outlet. As the initial concentration of the water injected into the soil is fixed, in this case the peak value of the breakthrough curve progressively increases and moves leftward as the fraction of new water composing the runoff increases (i.e., varying the mixing and spilling schemes from (a) to (d)). In particular, Fig. **??**a shows clearly that the best scheme assumes that the water particles leaving the control volume are randomly sampled (option (c)). Indeed, the schemes (a) and (b) largely underestimate the observed peak concentration (which in this case proceeds the peak of the hydrograph by 14 h), whereas the scheme (d) overestimate this important quantity. The graph shown by Figure **??**a also suggests that the preferential flows, though not entirely dominating the response of the plot to the tracer injection, significantly contribute to determine its features, and partially explain the early peak observed in the lithium flux concentrations.

Figure **??**b reports a comparison between modeled and observed flux concentrations in the case where the lithium injection is modeled through a stepwise change in the solute concentration of the immobile phase, rather than by introducing a solute mass into the soil through the mobile phase. From a physical point of view, incorporating the injection into the immobile phase is equivalent to assuming that the injected tracer instantaneously mixes with the immobile soil moisture. The graph reported in Fig. **??**b shows that the above modeling choice must be rejected, as all the modeled flux concentrations largely underestimate the peak of the lithium response during January, 16 and 17. Once again, the scheme (d) exhibits the worst performances among the various schemes investigated in this paper. The plot shown in Fig. **??** suggests that the initial and boundary conditions are crucial to properly mimic solute transport processes in soils, as already outlined, e.g., by *Botter et al.* [2005]. Note that at the end of the first event about 1/6th of the total Li^+ mass injected was recovered at the outlet, the remaining mass being trapped within the fixed soil phases or lost in deeper soil layers through deep percolation.

According to the numerical simulation performed, and taking into account the estimated fraction of lithium mass released toward deep soil layers, at the beginning of the second rainfall event the lithium mass stored in the soil system should not exceed 100 g ($\approx 2/3$ of the initial mass). The lithium response of the system to the second rainfall event considered in this study is reported in Figure **??**. The plot shows that, during the second rainfall event, a clear response to the rainfall event in terms of lithium concentrations lacks. In this case, in fact, distinguishing between the fluctuations of the flux concentration induced by runoff and those related to errors of measure is rather difficult. The lack of a clear response of the system in terms of lithium concentrations is also exhibited by the modeled behavior of C_L through time for all the spilling schemes adopted.

Finally, in order to further analyze the impact of the age distribution ω and of the initial and boundary conditions on the modeled solute response we have studied nitrate and lithium responses observed during a similar tracer experiment conducted during December, 2006 in the Piovega Tre Comuni test catchment. The latter experiment has been described in detail by *Botter et al.* [2008b]. The analyses presented therein are here extended to the testing of the effect of different age distributions and different initial and boundary conditions.

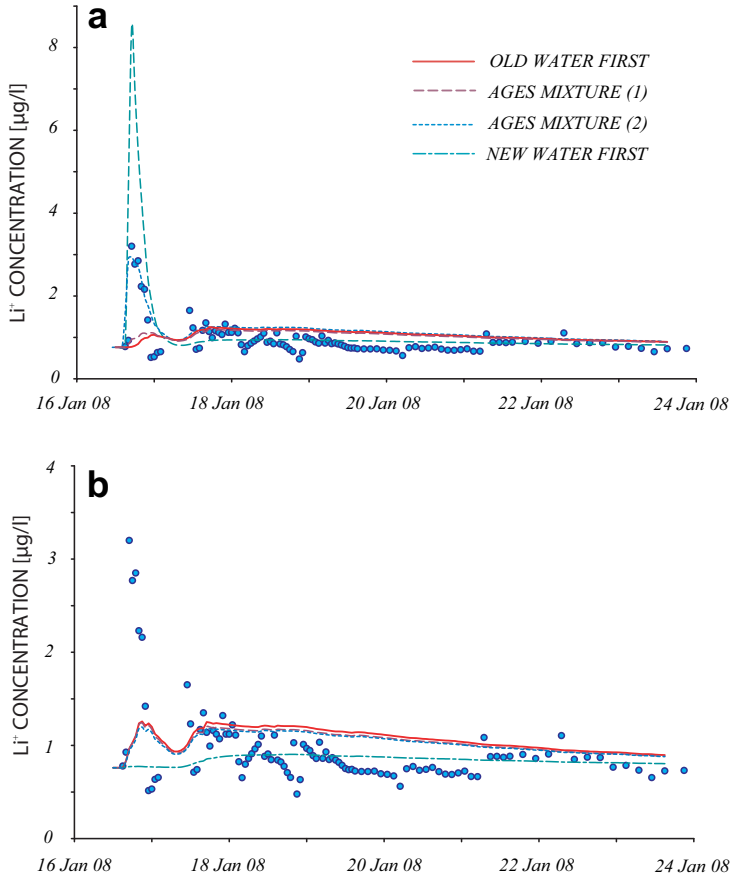

Figure 3.7: Comparison between measured and modeled Li^+ concentration during the first rainfall event resulting from the use of the four ages distribution described in the text. Lithium injection is modeled both as a solute mass introduced into the soil through the mobile phase (a) and as a stepwise change in the solute concentration of the immobile phase (b).

Figure **??** shows the comparison between modeled and observed NO_3 flux concentrations at the outlet during the rainfall event considered by *Botter et al.* [2008b] (12/06 - 12/22, 2006). Different lines in the plot correspond to the different mixing schemes (a)(d). After calibration of the initial nitrate concentration in the soil solution, the model proves able to satisfactorily reproduce nitrate flux concentrations observed at the outlet in all cases investigated. Interestingly, in this case all age distributions provide very similar responses, including the scheme according to which the new water is assumed to dominate the hydrologic response. This behavior is probably related to the fact that, differently from the other events, at the beginning of the simulation of the 2006 event the immobile soil moisture content was very close to field capacity, and no rainfall was recorded between the injection and the major event. Thus in this case the difference between the ages of the mobile

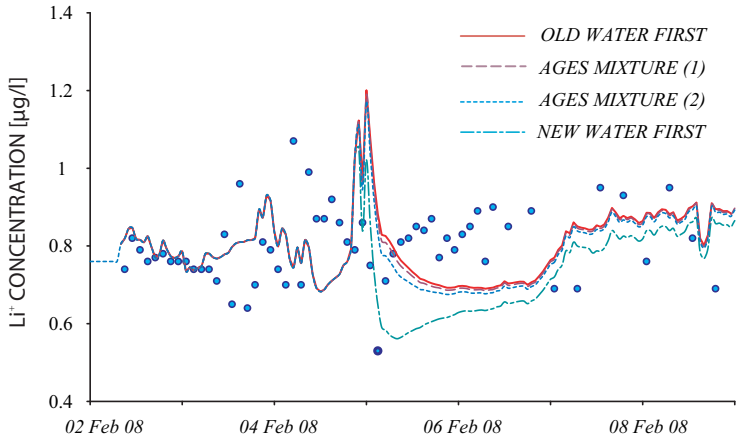

Figure 3.8: Comparison between measured and modeled Li^+ concentration during the period 01/16-01/24, 2008. The different lines show the flux concentration resulting from the application of the model employing different ages distribution (see text).

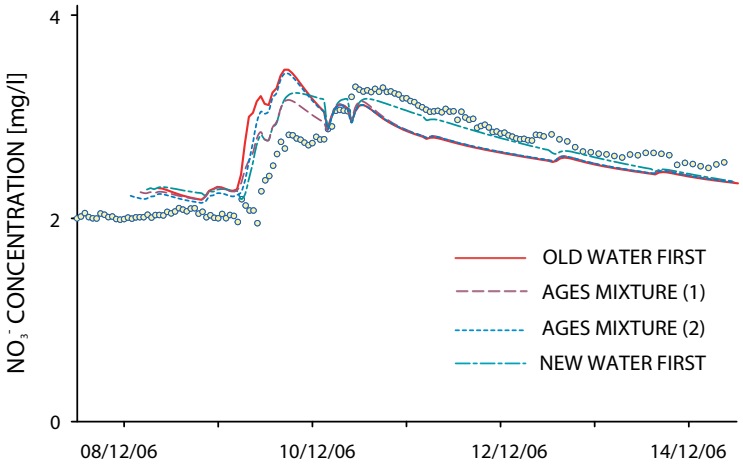

Figure 3.9: Comparison between measured and modeled NO_3^- concentration during the period 06/12-14/12, 2006. The rainfall event considered in this Figure is the one used by *Botter et al.b* (2008). The different lines show the flux concentration resulting from the application of the model employing different ages distribution (see text).

phase is less important. Possible differences induced by the choice of the specific mixing schemes can be effectively compensated by a different value of the initial nitrate concentration. Figure **??** further highlights the role of the shape of the age distribution and of different initial/boundary conditions which can be imposed on the transport problem when modeling the lithium release during the rainfall event occurred from 12/06 to 12/22, 2006. Note that in December 2006 the tracer was

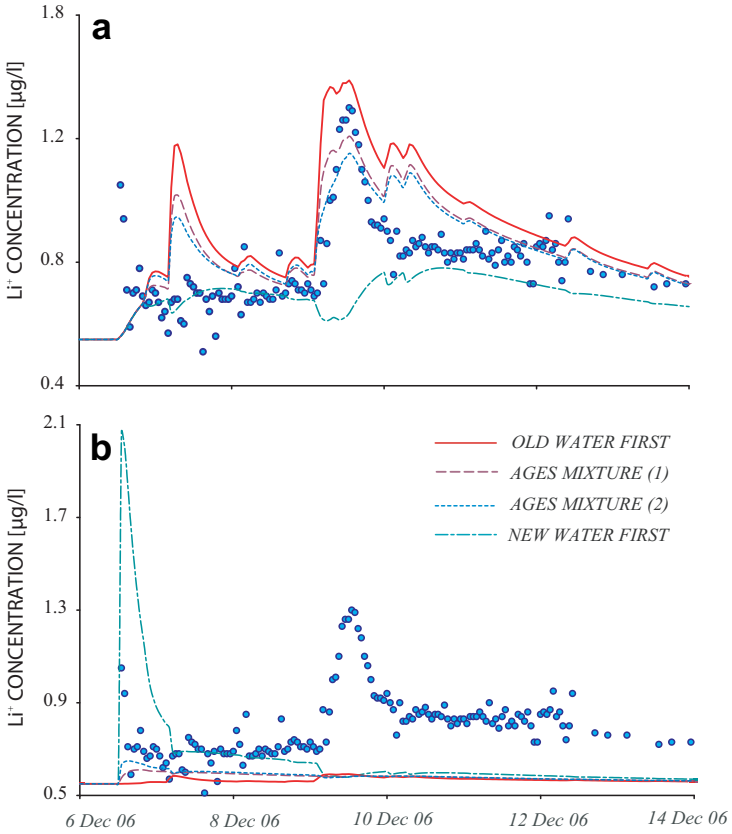

Figure 3.10: Comparison between measured and modeled Li^+ concentrations for the different spilling schemes employed during the period 12/06-12/14, 2006. Lithium injection is modeled both as a solute mass introduced into the soil through the mobile phase on 12/06 at 12:00 am (a) and as a stepwise change in the solute concentration of the immobile phase (b).

injected slowly (the injection operations took more than 2 h), and about 2 days before the beginning of the subsequent rainfall pulse. Fig. 10a shows the model performances for the event of 12/6 - 12/22, 2006 when the injection is incorporated as a step-wise increase of the lithium mass stored in immobile soil moisture. The plot reinforces the fact that, provided that a sufficiently large numbers of old water particles compose the runoff, the specific age distribution may be less important than other factors (such as rainfall forcing, the overall solute mass prone to leaching processes or the underlying residence time distribution) in determining the features of the solute response. Also, note that the best agreement with observed data during the peak of the breakthrough curve is ensured by the scheme (a) (according to which the old water dominates runoff), while the options (b) and (c) perform better during the recession phase. Once again, the scheme according to which new water dominates the hydrologic response offers the worst performance in terms of the agreement with the observed flux concentrations, as in particular it largely underestimates the

peak. Figure **??**b reports the comparison between modeled and observed Li^+ flux concentrations at the outlet during the same rainfall event considered in Figure **??**a, when the lithium injection is incorporated into a temporary increase of the input water concentration. Remarkably, in this case none of the curves corresponding to the four modeling schemes considered in this paper is able to satisfactorily reproduce the observed breakthrough curve. Only scheme (a) is able to partially capture the initial concentration peak produced during the first 2 days of the event after injection. This result strongly suggests that the initial and boundary conditions of plot- and catchment- scale solute transport models should be strictly related to the type of solute considered and to the modes of injection. Indeed data and the numerical exercises performed suggest that solutes native in precipitation, externally injected tracers and chemicals originally stored in soils may show vastly different dynamics in catchment during rainfall events.

Chapter 4

Anthropic Impact and Catchment response

In this Chapter a novel modeling approach is applied to a relevant case study in order to examine the dominant drivers of contaminant transport in intensively managed catchments and evaluate the predictability of catchment exports on the basis of a minimum level of model complexity. As it will be justified hereafter the human impact on catchment hydrologic and biogeochemical response, does not necessarily increase the complexity of the system but, in many cases produces a sort of 'functional homogeneity'.

The analysis is focused on the export of herbicide atrazine from Midwestern U.S. croplands, where this herbicide has been extensively used for more than 40 years [*Baldock et al.*, 1993; *Belluck et al.*, 1991], and is now at center of a tense debate as studies have shown that atrazine in drinking water, even at concentrations allowed by current regulations, may be associated with birth defects and reproductive problems among humans [*Winchester et al.*, 2009; *Ralston-Hooper et al.*, 2009; *Fuortes et al.*, 1997]. While our specific focus in this study is on atrazine, the overall approach is applicable to reactive chemical transport in agricultural catchments with strong impacts from human management practices.

This case study is also suitable for investigating the effects of rainfall on solute transport phenomena because field observations in the Midwestern U.S. watersheds have repeatedly shown that the fraction of seasonal loads are closely related to the few major storm events subsequent to herbicide application [*Leonard*, 1990; *Kladivko et al.*, 2001; *Gish et al.*, 1991], as well as on their timing [*Chiovarou and Siewicki*, 2007; *Luo and Zhang*, 2009]. The model proposed [*Zanardo et al.*, 2011b, *in review*] is based on the coupling of a large-scale Mass Response Function approach [*Rinaldo and Marani*, 1987; *Rinaldo et al.*, 1989] to a 'source zone' model that describes near surface pesticide dynamics.

In fact, the main difference between this modeling approach and the one presented in Chapter 3 is the introduction of the new 'source zone' module, which proves critical to capture the pesticide dynamics. Indeed the the strong linkage of pesticide loss mechanisms to the magnitude and the timing of rainfall requires a proper description of the processes occurring in top soil layer. Conversely in the modeling exercise shown in the previous chapter this is not necessary. Moreover,

a further goal pursued in the current chapter is the evaluation of the predictability of pesticide losses, which, as suggested by *Basu et al.* [2010a,b] is possibly enhanced because of the anthropic impact on the systems (see Section **??**). To this end the calibration of the model is reduced to a minimum, as opposed to the analysis in Chapter 3. Finally, given also the results produced by the previous modeling exercise, the current model considers only two water aging mechanisms within the soil: a 'perfect mixing' mechanism, where the water particles leaving the soil are randomly sampled among all the water particles present in the soil at a certain time; and 'preferential flow' mechanism, where no mixing occurs within the soil.

4.1 Managed Vs. Pristine Catchments: Observed Patterns

Basu et al. [2010b] have recently shown how, in certain cases, the extensive human alterations on catchments in many cases allow for an enhanced predictability of contaminant exports over a wide range of spatial scales. The authors, on the basis of a large body of observational data suggest that the anthropic impacts have resulted in the emergence of effective biogeochemical stationarity in managed catchments.

Long-term monitoring data from the Mississippi-Atchafalaya River Basin (MARB) and the Baltic Sea Drainage Basin (BSDB) reveal that inter-annual variations in loads, L_T, for total nitrogen, TN, and total phosphate, TP, and for geogenic constituents exported from a catchment are dominantly controlled by discharge, Q_T (Figure **??**). In particular, approximately linear relationships were found between annual exported nutrient loads and annual discharge. Moreover the annual flow-weighted concentrations ($C_f = L_T/Q_T$) computed for these catchment exhibited, relatively low inter-annual variability, implying that each of the catchments may characterized with a constant, mean flow averaged concentration, $\overline{C}_f$ (Figure **??**).

Such biogeochemical stationarity is explained therein by considering that nutrient sources can accumulate within the landscape elements - as a legacy of excessive fertilizer applications over several decades of intensive land management - which then provide the long-term memory to buffer the expected biogeochemical variations. Also other previous studies examining individual constituents in single, managed catchments provide supporting evidence for such build-up of subsurface nutrient memories [*Baresel et al.*, 2005; *Darracq et al.*, 2008]. The observed patterns indicate that nutrient export from managed catchments is transport- rather than supply-limited, such that contemporary distributed and point sources have lesser influence on inter-annual fluctuations in stream nutrient concentrations.

Additionally, *Kladivko et al.*, [1991] observed a general lack of correlation between L_T and Q_T for pesticide loads exported from catchments. Pesticides and other reactive constituents exhibit supply-limited responses, because short half-lives (e.g., 1 to 100 days for pesticides [*Wauchope et al.*, 1992]) preclude the buildup of legacy sources from annual applications. Moreover, a further database relative to 31 forested catchments located in the continental U.S. and Puerto Rico [Cambpell, 2009] showed that, under conditions of minimal anthropogenic influence, the $L_T - Q_T$ relationship was much more variable when compared to geogenic constituents, which have ubiquitous large sources. These trends lend further support the argument that biogeochemical stationarity for nutrients in impacted catchments arises from anthropogenic legacy of management, whereas for

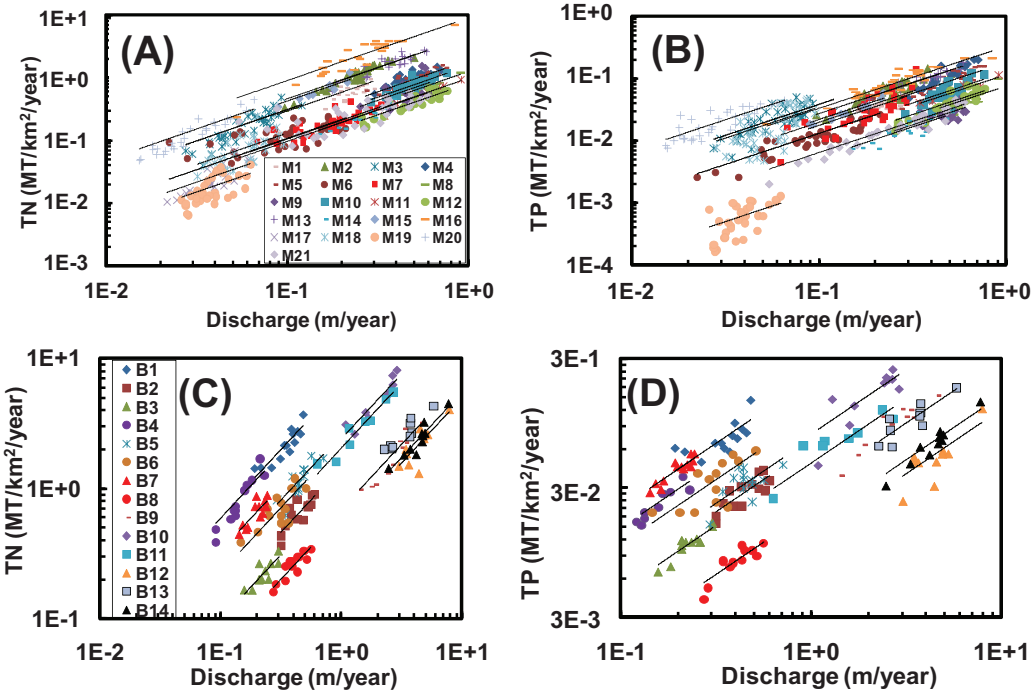

Figure 4.1: Dominance of hydrologic forcing on inter-annual variations in total-nitrogen (TN) and total-phosphorus (TP) loads exported from selected basins in the Mississippi-Atchafalaya River Basin (MARB) and the Baltic Sea Drainage Basin (BSDB). Annual loads (L_T; $MT/km^2/year$) of TN and TP are plotted against annual discharge (Q_T; $m/year$) for the MARB catchments in (A) and (B), and for the BSDB sub-basins in (C) and (D). The plots are presented on a log-log scale for visual clarity [after *Basu et al.*, 2010b].

the geogenic constituents catchment geologic legacy is the primary controlling factor. Based on the persistence of linear $L_T - Q_T$, annual nutrient loads can be robustly estimated as $L_T = Q_T \overline{C}_f$, where the hydro-climatic controls (e.g., precipitation, evapotranspiration) are manifested in Q_T, and the anthropogenic drivers (e.g., land-use; nutrient inputs) are reflected in $\overline{C}_f$. Emergent effective biogeochemical stationarity indicates that annual stream discharge can serve as a reliable surrogate for estimating annual loads of geogenic and anthropogenic constituents exported from managed catchments at diverse spatial scales.

Anthropic alterations have also been shown to enhance the predictability of the hydrologic response in agricultural catchments. *Basu et al.* [2010a] demonstrated the capability of a parsimonious threshold-based model (Threshold Exceedance Lagrangian Model – TELM), with no parameter calibration, to predict daily discharge at the outlet of the Cedar Creek Watershed (700 km^2) in Northeastern Indiana. The parsimony of the TELM approach was attributed to the unique geomorphic features and anthropogenic alterations of tile-drained Midwestern agricultural watersheds. These features rendered the watersheds to be 'functionally homogeneous' and generate equivalent

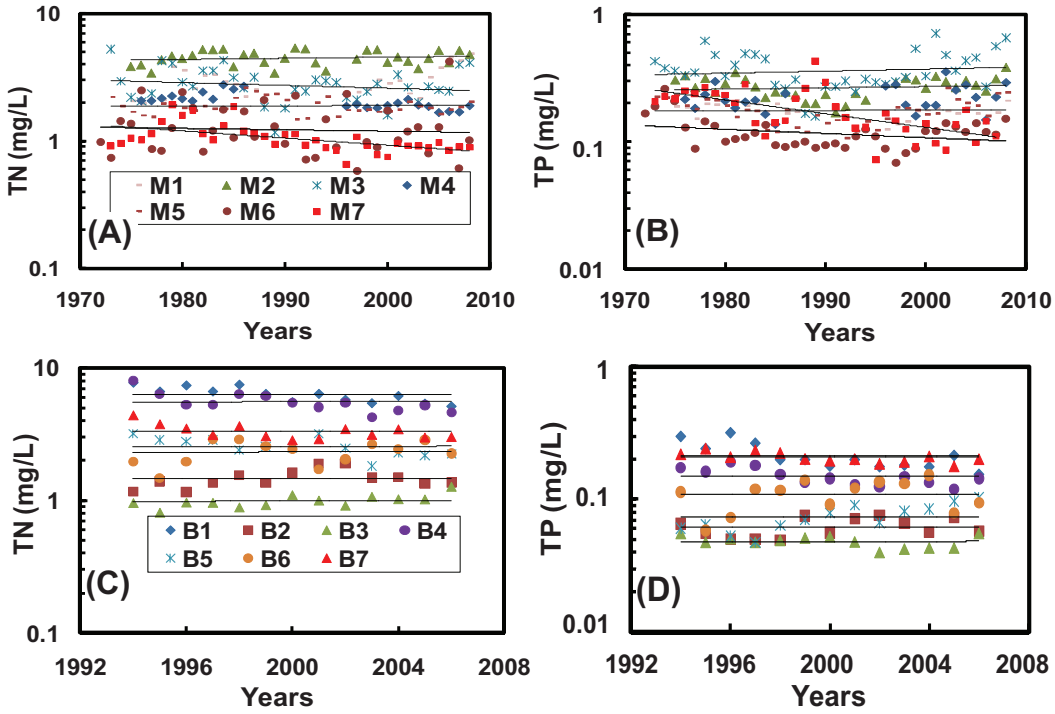

Figure 4.2: Annual flow-weighted concentration, C_f (mg/l), of total-nitrogen (TN) and total-phosposrus (TP) does not change significantly over time, despite one and a half times increase in fertilizer application in the Mississippi-Atchafalaya River Basin (MARB) (1976-2000) and decrease in inputs for the Baltic Sea Drainage Basin (BSDB) (1992-2008). TN and TP data for the MARB catchments are shown in (A) and (B), while the corresponding data for the BSDB catchments are shown in (C) and (D) [after *Basu et al.*, 2010b].

hydrologic responses in spite of their 'structural heterogeneities' expressed in spatial variability of soils and land use. A representative area of 10-20 km^2 was identified as the scale at which watersheds are functionally homogeneous.

4.2 Catchment-scale pesticide transport

Transport of reactive chemicals like pesticide has added layers of complexity over hydrologic response contributed by (1) soil biogeochemistry that affect pesticide sorption and degradation, and (2) land use and soil/crop management practices (e.g., cropped area, crop distributions and growth, planting dates, timing and amount of pesticide application), which is often an unknown at the spatial scale required for modeling. In the Midwestern U.S. agricultural catchments, the dominant cropping system is corn-soybean rotation, and more or less an equal split between the two crops is the norm. While an average 50-50 split may be a reasonable approximation at a regional scale (county or state level), yet within a specific watershed the planted area between corn and soybean

can vary significantly from year to year depending, say, on weather patterns or market fluctuations for grain prices. Accounting for areas planted to corn or soybeans is important both for hydrologic prediction and for pesticide export estimations. Rooting depths and patterns, and the crop growth during the season, are different for these two crops. Thus, the soil-water storage deficit created by evapo-transpiration, and the concurrent hydrologic response are influenced by the partitioning of area between corn and soybeans. Pesticide transport is even more strongly affected by the uncertainties arising from lack of knowledge of area planted to the two crops, as pesticides are applied on corn, but not on soybean fields. Furthermore, pesticide loads exported at the field, hillslope- or catchment-scales have been observed to be highly dependent on the timing of pesticide applications relative to major rainfall events [*Chiovarou and Siewicki*, 2007; *Luo and Zhang*, 2009]. Field observations in the Midwestern U.S. watersheds have repeatedly shown that only few major storm events subsequent to pesticide application export the largest fraction the total seasonal loads [*Leonard*, 1990; *Kladivko et al.*, 2001;. *Gish et al.*, 1991]. Critical data on variations in planting and application dates are not readily available for most catchments, and model implementation is based on either calibration or estimates from data available for much larger spatial units (e.g., single county or multiple counties). The conventional calibration-validation leads to issues of equifinality where multiple combinations of model parameters lead to the same integrated response at the watershed outlet. Possibly large uncertainties in the prediction of exported pesticide loads, arising from such choices, are usually not examined or explicitly acknowledged. These types of difficulties and challenges motivate a parsimonious modeling approach that is based on a minimum level possible model complexity, includes the major drivers and pathways for pesticides, and uses pragmatic model assessments based on a set of hierarchical criteria. The objective is not to develop the most detailed model for pesticide transport, but rather to use the model as a 'learning tool' to understand the dominant controls, and associated allometric and epistemic uncertainties.

The first attempts to model water quality began in 1970 after the Clean Water Act. The Chemicals, Runoff and Erosion from Agricultural Management Systems (CREAMS) model was proposed by *Knisel* [1980] and aims to predict runoff, erosion, and chemical transport from agricultural management systems. The CREAMS approach considered only surface runoff, while the groundwater component was neglected. This was later modified in the *Groundwater Loading Effects of Agricultural Management Systems* (GLEAMS) model [*Leonard et al.*, 1987] that explicitly considered groundwater loadings. The model was developed to evaluate edge-of-field and bottom-of-root-zone loadings of water, eroded soil, and agricultural chemicals from alternate management systems. The GLEAMS model has been frequently applied by researchers [*Leonard and Knisel*, 1989; *Smith et al.*, 1994;], usually at the field scale ($\sim ha$). The pesticide component of the model assumes that the contaminant undergoes sorption and chemical decay while the principal hydrologic drivers for pesticide losses are surface runoff and percolation. Partitioning of soluble pesticide between percolate and surface runoff is defined by a calibration parameter. The GLEAMS algorithm is also used in the SWAT model [*Arnold et al.*, 1993] to model pesticide fate and transport at the watershed scale ($\sim 10^3\ km^2$). SWAT model is applied to relatively large scale therefore it also incorporates a simple mass balance controlling pesticide transport and transformations within streams [*Chapra*, 1997], and the *Erosion Productivity Impact Calculator* (EPIC) algorithm, that governs pesticide

movement from land areas to the stream network [*Williams et al.*, 1984]. The transport process in land areas is based on a piston flow scheme where no diffusive flow is considered within the soil. However, this component of transport may be important in modeling solutes at a catchment scale as it introduces the effects of water age as well as the mixing among water volumes with different ages. Diffusive mass-transfer is considered, for example, by *Larsbo et al.* [2005] with the MACRO model that simulates the solute transport in the vadose zone. The model uses a two-domain approach by coupling a high-conductivitylow porosity macropore domain to a low-conductivity high porosity domain representing the soil matrix. The diffusive component has been also included by other authors through simpler, lumped approaches. With these methods, the underlying transport mechanisms of a hillslope/catchment are implicitly embedded within an assumed system response function which can be the analytical solution of the advection-dispersion equation [*Stewart and McDonnel*, 1991; *Maloszewski et al.*, 1992], or the water travel time distribution [*Stewart and McDonnel*, 1991; *Rinaldo and Marani*, 1987; *Rinaldo et al.*, 1989]. In particular, the water travel time distribution serves as a descriptor of the whole transport mechanism as it merges together all the sources of uncertainty of heterogeneous environments. *Rinaldo and Marani* [1987] proposed the so called Mass Response Function (MRF) approach for solute transport modeling. The main idea underlying the MRF approach is that mass transformations are mostly driven by the time spent by the water within the soil rather than the individual trajectories followed by each water particle. It is also acknowledged that an important contribution to the overall pesticide transport process is given by the near-surface soil layer (e.g., *Ahuja et al.*, 1981) Previous studies have shown that pesticides often persist in the this layer for a long time after the application [*Flury et al.,* 1995]. Therefore a characterization the shallow region of the soil should be included when modeling pesticide transport. *McGrath et al.* [2009], proposed a simple source zone model, able reproduce many of the signatures of pesticide transport. *Steenhuis et al.* [1994] coupled a superficial mixing zone to a preferential flow model, producing a closed form equation for preferentially moving solute concentrations.

We follow the hydrologic modeling approaches suggested by *Basu et al.* [2010a], and the mass-response function approach [*Rinaldo et al.*, 1987] to model pesticide transport through the hillslopes. We also add a new two-compartment source function model to describe the temporal dynamics in a shallow surficial soil layer in which the applied pesticide is assumed to reside, and provide episodic pulses of pesticide loads to the catchment. The model provides, predictions for both water discharges and pesticide concentrations and loads. However, instead of using the conventional calibration-validation approach, we choose to pursue the alternate path of using the model as a "learning tool" to understand the dominant drivers of pesticide export. The ranges of critical model parameters required to produce the measured concentrations at different scales (tile and watershed) are examined to understand the range of variability and uncertainties in model predictions. Further, we adapt a set of hierarchical criteria for model assessments, where the first level of model assessment is based on seasonal pesticide loads, then on monthly and daily loads. Finally, we adopt an overall risk assessment framework to evaluate model performance. That is, our focus is not solely on point-to-point matching of hydrographs and chemographs, but also on probabilistic comparisons of concentration exceedance probabilities.

4.3 Contaminant mobilization from the top-soil layer

It is commonly accepted that pesticides transport occurs under non-equilibrium conditions [*Brusseau and Rao*, 1989; *Brusseau et al.*, 1989]. Processes responsible for non-equilibrium are usually classified into two general groups: i) transport-related non-equilibrium (TRN), and ii) sorption-related non-equilibrium (SRN). In the first group the flow domain is characterized by regions of minimal advective flow that exchange mass with the advective flow region through diffusive transport. The breakthrough curves in this type of process are characterized by early breakthrough due to advective transport, and long tails resulting from rate-limited mass transfer between advective (mobile) and non-advective (immobile) domains. It is important to notice that TRN affects both sorbing and non-sorbing solutes. This is not the case for SRN, which is a result of both chemical interactions between solute and specific sorption sites and intrasorbent diffusion.
The occurrence of TRN has been shown from both laboratory experiments [*Van Genuchten and Wierenga*, 1977; *Rao et al.*, 1980; *Nkedi-Kizza et al.*, 1982] and field studies [*Rao et al.*, 1974; *Bowman and Rice*, 1986; *Jury et al.*, 1986]. However, other works [*Davidson and Chang*, 1972; *Rao et al.*, 1979] suggest that for sorbing solutes non-equilibrium transport is also a result of sorption-related mechanisms [*Brusseau and Rao*, 1989a]. Thus it is appropriate, when dealing with highly sorbing chemicals such as pesticides, to recognize and evaluate both sources of non-equilibrium.
In our model, the catchment is conceptualized as composed by two serial control volumes: a production, or source zone, where the contaminant is applied, and a transport volume, where the contaminant is transported through. In the source zone, both the effects of TRN and SRN will be evaluated through a 4-compartment idealization of the soil system, whereas the transport volume, following *Rinaldo et al.* [2006a,b], is characterized by mobile and immobile domains.
In our framework the source zone is defined as the very shallow soil layer. Depending on the application and tillage methods and on land use, the agrochemicals may be reasonably thought of being uniformly distributed on within this layer. Most of the contaminant applied is assumed to be retained in this zone, and gradually depleted by rainfall events and the ensuing leaching.
Two relevant time scales for pesticide dynamics within the source zone can be identified: 1) the time between storm events, and 2) the duration of storm events. Between storm events the solute undergoes biogeochemical transformations (decay, production, sorption) as well as mass transfer. We also assume that, during that time period, advective and dispersive fluxes may be neglected. During storm events, advective and dispersive fluxes in/from such zone are triggered and a certain fraction of the pesticide stored in the source zone is flushed out, the load depending on the volume of the storm event and the solute concentration in the source zone. This conceptualization and the assumptions we have made are in agreement with the framework proposed by *McGrath et al.* [2009], although mass transfer was not considered therein.
The source zone is schematized as a two-compartment box (Fig. **??**). One compartment represents the mobile region, where the contaminant is readily available to the rainfall pulses coming through. The second compartment represents the immobile region, where there is no advective flow. Within each compartment, a certain amount of pesticide may be in the sorbed phase and the remaining part is in the dissolved phase. For pesticides that do not undergo sorptive processes, all the mass is present within the dissolved phase. Microbial or abiotic transformations (degradation/production)

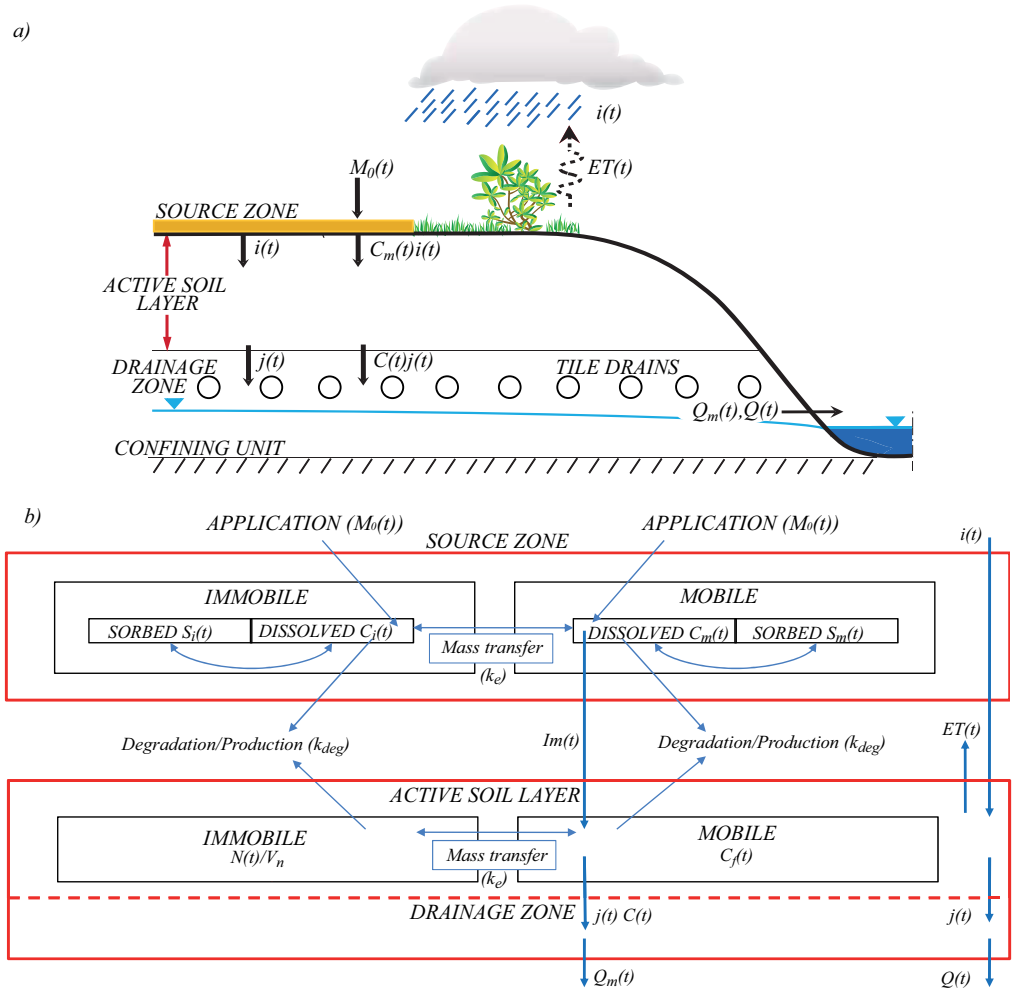

Figure 4.3: Physical (a) and conceptual (b) representation of the hydrological and biogeochemical models.

and mass transfer are assumed to occur only in the dissolved phase.
Between storm events, pesticide dynamics in the two source-zone compartments are driven by the general continuity equation:

$$\frac{\partial C(t)}{\partial t} + \frac{\rho}{\theta}\frac{\partial S(t)}{\partial t} = \pm\frac{\psi(t)}{\theta}, \tag{4.1}$$

where $C(t)$ $[ML^{-3}]$ is the dissolved concentration, $S(t)$ $[MM^{-1}]$ is the sorbed concentration, θ is the volumetric water content, ρ $[ML^{-3}]$ is the bulk density, and ψ $[ML^{-3}T^{-1}]$ is the source/sink term, which includes the decay and/or generation as well as mass transfer between mobile and

immobile phases. In Equation **??**, an advective term is not shown, as it is assumed that advective fluxes can be neglected within the source zone during inter-storm periods.
It is further assumed that the sorption process is linear and reversible and that the equilibrium is reached instantaneously. The sorbed pesticide concentration is then linearly related to the dissolved concentration through the partition coefficient, k_D ($= C(t)/S(t)$). In general, the sink/source, ψ term is a function representing decay, mass-transfer between phases, anthropic applications and losses due to storm events. First-order decay of pesticide is represented by the rate constant k_{deg} $[1/T]$. Mass transfer between phases is assumed to be driven by the gradient of concentrations through a first-order process with rate k_e $[1/T]$. Therefore, between storm events, the continuity equations for mobile and immobile phases may be expressed as follows:

$$\frac{\partial C_i(t)}{\partial t} R_i = k_e(C_m(t) - C_i(t)) - k_{deg} C_i(t), \tag{4.2}$$

$$\frac{\partial C_m(t)}{\partial t} R_m = -k_e(C_m(t) - C_i(t)) - k_{deg} C_m(t), \tag{4.3}$$

where R ($= 1 + k_D\rho/\theta$) is the retardation factor , k_e is the mass transfer rate constant $[T^{-1}]$, and the subscripts m and i indicate the mobile and immobile zones respectively.
Pesticide applications and losses due to storm events are assumed to occur instantaneously, producing stepwise jumps in the source-zone concentration. The pesticide may be applied in both the mobile and immobile phases, according to a coefficient Γ which defines the fraction of pesticide applied in the mobile phase. While pesticide applications are imposed through initial conditions in the model, losses depend on the magnitude and timing of the rain events and on the concentration in the source zone. As hypothesized, mass can be flushed out only from the dissolved mobile phase, the mass flux, $\phi_m(t)$ $[MT^{-1}L^{-2}]$, is then given by the following equation:

$$\phi_m(t) = i(t) C_m(t), \tag{4.4}$$

where $i(t)$ $[L]$ is the magnitude of the storm event.
Note that the various dissolved or sorbed pesticide concentrations employed herein are assumed as dependent only on relevant timescales (application times and contact times between phases) and not on spatial variables. It has been shown, in fact, that as long as the application/source areas are large with respect to typical spatial correlation scales of heterogeneous properties of the catchment (e.g. soil type, permeability of subsurface zones, macroscales of instantaneous rainfall patterns) this is a viable assumption [*Botter et al.*, 2008]. This is indeed typically the case for non-point sources transport at the catchment scale [*Rinaldo et al.,* 2006a; *Rinaldo et al.,* 2006b], and, in particular, for the case study at hand.

4.4 Transport through the unchanneled transport volumes

4.4.1 Hydrologic response

The hydrologic response is modeled by means of the Threshold Exceedance Lagrangian Model (TELM), already successfully applied to the Cedar Creek watershed (700 km^2) in Northwestern

Indiana [*Basu et al.*, 2010a]. The parsimony of the TELM approach, highlighted by the need to calibrate no parameters, was attributed to the unique geomorphic features and anthropogenic alterations of tile-drained Midwestern agricultural watersheds. These features rendered the sub-watersheds within the Cedar Creek to be 'functionally homogeneous' in generating equivalent hydrologic responses despite their structural heterogeneity expressed in spatial variability of the soils and land uses.

For a single geomorphic unit, the discharge, $Q(t)$ $[L^3]$, can be expressed by the following equation:

$$Q(t) = A \int_{\infty}^{t} j(t_i) g(t - t_i) dt_i + BF(t), \tag{4.5}$$

where: $g(\cdot)$ $[T^{-1}]$ is the system response function, and $j(t)$ $[L]$ is the net rainfall, which is the excess water that leaves the system at time t; $BF(t)$ represents the slow component of the discharge (base flow), and A is the drainage area. In tile-drained watersheds, the discharge recessions have been shown to follow an exponential trend [*Schilling and Helmer*, 2008; *Kladivko et al.*, 2001]. In the model, the system response function is expressed as an exponential distribution with the rate equal to the inverse of the mean water travel time, t_r.

Net rainfall events are assumed to be triggered instantaneously, as soon as available soil-water storage exceeds a critical level, equal to the field capacity. This implies that the restoring of soil-water deficit occurs before the soil begins to drain. The process is therefore threshold-driven and only the field capacity (i.e. the threshold) needs to be estimated. There exists more complicated models for the water leakage process from the source zone, for instance, *Clapp and Hornberger* [1978] assume that the net rainfall is a power function of the soil water content: $j(t) = K_{sat} s(t)^c$, where K_sat is the saturated hydraulic conductivity, $s(t)$ is the relative soil moisture and c is the so called Clapp coefficient. However, along the lines of parsimonious modeling process we choose to use the approach by *Basu et al.* [2010a] and evaluate its predictive capabilities as well as its limitations.

Runoff production due to infiltration excess mechanisms is neglected, as it usually represents a minor contribution to the total discharge in extensively managed, tile-drained agricultural watersheds, except under extreme hydrologic conditions.

The effective rainfall production is driven by the following water balance equation in the active soil layer:

$$\frac{dS_t(t)}{dt} = i(t) - ET(t) - T(t), \tag{4.6}$$

where S_t $[L^3]$ is the water content in the active soil layer, $T(t)$ $[L^3/T]$ is the excess rainfall, and $ET(t)$ $[L^3/T]$ is the actual evapotranspiration rate.

The effective rainfall, $j(t)$ is then computed as follows:

$$j(t) = (1 - g_f) T(t), \tag{4.7}$$

where g_f represents the fraction of recharge, which constitutes the slow flow component of discharge. The actual evapotranspiration was estimated following *Basu et al.* [2010a], where a root-growth term is added to the FAO approach [*Allen et al.*, 2005], in order to account for variable water extraction from the soil during the the different growth stages. This term conceptualizes the growth

process as divided in three stages: an early constant growth stage when roots are still shallow, a silking (for corn) stage where roots progressively up to the crop maturation and a maturity stage where roots stay constant at their maximum level until harvest.

4.4.2 Biogeochemical response

This part of the model concerns the transport of pesticides from the source zone to the catchment outlet. As suggested e.g. by *Botter et al.* [2010c], the nonlinear character of the relevant processes may be captured by dividing the transport volume into an active soil layer, where evapotranspiration fluxes are assumed to occur, and a drainage zone where the net rainfall exiting the active soil layer is linearly and invariantly routed to the streams (Figure **??**).
Resident pesticide concentration of water particles transported through the unchanneled transport volume decreases in time due to biogeochemical degradation. Moreover, the flux concentration at the outlet is also affected by the mixing of particles with different ages occurring in hillslopes due to local diffusion and convective dispersion.
Analogously to the conceptualization of the source zone, a first-order pesticide decay with rate constant k_{deg} is considered in both the active soil layer and the drainage zone. Moreover, we assume that water mixing occurs eminently in the active soil layer, while the drainage zone acts as a linear reservoir for both water and mass (see Figure **??**). On this basis, the mass flux $Q_M(t)$ at the outlet can be expressed as follows:

$$Q_M(t) = A \int_{-\infty}^{t} \phi_j(t_j) e^{-k_{deg}(t-t_j)} g(t-t_j) dt_j, \tag{4.8}$$

where $\phi_j(t_j)$ is the mass flux exiting the active soil layer at time $t = t_j$ and $g(\cdot)$ is the unit hydrograph used in Equation **??**. Equation **??** implies that after the water pulses exit the active soil layer, water mixing ceases and the only variation of resident concentration is due to biogeochemical decay.
The flux ϕ_j is thus related to the mixing processes occurring in the active soil layer. To calculate ϕ_j, we will consider and evaluate two different modeling schemes.

Preferential flow

The first scheme aims at simulating a system where water is predominantly routed through preferential/bypass flow paths and will be thus referred to as preferential flow (PF) scheme. According to such scheme, no mixing takes place in the active soil layer and, when an effective rainfall event is generated, all the water leaving the active soil layer belongs to the same rainfall pulse that triggered such event. In this case, the partitioning of the total rainfall into evapotranspiration and effective rainfall, is decoupled from the underlaying biogeochemical dynamics.
The mass flux leaving the active soil layer is simply given by the product of the effective rainfall and the instantaneous concentration, C_m, in the labile region of the source zone:

$$\phi_j(t) = C_m(t) j(t) \tag{4.9}$$

Motivations for this scheme can be found in several studies, which have shown that in agriculture dominated landscapes, such as the Midwestern US, hydrology has been modified to promote rapid drainage of low permeability soils necessary for intensive crop production. Presence of extensive networks of artificial (tile drains, ditches) and natural (cracks, root holes, bio-channels) preferential flow paths, has significantly altered the hydrologic responses [*Evans and Fausey*, 1999; *Radcliffe and Rasmussen*, 2000; *Kladivko et al.*, 2001; *Schilling and Helmers*, 2008]. Similar pedologic features arising from landscape modification for crop production are also found in European catchments [e.g. *Olli et al.*, 2009].

Perfect mixing

The second modeling scheme assumes that mixing occurs within the active soil layer, implying the coupling of hydrologic and biogeochemical dynamics. Mixing is assumed to happen among water particles with different ages, as well as through mass transfer between mobile and immobile soil regions, analogously to the conceptualization of the source zone. The mass transfer is proportional to the gradient of concentration between mobile and immobile zones with a rate constant k_e (see Figure **??**) [*Rinaldo et al.*, 2006a,b]. The main idea underlying the MRF approach, which we refer to, is that mass transformations are mostly driven by the time spent by the water within the hillslope rather than the individual trajectories followed by each water particle. The approach has been recently generalized by *Botter et al.* [2010] through a comprehensive mathematical framework. In our study we evaluated the simplifying assumption of perfect mixing (PM) of water particles within the active soil layer. This implies that during evapotranspiration and mobilization the water particles that leave the system are randomly sampled among all the water particles in the active soil layer and, analogously, the mass transfer between mobile and the immobile zones is proportional to the difference of their perfectly mixed resident concentrations. This conceptualization translates into the following water and mass balance equations:

$$\frac{dS_t(t)}{dt} = i(t) - j(t) - ET(t) \tag{4.10}$$

$$\frac{d(S_t(t)C(t))}{dt} = C_m(t)i(t) - C_f(t)j(t) + \left(\frac{dM}{dt}\right)_{react} \tag{4.11}$$

where $S_t(t)$ is the water stored in the active soil layer, $ET(t)$ is the actual evapotranspiration, and $C_f(t)$ is the perfectly mixed concentration of the mobile phase. The reaction term $(dM/dt)_{react}$ is then given by

$$\left(\frac{dM(t)}{dt}\right)_{react} = -k_{deg}S_t(t)C_f(t) + k_eV(N(t) - C_f(t)), \tag{4.12}$$

where $N(t)$ is the solute concentration in the non-advective zone, and V is a characteristic volume in which the mass-transfer dynamics take place. The closure of the problem is finally given by the mass balance within the non-advective region:

$$V_N\frac{dN(t)}{dt} = -k_{deg}V_NN(t) - k_eV(N(t) - C_f(t)), \tag{4.13}$$

where V_N is the volume of the non-advective region, which is here assumed equal to the product of the depth of the active soil layer, Z, and soil-water wilting point, θ_{wp}. Without less of generality it is further assumed $V = V_N$, the purpose of the latter assumption is only to simplify the estimation of the parameters and does not affect our conclusions.
Coupling Equations **??** and **??** and substituting Equation **??** in **??** yields:

$$S_t(t)\frac{dC_f(t)}{dt} = i(t)(C_m(t) - C_f(t)) + C_f(t)ET(t) - k_{deg}S_t(t)C_f(t) + k_eV(N(t) - C_f(t)). \quad (4.14)$$

The concentration $C_f(t)$ is then obtained by solving Equations **??** and **??**. The mass flux, ϕ_j to be used in Equation **??** is finally given by:

$$\phi_j(t) = C_f(t)j(t). \quad (4.15)$$

consistently with the above formulation.

4.5 Field Monitoring Data: the Little Vermilion River Watershed

The Little Vermilion River Watershed (LVRW) is a 490 km^2 catchment located in central Illinois (Figure **??**), at the boundary of Champaign and Vermilion Counties. The topography is flat with slopes reaching at most a 1%. Soils in this area are predominantly characterized by Drummer silty clay loam and Flanagan silt loam. Approximately 90% of LVRW area is agricultural land used for corn-soybean production, while the remainder consists of grassland, woodland, roadways and farmsteads [*Kalita et al.*, 2004]. The yearly area planted to corn is approximately equal in size to that of soybeans [*Algoazany et al.*, 2007]. Given the flat topography, agriculture activities require subsurface tile networks for enhanced drainage. Tile drains have long been installed across the Midwestern United States dramatically altering the hydrologic response of these regions [*Schilling and Helmers*, 2008]. Such drains usually discharge into surface ditches, which eventually flow into stream networks.
Beginning in 1991, a decade-long research project was conducted in LVRW by a research group from the University of Illinois at Urbana Champaign to investigate water quality issues [*Mitchell et al.*, 2003; *Kalita et al.*, 2004]. Discharge data were collected from 1991-1999, while atrazine monitoring was done between 1993 and 1999. Monitoring was done at multiple scales — (a) co-located sub-surface (tile-drain) and surface runoff stations, (b) river stations. There were seven sub-surface stations (A-G), four surface runoff stations (As, Bs, Cs and Ds) and seven river stations (R1 - R7). Figure 2 shows the locations of the gauging stations across LVRW. Each sub-surface station was located at the outlet of a network of tile drains. We focused our analysis on two subsurface stations (A and B - drainage areas 0.05 km^2 and 0.03 km^2), and on one of the river stations (R5 - drainage area 69 km^2), since there were questions regarding the validity of some of the other datasets. The surface stations were not considered in our analysis, as surface runoff events were rare, and the overall volume of surface runoff was $< 4\%$ of the total discharge.
Detailed information on the data collection as well as the water sample analyses for the LVRW can be found in *Yuan et al.* [2000], *Mitchell et al.* [2003], *Kalita et al.* [2004], and *Algoazany et al.* [2007]. Daily rainfall was recorded using tipping buckets at every subsurface station except station

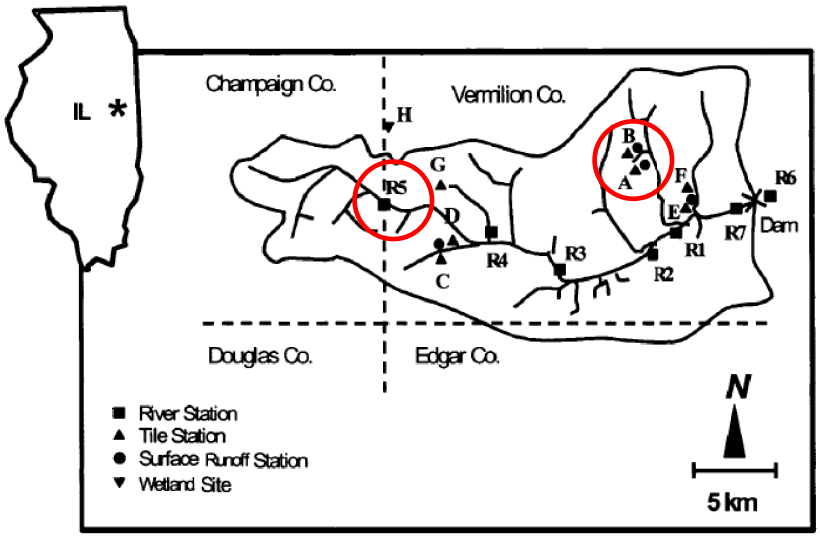

Figure 4.4: Schematic of the Little Vermilion River Watershed with locations of the sub-surface stations, surface stations, river gages and precipitation stations. Figure from *Algoazany et al.* [2007]. The circles highlight the stations considered in the thesis [after *Algoazany et al.*, 2007].

B since it was adjacent to station A. At the subsurface stations, drain flow was monitored continuously by Palmer-Bowls flumes installed at each drain system outlet. For water quality analyses, samples were obtained bi-weekly during most of the year, with additional samples taken by pump samplers activated by the data logger during storm events [*Mitchell et al.*, 2003]. The number of measurements available for this study ranged from 3-4 per month to 5- 6 per week. At the river stations, flow was monitored daily through stage gage readings. Samples were transported and stored in the Water Quality Laboratory of the Department of Agricultural and Biological Engineering at the University of Illinois. Atrazine concentrations were measured using a liquid/liquid extraction method with methylene chloride and gas chromatography. As water samples were not taken every day that flow occurred, atrazine loads were computed by multiplying the concentration for a sample collected at a specific time by half the flow volume from the previous concentration measurements plus half the flow volume from the following concentration measurement. This procedure continued from the start to the end of recording for each station.
Total discharge, rainfall, and atrazine losses during the growing season are reported in Table **??** and **??** along with the discharge-rainfall ratios and the Load As Percentage of Use (LAPU).
In a study conducted on 180 fields (drainage area lower than 100 *ha*) *Capel and Larson* [2001] found a mean atrazine LAPU of 1.71, with a standard deviation of 2.98. Values shown in Table **??** fall within the confidence interval provided, although they are always lower than the mean LAPU observed by the authors. Table **??** also shows that at station A, in the years with no application (even years), atrazine is observed in subsurface flow because of the carry-over from odd years. At station B, such carry-over contribution to the pesticide is less important.

Table 4.1: Atrazine application rates and loads, water discharge, discharge-rainfall ratio, and total loads as percentage of used (LAPU) observed at station A and B from 1993 to 1999.

Year	Atrazine application rate $[Kg/km^2]$	Growing season subsurface flow $[mm]$	Growing season rainfall $[mm]$	discharge-rainfall ratio $[-]$	Growing season atrazine loss $[Kg/km^2]$	Atrazine LAPU [%]
Station A						
1993	200.1	265	949	0.28	0.24	0.17
1994	0	170	599	0.28	0.08	0.04[1]
1995	144.5	96	538	0.19	0.28	0.21
1996	0	217	759	0.29	0.08	0.06[1]
1997[2]	200.1	58	472	0.12	0.053	0.03
1998	0	203	931	0.22	0.08	0.04[1]
1999	139	21	477	0.04	0.001	0.001
Station B						
1993	0	146	949	0.15	0.09	-
1994	200.1	151	599	0.25	0.24	0.12
1995	0	49	538	0.09	0.044	0.02[1]
1996	180.7	132	759	0.17	0.31	0.17
1997[2]	0	35	472	0.07	0.036	0.02 [1]
1998	150.8	200	931	0.21	0.70	0.47
1999	0	15	477	0.031	0.007	0.005[1]

Table 4.2: Atrazine losses and flow volumes at station $R5$. The last column reports the average annual application rates estimated by the USDA National Agricultural Statistical Service [2006] for the State of Illinois.

year	Growing season rainfall $[mm]$	Growing season discharge $[mm]$	rainfall-discharge ratio [-]	Growing season atrazine losses $[Kg/km^2]$	Flow-averaged concentrations $[\mu g/L]$	Atrazine average app. rates in Illinois $[Kg/km^2]$
1993	849	211	0.25	0.15	0.71	134
1994	543	75	0.14	0.31	4.1	134
1995	530	38	0.07	0.09	2.37	125
1996	731	81	0.11	0.35	4.32	134
1997	455	34	0.08	0.08	2.35	133
1998	748	159	0.21	0.97	6.1	145
1999	518	26	0.05	0.02	0.77	142

4.6 Uncertainties in parameter estimation

Catchment scale studies often need to face notable difficulties in estimating effective parameters at the spatial and temporal scales of resolution required. Model parameters, somewhat simplifying matters, can be classified as: (a) management parameters, like e.g. land use, planting dates, application dates; (b) hydrologic and biogeochemical parameters that describe the filtering action of the catchment and sum the relevant dynamics at the scale prescribed by the chosen control section.

While estimation of the second class of parameters appears to be complex owing to significant landscape heterogeneity and to the need to synthesize complex basin-scale dynamics, it must be noted that the first class of ideally 'known' parameters are also often difficult to estimate at the spatial scales of interest here. Most studies on pesticide transport have focused on the scale of individual fields or plots where land-use and atrazine application rates are known. These models may be calibrated for a large number of parameters that describe advective and dispersive fluxes [e.g. *Larsbo et al.*, 2005]. In contrast, studies at larger scales have mostly used simpler models, and calibrated uncertain parameters such as pesticide application dates [e.g. *Larose et al.,* 2007; *Neitsch et al.*, 2002]. Average estimates of such information are available at the larger scales (e.g., 10^4 km^2), but often spatial variability in land-use patterns, as well as land management choices, result in downscaling errors.

With regard to the study at hand, we note that in the Midwestern U.S. croplands the dominant land use is corn-soybean rotation, and an equal subdivision between the two crops is the norm. While an average 50% split may be a reasonable approximation at a regional scale (county or state level), within a specific watershed the planted area between corn and soybean can vary significantly from year to year depending, say, on market fluctuations for grain prices. Accounting for areas planted to corn or soybeans is important both for hydrologic prediction and for pesticide export estimations. Rooting depths and patterns, and the crop growth during the season, are different for these two crops; corn rooting depths at mature stages can extend down to the confining clay unit that characterizes the site (1 to 1.5 m), while soybean maximum rooting depths are shallower, extending down to about 50-60 cm. Thus, the soil-water storage deficit dynamics, created by evapotranspiration, and the stochastic behavior of the hydrologic response may indeed be influenced by the area partitioning o between corn and soybean.

Pesticide transport is strongly affected by uncertainties arising from the lack of knowledge of the spatial distribution of planted areas because pesticides are applied only on corn fields. Thus, area coverage of each crop type needs to be known to estimate the total pesticide mass applied across the catchment. Furthermore, pesticide loads exported at the field or catchment scales have been observed to be highly dependent on the timing of pesticide applications relative to major rainfall events [*Chiovarou and Siewicki*, 2007; *Luo and Zhang*, 2009]. Field observations in the midwestern U.S. watersheds have repeatedly shown that only few major storm events subsequent to pesticide application export the largest fraction of the total seasonal loads [*Leonard*, 1990; *Kladivko et al.*, [2001];. *Gish et al.*, 1991]. It must be noted that critical data on variations in planting and

[11] This percentage refers to the mass applied the previous year

[22] Water table control installed

application dates are not readily available for most catchments, and model implementation is often based on either calibration or estimates from data available for much larger spatial units (e.g., single county or multiple counties) [*Chiovarou and Siewicki*, 2007; *Luo and Zhang*, 2009].

4.6.1 Management parameters: land use, planting dates, application rates/date

In the case study at hand, explicit information on these parameters at the tile station was available, but specific information at the river station was missing. In brief, in odd years all the crop fields draining at station A were planted to corn, while all the crop fields drained at station B were planted with soybean – and vice versa in even years. Because atrazine is not applied to soybean fields, our analysis was limited to data from alternate years at the two stations. Information on planting dates and atrazine application rates (1.4-2 kg/ha) was also available at such scale.
In contrast, significant uncertainty existed in the estimation of: i) percent land planted to corn and soybean, ii) planting dates, and iii) atrazine application rates at the scale of the river station. Agricultural statistical data for the LVRW (490 km^2), indicate that the cropland was equally subdivided between corn and soybean. However, large-scale statistics do not often capture land use dynamics at field scales, where corn-soybean rotations may be different. We explored the effect of such variability at the river station (69 Km^2) by carrying out simulations using a 50%-50% and a 70%-30% corn-soybean rotation. The latter choice indicated that in even years 70% of the cropland was planted to corn, and 30% to soybean; and vice-versa in odd years. The choice was motivated by the inter-annual fluctuations observed in the growing season flow-averaged concentrations (i.e. growing season loads divided by growing season discharges). As shown by Table **??**, a clear pattern of greater flow-averaged concentrations of atrazine in alternate years is observed, which led to our choice of a $70 - 30$ corn-soybean rotation in the actual simulations.
In addition to land use, which defines the total mass of atrazine applied to LVRW, other important factors determine atrazine releases. In particular, the timing of application relative to major hydrologic events is known to play a key role [e.g. *Chiovarou and Siewicki*, 2007; *Luo and Zhang*, 2009]. While, the exact application dates of atrazine is often unknown, they are strongly correlated to corn planting dates [*Vasquez-Amabile et al.*, 2006; *Larose et al.*, 2007]. Planting dates are variable over the landscape, and correlated to climatic variables (rainfall and temperature). Information on inter-annual variability in planting dates over Eastern Illinois is available from the USDA National Agricultural Statistical Service, which, for each year, provides acreage planted curves (see Figure **??**). However, downscaling such information to 69 km^2 scale poses challenges arising from spatial variability. Climatic parameters are expected to be relatively homogeneous at this scale, leading to lower variability in planting dates than indicated in Figure **??**.
We considered two different ways of estimating atrazine application dates. First, we used the acreage planted curves as indicators and assumed that atrazine was applied only on the area of land that was progressively planted as reported by the curves. We then used a single planting date for each year, estimated as follows. Previous works suggested ways to estimate planting dates through climatic data, for example, *Wallace and Bressman* [1937] and *Shaw* [1977] suggested mean air temperatures of 16 C° and 14 to 15 C° respectively, for corn planting in Iowa. Here it is assumed that corn was planted as soon as a mean air temperature of 15 C° is reached, as long as this occurs after April 4th, as this was the earliest corn planting date observed by *Kucharik* [2006] in his

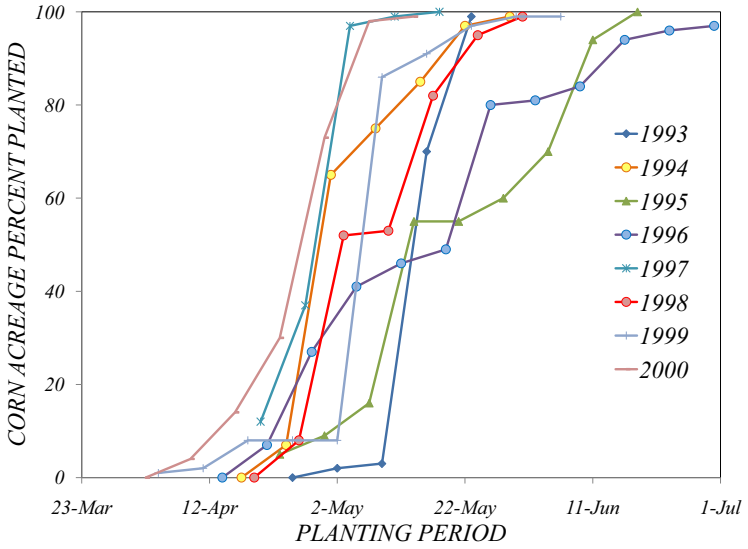

Figure 4.5: Cumulative distribution of acreage planted in the Eastern region of Illinois ($\sim 10^4\ km^2$). *USDA National Agricultural Statistical Service.*

study on the trend of corn planting dates in the Corn Belt. Application rates may vary depending on farmer choices, pesticide prices and regional regulations. The values reported in literature, regarding atrazine applications in the U.S., usually range from 1 to 3 Kg/ha [e.g., *Ribaudo and Bouzaher*, 1994]). However, for the whole State of Illinois, the application rates reported by the USDA National Agricultural Statistical Service are generally lower (Table **??**), and such values were used for our study.

4.6.2 Climatic and hydrologic parameters

Rainfall data at the sub-surface stations were based on the co-located rain-gages, while at the river station R5 rainfall was estimated via the rain-gage measurements at station C. This is the closest station where rainfall measurements are available, and is located approximately 6 km South-East of station R5. Given the relatively large drainage area, a single rain-gage station located outside the catchment may not provide accurate estimates of rainfall within the catchment, although the flat terrain somewhat simplifies the assumption of homogeneity.

Evapo-transpiration was estimated using the Penmann-Monteith Equation, modified by the FAO approach following the procedure outlined in *Basu et al.* [2010a]. Climatic data, necessary to compute evapotraspiration, were collected through METAR reports at station KCMI (ICAO code), at University of Illinois-Willard airport, (Champaign County, IL). Information on crop planting dates was available for the tile station, while it was estimated using the technique described above for the river station.

The hydrologic model required the estimation of the following parameters: (a) the depth to the

limiting layer Z, (b) the recession constant k, (c) soil-water storage characteristics (field capacity θ_{fc}, and wilting point θ_{wp}), and (d) the groundwater recharge fraction g. Information on the soil-water storage characteristics and the depth to limiting layer was obtained from Soil Survey Geographic (SSURGO) databases. Suffice here to recall that the watershed is composed of silty loam and silty clay loam soils [*Mitchell et al.*, 2003]. Because approximately 50% of the soil is characterized by a single soil type (Drummer silty clay loam, [*Algoazany et al.*, 2007]) with $\theta_{fc} = 0.35$, $\theta_{wp} = 0.22$ and $Z = 120$, we assumed LVRW to be functionally homogeneous with respect to soil characteristics, and adapted these values directly into our model at R5. Despite functional homogeneity at the scale of R5, these parameters, especially Z, can be expected to be relatively variable at the scale of the individual tile stations. For simplicity, we assumed θ_{fc} and θ_{wp} to be constant, but calibrated the results at the tile stations to estimate Z. Comparison between the calibrated Z at tile scale, and the measured Z at the watershed scale provides insight into the spatial patterns in Z that are not captured by soil databases.
The mean travel time was estimated as the inverse of the decay constant obtained by fitting hydrologic recessions with exponential distributions [*Kladivko et al.*, 2001; *Basu et al.*, 2010a] at both tile and river stations. The groundwater recharge fraction, g_f, was assumed to be zero at the tile station, whereas, at the river station it was estimated to be equal to the baseflow fraction (BF). BF was estimated from streamflow data at R5 using the filter program for BF separation [*Arnold and Allen*, 1999]. Only the first year of data in each of the tile stations was used to estimate Z (i.e. 1993 for station A and 1994 for station B), while the hydrologic model at the river station was uncalibrated, as suggested by *Basu et al.* [2010a].

4.6.3 Biogeochemical Parameters

Ranges of values for atrazine half-life, DT_{50}, and sorption coefficient, k_{oc}, were found in *Wauchope at al.* [1992] and *Hornsby et al.* [1995]. Retardation, R, is calculated as $1 + \rho k_{oc} f_{oc}/\theta$, and ranges for the bulk density, ρ, the fraction of soil organic carbon, f_{oc}, and the volumetric water content, θ, were estimated from the Soil Survey of Vermilion County [2006] by assuming that the Drummer Silty Clay Loam is the dominant soil type. The volume of the source zone, which is assumed to be constant, depends on the depth at which the pesticide is applied, as well as the average water content. Given the range of variability in these parameters, it is difficult to estimate small ranges for the parameter values. However, in order to keep the amount of information needed to a minimum, we calibrate the model to estimate these quantities using only the first year of data at Station A and then use the calibrated values for the other years in both tile and river stations. This necessarily decreases the accuracy of model predictions although is useful to evaluate the predictability of the chemical response. The mass transfer coefficient, k_e, is difficult to assess as its relationship to physical parameters is complex. *Haggerty et al.* [2004] compared estimates of mass-transfer timescales to physical characteristics of the transport process (e.g., pore-water velocities and travel times) and identified correlations between these quantities for saturated zones. In addition to these factors, for pesticide applications the mass transfer coefficient in the source zone may also be dependent on the application method employed, on the soil-water content at the time of pesticide application, as well as the cultivation method. For example, it is reasonable to assume that when the soil is wet the inter-connections between mobile and immobile phase are enhanced with respect

Table 4.3

Parameters	STATION A	STATION B
Hydrologic model		
Soil field capacity θ_{fc}	0.35	0.35
Wilting point, θ_{wp}	0.22	0.22
Depth to limiting layer, Z $[mm]$	700	600
Water travel time τ $[d]$	2.1	2.1
Fraction contributing to groundwater recharge g_f	0	0
Biogeochemical model		
Source zone volume $[mm]$	20	20
Retardation, R	4	4
Half-life, DT_{50} $[d]$	46	46

to a drier soil condition. Therefore, if pesticide applications occur after a heavy rain event the mass transfer coefficient should be larger than that relative to an application on dry soil. These dependencies are important because they endow k_e a marked variability for different applications. Given the above, we have chosen to calibrate k_e in all years of simulation and examine its yearly variation.

The application coefficient, Γ, which describes the fraction of the pesticide that partitions into the mobile zone at the time of application, is also related to the application techniques and the tillage methods, as well as the antecedent soil-water content of the top soil layer during the application. In this study we assume that atrazine is only applied onto the immobile domain ($\Gamma = 0$). This assumption may be justified by acknowledging that, on bare soil, evaporative losses tend to dry soil faster than in deeper layers. Therefore, the applied pesticide – which is in the dissolved phase – is likely to first fill the micro-pores of the diffusive zone. As a further justification for this assumption, preliminary simulations were run with the model and the results were compared with the LAPU (load as a percent of used) values observed by *Capel and Larson* [2001]. The tests showed that to reproduce the physical values of LAPU, the application coefficient, Γ, needs to be relatively small (i.e., $\Gamma < 0.1$).

A summary of the main hydrologic and biogeochemical parameters used in the analysis is presented in Tables **??** and **??**.

4.7 Interpretation of Model Results

4.7.1 Model Performance Evaluation

The performance of the hydrologic model is evaluated by comparing observed daily hydrographs with predicted ones, as customary. The evaluation of the biogeochemical model is based on comparative analysis of computed/measured loads and flux concentrations at the control sections. Both are in fact relevant measures of environmental risk, as loads are responsible for chronic stresses of

Table 4.4

Parameters	Station R5
Hydrologic model	
Soil field capacity θ_{fc}	0.35
Wilting point, θ_{wp}	0.22
Depth to limiting layer, Z $[mm]$	1200
Water travel time τ $[d]$	2.5
Fraction contributing to groundwater recharge g_f	0.4
Base flow recession constant α $[d^-1]$	0.07
biogeochemical model	
Source zone volume$[mm]$	20
Retardation, R	4
Half-life, DT_{50} $[d]$	46

aquatic ecosystems, whereas acute exposure hazards are related to concentration levels.
The efficiency criterion used for calibration is based on the mean absolute error, as we divide the index by the mean value of the set of observations in order to compare different sets, yielding the mean relative error (MRE) defined as:

$$MRE = \frac{\sum_{i=1}^{N} |X_i - Y_i|}{N\bar{X}_i}, \tag{4.16}$$

where X_i and Y_i are, respectively, the i^{th} observed and predicted values, N is the size of the dataset and $\bar{X}_i$ is the mean observed value. The evaluation of the hydrologic predictions relies on both MRE and the Nash-Sutcliffe efficiency coefficients, E_{NS}, defined as:

$$E_{NS} = \frac{\sum_{i=1}^{N}(X_i - Y_i)}{\sum_{i=1}^{N}(X_i - \bar{X}_i)}. \tag{4.17}$$

Such criterion was not used to evaluate the biogeochemical predictions because concentration datasets have a relatively small size and high variance, producing unreliable evaluations via E_{NS}. Performance indicators relative to the analyses at station A, B and R5 are reported in Table **??** and **??**.

4.7.2 GLUE methodology for sensitivity analyses

The sensitivity analysis of the model parameters was carried out using the Generalized likelihood Uncertainty Estimation (GLUE) approach [*Beven*, 2001]. The rationale of the method is as follows: in modeling physical processes, there usually exist several parameter sets that give equally acceptable predictions, i.e. the equifinality assumption [*Beven et al.*, 1996], and, in practice, the concept of an optimal parameter set is considered misleading. Additionally, the importance of each

parameter in achieving acceptable predictions may be very different, providing motivation for a robust sensitivity analysis.
The GLUE approach consists of running a large amount of model simulations where, for each of them, the value of all the parameters is randomly drawn from a feasible range. By comparing predictions with data, for each simulation the efficiency of the model is evaluated by a suitable efficiency criterion. This procedure generates a large set of values of efficiency indicators based on random parameter sets. A cutoff is then defined, somewhat arbitrarily, to divide simulations into a behavioral and a non-behavioral set. Finally, the cumulative probability distributions for each parameter in the behavioral and non-behavioral sets are computed. Comparison of such distributions provides an evaluation of the model sensitivity to the parameters considered, as indeed the more different are the distributions, the more sensitive is the model to that particular parameter.

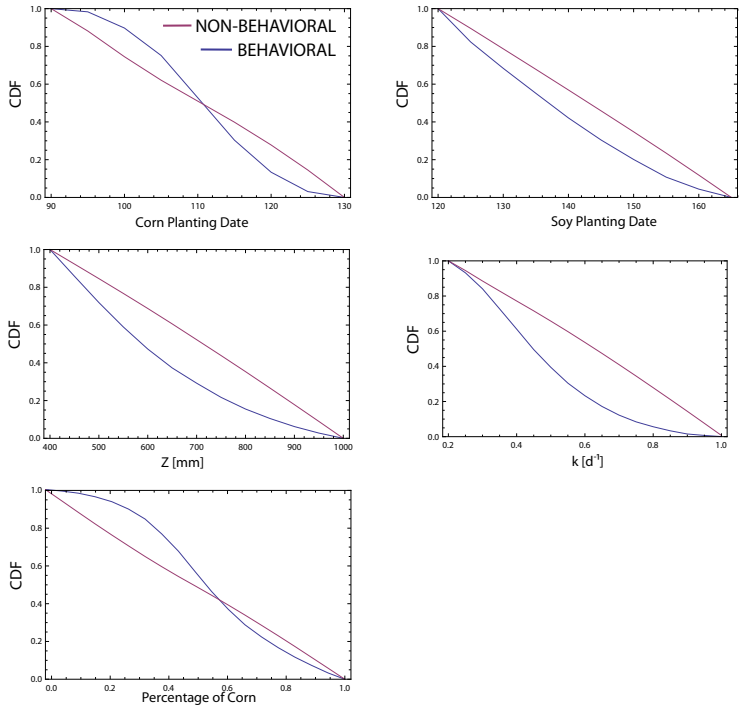

Figure 4.6: Sensitivity analysis on the parameters of the hydrologic model through the GLUE methodology.

We have applied this method to the hydrologic and chemical data collected in 1993 at the LVRW tile station A. Parameters are randomly picked within the ranges defined in Table **??** and the efficiency of simulations is evaluated through the MRE index. Once the cutoff criterion is defined, all the simulations that yield a MRE lower than the cutoff criterion are labeled as behavioral (all others are considered non-behavioral). Results of the GLUE analysis are sensitive to the choice of the cutoff criterion. In this analysis we have used a cutoff equal to the 10^{th} percentile of the distribution of MRE's produced with the hydrologic and biogeochemical simulations, that is,

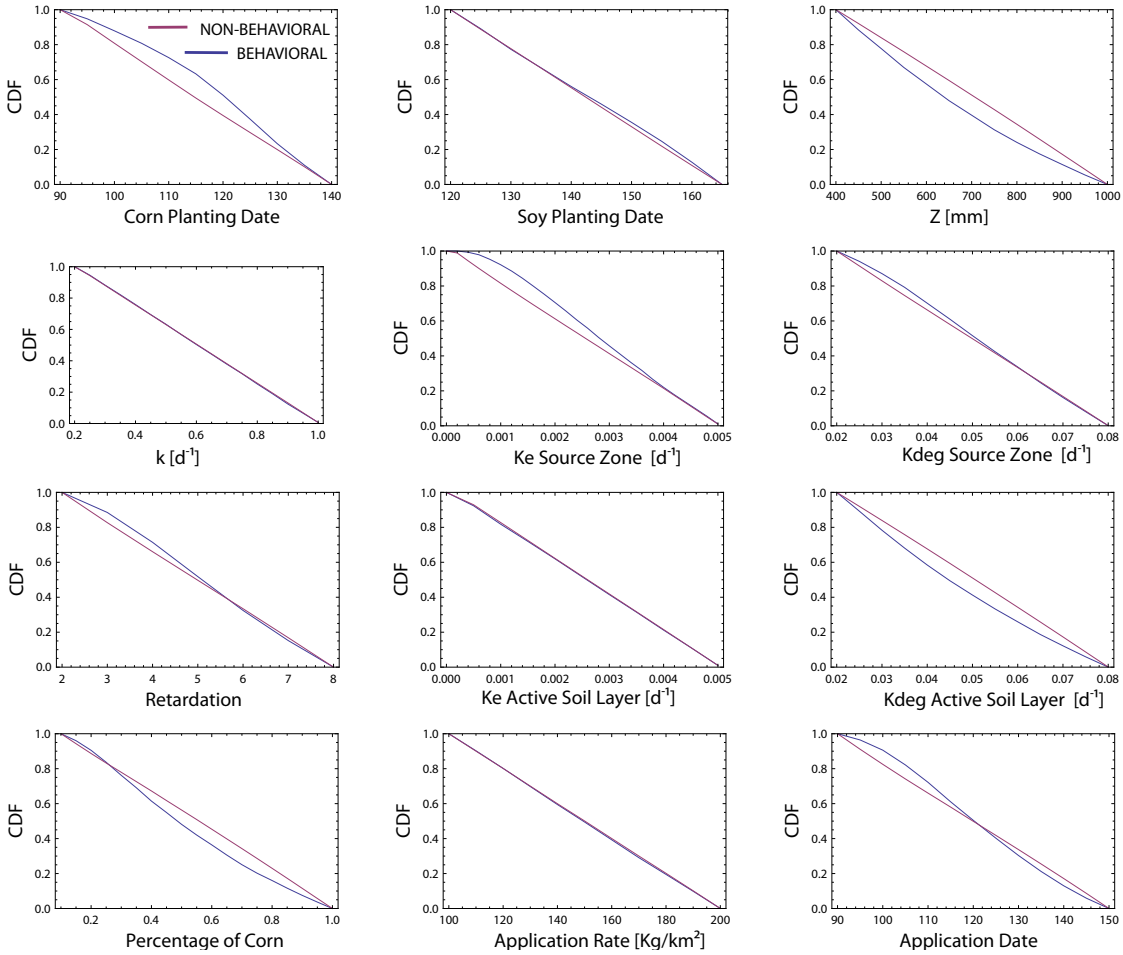

Figure 4.7: Sensitivity analysis on the parameters of the biogeochemical model through the GLUE methodology.

respectively, $MRE = 0.67$ and $MRE = 0.5$.

Table 4.5: Ranges of parameters used for the GLUE analysis.

Parameter	Lower bound	Upper bound
Z $[mm]$	400	1000
Corn planting date	April, 1	May, 15
Soy planting date	May, 1	june, 15
k $[d^{-1}]$	0.2	1
Percentage of land planted with corn	0.1	0.9
k_e source zone $[d^{-1}]$	0.0005	0.005
k_e active soil layer $[d^{-1}]$	0.0005	0.005
k_{deg} source zone $[d^{-1}]$	0.02	0.08
k_{deg} active soil layer $[d^{-1}]$	0.02	0.08
R	2	8
Atrazine application rate $[Kg/km^2]$	100	200
Atrazine application date	April, 1	May, 15

Cumulative distributions obtained with the GLUE method for each of the hydrologic parameter are reported in Figure **??**. The plots suggest that the most important control on the hydrologic response prediction is given by water recession constant, k, followed by the depth to the limiting layer, Z, and then by the crop, which is here represented by corn and soy planting date as well as the percentage of land-use. The importance of the parameters stressed by the GLUE analysis is to be understood in terms of equifinality. For example, the analysis shows that the choices of k affect model predictions more than those of Z. This was expected because the role of Z is mainly that of reducing/increasing the volume of effective runoff and this effect is partially produced also by land-use percentages or by planting dates. On the other hand, none of the other parameters is capable of reproducing the effects of k (that is, capable of modifying hydrograph recessions).
The sensitivity analysis applied to the biogeochemical model refers to 12 parameters: Z, k, soy and corn application date, mass transfer rate constant, k_e, in the source zone and in the transport zone, degradation rate constant, k_{deg}, in the source zone and in the transport zone, atrazine application rate and date, retardation, R, and land use. In such analysis we differentiate between mass transfer and degradation coefficients in the source and in the active soil layer. However, when applying the model to our dataset, in order to reduce the number of parameters, we no longer make this distinction. Results for the biogeochemical model (Figure **??**) suggest that acceptable predictions are insensitive to the choice of soy planting date, the water mean travel time, the mass transfer coefficient in the active soil layer, and the application rate. In other words, the effects of these parameters are clouded by the global effect of the whole set of parameters. For example, for each value of the application rate there exist a set of parameters that produces, with equal probability, a behavioral and a non-behavioral prediction. In fact, the only effect of the application rate is to increase or decrease the atrazine concentration and the same effect is achieved, for example, by the percentage of land planted with corn (because atrazine is only applied to corn fields).
The analysis also shows that behavioral concentration prediction essentially does not depend on the value of the mass transfer rate constant in the active soil layer (Figure **??**). This gives a further

motivation for the choice of the preferential flow scheme over the perfect mixer scheme. This choice is also in accord with field observations and modeling exercises that emphasize fast preferential flow [*Kladivko et al.*, 2001]. Among the parameters of the biogeochemical model, the mass transfer rate constant in the source zone, the depth, Z, the degradation rate in the active soil layer, and land-use seem to be the most relevant as the probabilities of behavioral and non-behavioral predictions for these parameters are markedly different.
Overall, the GLUE analysis shows that, in the hydrologic model, all the parameters considered have an important impact on model predictions whereas a significant degree of equifinality is present among the parameters of the biogeochemical model. This implies that for the biogeochemical model the calibration of specific parameters can make up for the lack of knowledge of other parameters and still produce satisfactory results. However, when the overall purpose of the model is simply to predict the response of the physical system, calibration should be minimized if not removed. The effect of each parameter has to be taken into account and, given the high degree of equifinality of the biogeochemical parameters, such variables require a careful estimation.

4.7.3 Tile Stations

The ability of the model to predict daily discharges, atrazine concentrations and loads was evaluated during the cropping season (April-October) in the years 1993 - 1998, at both tile stations. The years 1997 and 1999 were not considered in our analysis because in 1997 a water table control was installed, while 1999 was a relatively dry year where no significant rainfall event was observed.
The hydrologic model was calibrated for the depth to the limiting layer only for the year 1993. The remaining five years were used exclusively for model validation. Calibration was done by minimizing the mean relative error (MRE) between observed and predicted daily discharge values.
The biogeochemical model was calibrated to estimate R, DT_{50} and the depth of the source zone, Z_s, at station A for the year 1993. The calibrated R, DT_{50}, and z values were then used for all years, and at both the tile stations and the river station. The mass transfer exchange parameter is difficult to estimate at the field scale and was thus calibrated for all years at all locations. The range of variability in the calibrated mass transfer was explored.
Figure **??** shows the comparison between observed and predicted daily hydrographs at station A (a, c) and station B (b, d, e). The model, in general, was able to reproduce the measured trends; however, few flow events were not well captured. In 1994, for example, the higher peaks were underestimated whereas the opposite behavior was noted in 1998. Model performance is evaluated using E_{NS} and MRE (Section **??**). Following, *Van Liew and Garbrecht* [2003], the results may be considered good if $E_{NS} \geq 0.75$ and satisfactory if $0.35 < E_{NS} < 0.75$. Using this evaluation criterion the predictions are, in most of the cases, satisfactory, except for the prediction of the year 1998, that shows a negative E_{NS}. Negative values of E_{NS} imply that the observed mean in the dataset is a better predictor than the model. The predictive ability of the model (see Table **??**) is very satisfying, considering that a single calibration parameter (i.e. $Z = 700$ mm at station A and $Z = 600$ mm at station B) based on a single year of data was used. This is in contrast to most catchment- scale hydrologic models that use a large number of parameters (e.g. SWAT, *Arnold et al.* [1993]) and consistent with our philosophy of parsimony.
For each year, we calibrated the mass transfer rate constant, k_e by minimizing the MRE between

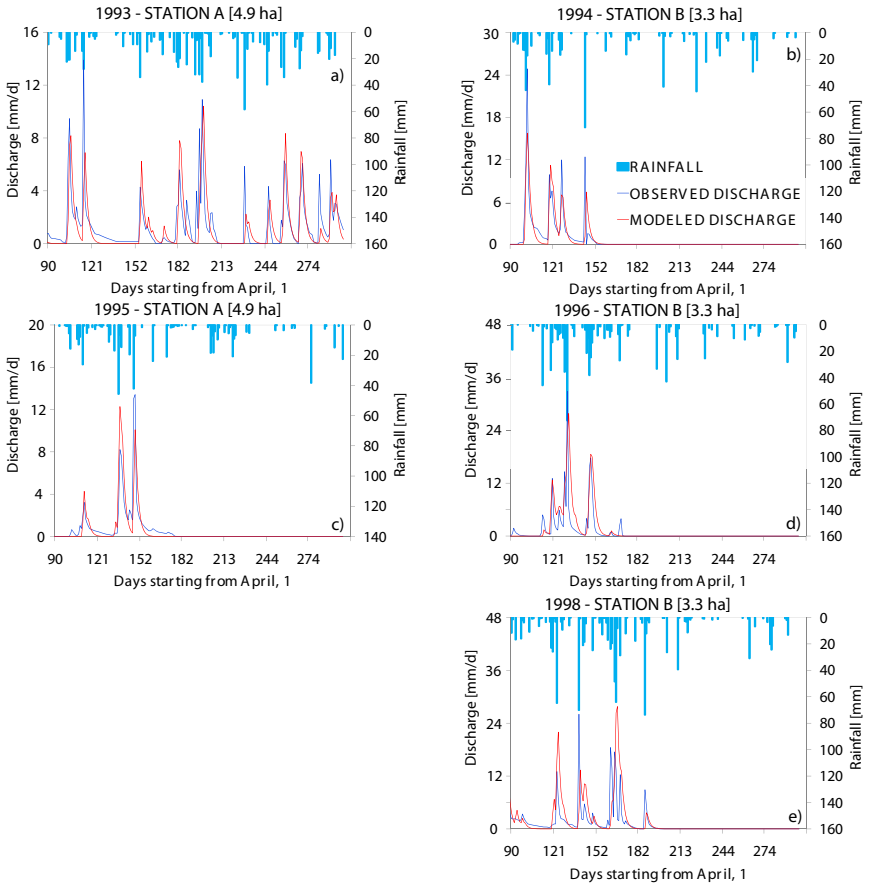

Figure 4.8: Comparison between observed and predicted hydrographs at station A (a, c) and station B (b, d, e). Soil properties were obtained from SOLIM simulations in the LVRW, except the depth to the limiting layer, Z, which was calibrated to fit the data: $Z = 700$ $[mm]$ at station A; $Z = 600$ $[mm]$ at station B. Year 1997 and 1999 are not shown because, in 1997 water table control was installed and therefore we did not model it, whereas 1999 was a relatively dry year and no significant discharge events were observed.

predictions and observations, while the other biogeochemical parameters were calibrated using only the first year of data at station A. This gives a range of variability for k_e and allows to evaluate the sensitivity of the model to such parameter. In general, k_e can be calibrated in order to minimize either the MRE of concentrations predictions or the MRE of loads predictions. Available concentration measurements represent water samples collected instantaneously, therefore, given their relatively high variability, the comparison with concentrations predicted at the daily time scale at which the model is run may not be completely significant. For this reason, an integrated metric has been preferred. Our data, as well as previous works [e.g. *Kladivko et al.*, 2001] show that the highest pesticide loads usually occur right after application closely followed by intense storms.

We thus calibrated k_e considering only the early period after application, when most of the annual pesticide losses are released. For an objective evaluation, we considered the period in which 80% of the total annual losses is released. Such period is usually short, ranging from 17 days in 1994 to 46 days in 1998, the only exception being the year 1993 when it lasted 190 days.

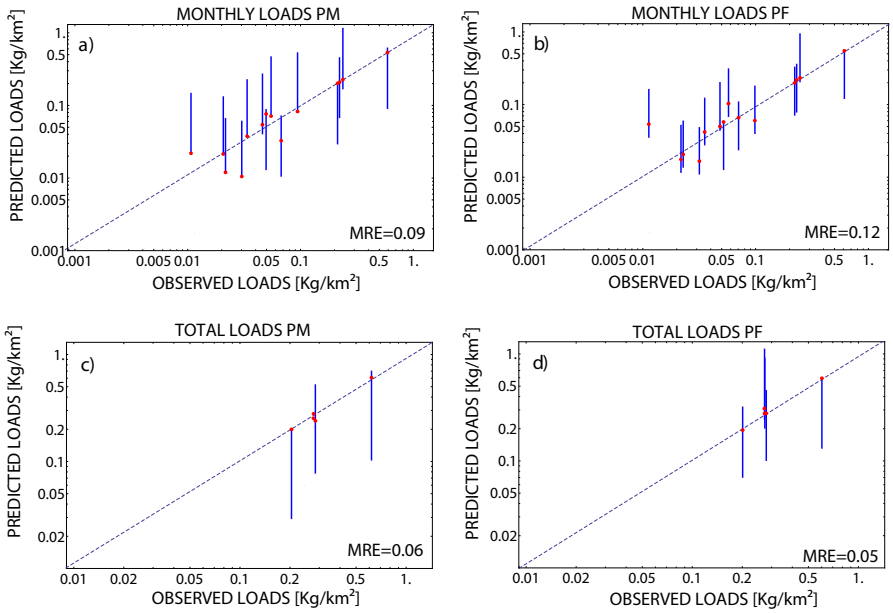

Figure 4.9: Comparison between simulated and observed loads accumulated on monthly (a,b) and seasonal (c,d) time scale with the perfect mixer (a,c) and the preferential flow (b,d) scheme, after calibrating k_e (red dots). k_e's are calibrated by comparing observed and predicted monthly loads. The bars represent the maximum deviations from the actual loads, using all the calibrated k_e's. The axes are represented in a logarithmic scale.

Figure **??** illustrates the comparison of monthly and total loads obtained using the perfect mixer (PM) (a, c) and the preferential flow (PF) (b, d) schemes (see Section **??**). Note that the parameter k_e is calibrated on a monthly basis except in those years when 80% of the annual loads is lost in less than a month (e.g. 1994). For each year a different value of k_e is obtained by calibration. In Figure **??** the dots represent the loads simulated with the calibrated k_e whereas the bars represent the maximum deviation between predicted and observed loads using the k_e's calibrated in all the years. Values of k_e range from $9 \cdot 10^{-4}$ to $62 \cdot 10^{-4}$ $[d^{-1}]$ for the PM scheme and from $6 \cdot 10^{-4}$ to $18 \cdot 10^{-4}$ $[d^{-1}]$ for the PF scheme. In general, a good agreement between estimated and simulated atrazine loads was noted, the 1:1 dashed line represents optimal prediction, and is captured by the confidence interval in most cases. The overall MRE's for each set of simulations are reported in the graphs and show that the performance of the two schemes discussed are equally good. It should be noted, however, that the range of k_e's calibrated for the PF scheme is significantly smaller than that calibrated for the PM scheme. A narrow range of values for k_e is an encouraging result because

suggests a rather invariant (in space and time) character of such parameter, which is indeed an indicator of robustness of the proposed framework.

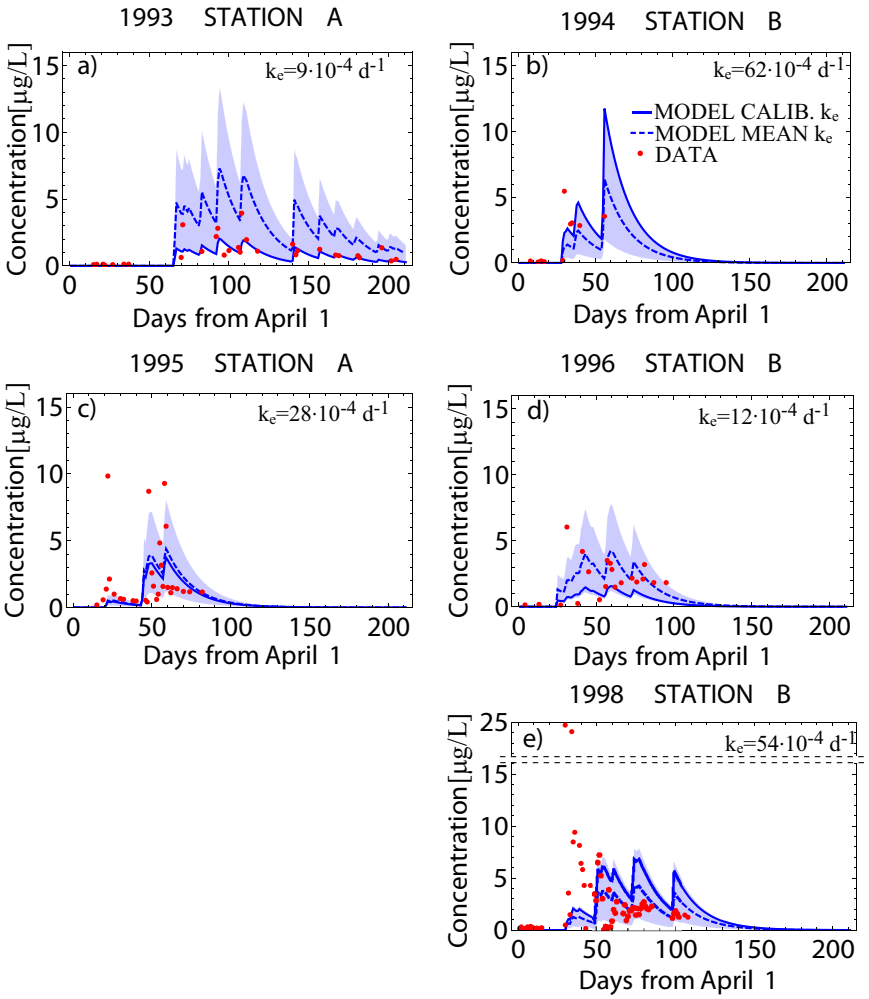

Figure 4.10: Observed and predicted concentrations at station A (a, c) and station B (b, d, e) with the perfect mixer scheme. The shadowed area represents all possible predictions with any k_e comprised between the minimum and the maximum values calibrated in all the years. Year 1997 and 1999 are not shown because, in 1997 a water table control was installed and therefore we did not model it, whereas 1999 was a relatively dry year, only one concentration measurement is available. The dashed lines represent the concentration prediction using a k_e averaged among all the calibrated k_e's, i.e. $k_e = 33 \cdot 10^{-4}$.

Figures **??** and **??** show the comparison between observed and predicted concentrations, using k_e's calibrated with monthly loads. Given the limited number of concentration measurements it is difficult to compare predictions with observations. The figures report the predictions with the

Table 4.6: Efficiency in model predictions at station A and B: Nash and Sutcliffe efficiency coefficient, E_{NS}, and Mean Relative Error, MRE. E_{NS} is used only for discharge, MRE is used for discharge, and concentrations. Both the perfect mixer (PM) and preferential flow (PF) scheme are shown.

year	**Discharge** E_{NS}	**Discharge** MRE	**Atrazine concentration, PM** MRE	**Atrazine concentration, PF** MRE
1993	0.39	0.66	0.51	0.55
1994	0.69	0.79	2.23	1.38
1995	0.67	0.61	0.83	0.76
1996	0.4	1.53	0.85	0.93
1998	-0.36	1.52	1.58	1.01

calibrated k_e (solid lines) as well as the band of predictions obtained with any k_e comprised between the maximum and the minimum calibrated value among all the years (shadowed areas). This gives a visual representation of the sensitivity of predictions to k_e but also allows to evaluate the maximum errors in prediction that one may make by calibrating k_e using only one year of data. Figures **??** and **??** (except panel f) also show predictions produced with a k_e averaged among the calibrated k_e's (dashed lines in figure), i.e. $k_e = 33 \cdot 10^{-4}$ for Figure **??** and $k_e = 9.6 \cdot 10^{-4}$ for Figure **??**. Averaged k_e's, especially for the PF scheme, provide relatively good predictions, which is encouraging, given the difficulties in estimating such parameter. It should be observed that in the case of the year 1996 the prediction yielded by the averaged k_e is even better than that relative to the calibrated k_e, this can be explained considering that in 1996 discharge is generally over-predicted and, since k_e is calibrated using the loads, this translates into a biased evaluation of the parameter.
The MRE's of predictions obtained with the preferential flow scheme (see Table **??**) are, on average, lower than those relative to the perfect mixing scheme. Given also the fact that the range of k_e's calibrated with PF is narrower than the range calibrated with PM, we argue that the preferential flow scheme should be preferred to the perfect mixing scheme.
Overall, the main weakness of the model seems to lie in the prediction of the early peaks of concentration, which are not always captured satisfactorily. This may be attributable to the different scales at which the model and the data collection work, as model predictions are averaged on a daily basis whereas the scale of observation is that of the water samples, which in this context may be considered instantaneous. Additionally, a value of the initial partition coefficient, Γ, different from zero may provide a better prediction of the early peaks as some atrazine would be readily available to the rainfall coming through the source zone. For example, we note that at station B in 1998 (Figure **??**) the first peak of concentration is significantly larger than the concentration values observed in other years and at other stations. Such a large event may be explained by considering that in 1998 a very intense rainfall event occurred only 3 days after the pesticide application and, therefore, was likely to carry along a large amount of pesticide mass just applied. On this basis, it can be argued that, in that case, a significant amount of mass was already available for transport right after application, and this also explains why the model could not predict that extreme event using $\Gamma = 0$. Figure **??**f reports the chemograph predicted in 1998 assuming $\Gamma > 0$, in this way,

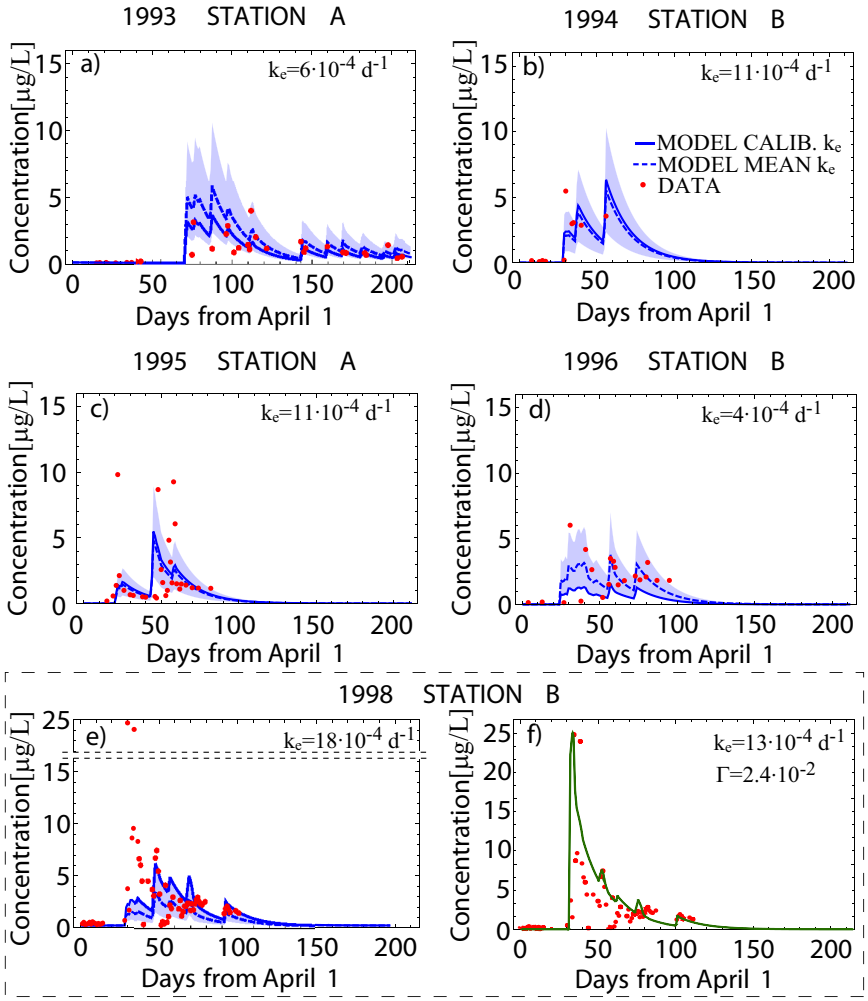

Figure 4.11: Observed and predicted concentrations at station A (a, c) and station B (b, d, e) with the preferential flow scheme. The shadowed area represents all possible predictions with any k_e comprised between the minimum and the maximum values calibrated in all the years. The dashed lines represent the concentration prediction using a k_e averaged among all the calibrated k_e's, i.e. $k_e = 9.6 \cdot 10^{-4}$. Panel f) shows the prediction obtained with $\Gamma > 0$, i.e. assuming that a fraction of pesticide mass is applied into the mobile domain.

both the first high peak of concentration as well as the later events can be captured. A similar improvement due to $\Gamma > 0$ can be achieved also in the other years (not shown), however, the values of Γ, adjusted to fit the data, vary over an order of magnitude and are difficult to estimate on the basis of phenomenological criteria. Reasonably, Γ could be related to the pesticide application method and to the water content of the shallow soil layer before pesticide application.

Table 4.7: Efficiency of model predictions at station R5: Nash and Sutcliffe efficiency coefficient, E_{NS}, and Mean Relative Error. E_{NS} is used only for discharge, MRE is used for discharge, loads and concentrations. Three different planting/application schemes are shown.

year	Discharge E_{NS}	Discharge MRE	Atrazine monthly loads MRE	Atrazine concentrations MRE
Single planting/application dates				
1993	0.25	0.61	0.75	0.83
1994	0.53	1.01	0.87	1.54
1996	-1.5	2.36	0.16	1.03
1998	-0.44	1.03	0.14	0.86
Distributed planting/application dates				
1993	0.11	0.65	0.75	0.7
1994	0.62	0.60	0.94	0.58
1996	-0.53	1.63	0.88	0.75
1998	0.66	0.73	0.26	1.23
Distributed planting/application dates, 70-30% corn-soybeans				
1993	0.12	0.64	0.74	0.70
1994	0.62	0.61	0.92	0.61
1996	-0.44	1.55	0.88	0.76
1998	0.7	0.71	0.2	1.28

4.7.4 River Station

We deliberately kept the hydrologic model un-calibrated in the analysis at the river station, whereas for the biogeochemical predictions we calibrated only the mass transfer coefficient, k_e, keeping all other parameters equal to those used at the tile stations.

Hydrographs are presented in Figure **??**, while the predictions of the biogeochemical model are presented in Figure **??** (loads) and Figure **??** (concentrations). In each of these figures, three different cases are simulated, corresponding to different management scenarios, to evaluate the effect of such uncertainties on model predictive ability. These are: (a) Single corn planting and application date and $50\% - 50\%$ corn-soybean split, (b) distributed planting dates and $50\% - 50\%$ corn-soybean split, and (c) distributed planting dates and $70\% - 30\%$ corn-soybean split. Details on methodology for estimation of the planting dates are presented in Section **??**.

Hydrologic predictions are minimally affected by the choice of land-use percentage (Figure **??**). However, a more clear difference can be seen between a single corn planting date and a distributed corn planting dates scheme, in fact, more events are usually predicted with the single planting date scheme. This result suggests that the crop growth stage evolution may be more important than the maximum rooting depth for predicting discharges. In general predictions are less accurate

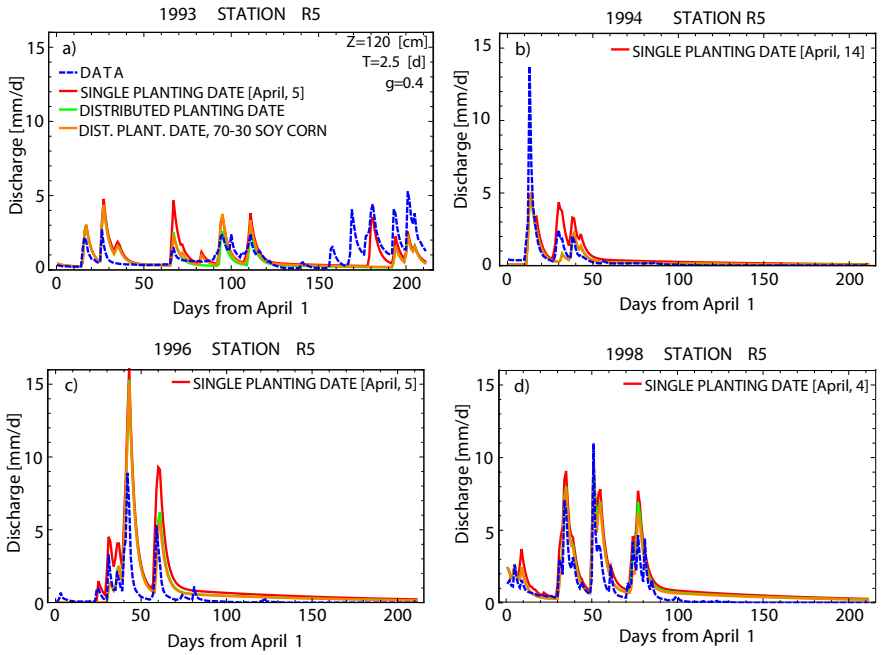

Figure 4.12: Comparison between observed and predicted discharge at the river station. The dashed line represents data, whereas the other lines represent in order: 1) discharge predictions with a single corn planting date and $50\% - 50\%$ corn-soybeans; 2) discharge predictions with distributed corn planting dates and $50\% - 50\%$ corn-soybeans; 3) discharge predictions with distributed corn planting dates and $70\% - 30\%$ corn-soybeans.

than those relative to the tile stations (see performance indicators in Table **??** and **??**). A full calibration of the hydrologic parameters does improve predictions in 1993 and 1998 (not shown), but no difference in the performance of the calibrated and the uncalibrated model is observed in 1996 and 1997. This suggests that poor predictions may be attributable to the rainfall data collected at station C, which is located outside the drainage area of station R5 and, therefore, may not be reliable.

Given the results obtained with the analysis at the tile stations, for station R5 only the preferential flow scheme was applied for the biogeochemical model. Comparisons between predicted and observed monthly loads are reported in Figure **??** for the three planting/application schemes. Each plot represents all the years considered (1993, 1994, 1996, and 1998), and the reported MRE indicates the overall performance for all the years. The plots report the mass transfer coefficient, k_e, calibrated for each year and for each scheme, using only the preferential flow conceptualization. Dissimilarly from the tile station simulations, the values of k_e are relatively different from year to year. Quality of predictions is rather similar for the three different management schemes.

Similarly to the hydrologic model, the choice of land-use proportion does not seem to affect concentration predictions (Figure **??**). This result is not surprising because the hydrologic simulations

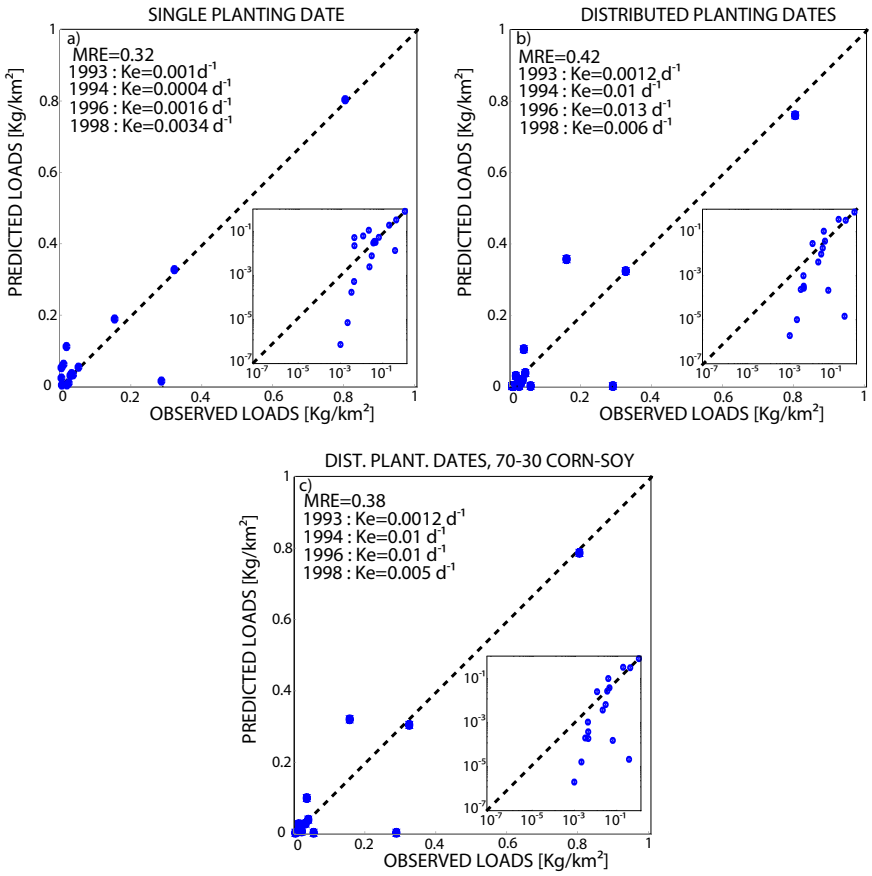

Figure 4.13: Comparison between observed and predicted monthly loads at the river station using the preferential flow scheme. The three plots represent the single planting date scheme (a), the distributed planting dates scheme (b), and the distributed planting dates scheme with $70\% - 30\%$ corn-soybeans proportion (c). Each plot represents the comparison between predictions and observations for 1993, 1994, 1996, and 1998. The mass transfer coefficient, k_e, is calibrated every year, its values are reported in figure. The dashed line is the $1:1$ diagonal. In each plot the mean relative error (MRE) relative to all the years of simulation is reported. The insets show the same plots using a logarithmic scale for the axes.

have already shown that land-use percentage has a small effect on discharge, therefore, the only effect expected in the biogeochemical simulations is simply a uniform variation of simulated loads, which is generally clouded by the calibration of the mass-transfer coefficient, k_e. On the other hand, when considering single vs. distributed planting/application schemes, we note a rather evident difference in the predictions. The largest errors are always observed in correspondence to the first concentration peaks of each year. In some cases this is attributable to a wrong estimation of pesticide application dates, for example in 1994 it is clear that the actual application occurred earlier than when it was estimated. On the other hand, in both 1996 and 1998, the distributed

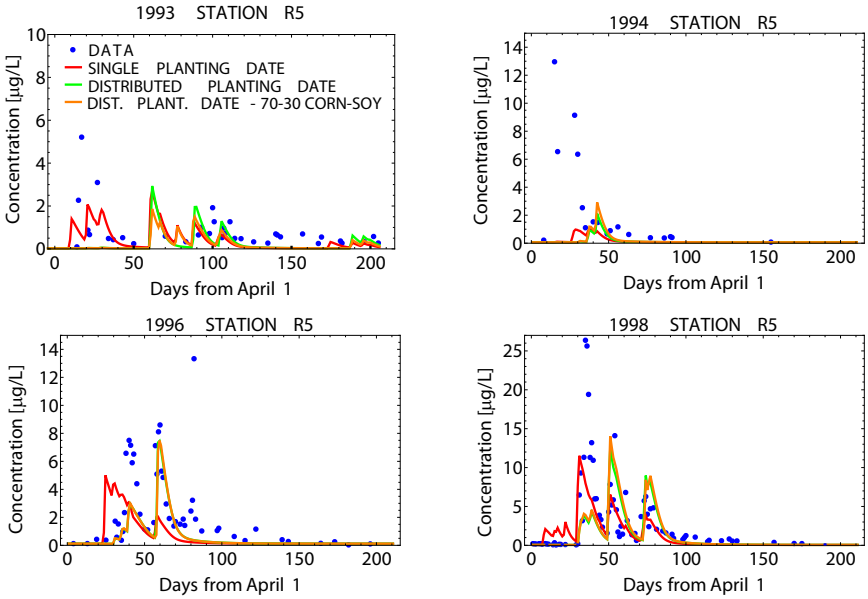

Figure 4.14: Comparison between observed and predicted concentrations at the river station using the preferential flow scheme. The dots represent data, whereas the other lines represent in order: 1) discharge predictions with a single corn planting date and $50\% - 50\%$ corn-soybeans; 2) discharge predictions with distributed corn planting dates and $50\% - 50\%$ corn-soybeans; 3) discharge predictions with distributed corn planting dates and $70\% - 30\%$ corn-soybeans.

planting date schemes captured all the peaks even though the first ones are consistently under-estimated. Given the fact that the magnitude of later concentration peaks is captured fairly well, the under-estimation of the first peaks may be attributable to the presence of a certain amount of mass readily available for transport right after the application (i.e. $\Gamma > 0$), analogously to what was observed at the tile stations. Additionally, when the hydrologic model does not properly predict a discharge event for whatever reason, the respective concentrations are obviously poorly predicted by any management scheme (e.g., year 1993 and 1996). Overall, given the uncertainties in the estimation of the actual application date it is difficult to give a preference to one scheme over the other, however, the results in Figure **??** suggest that lacking of any better information the distributed planting dates scheme should be preferred.

The indices of performance (E_{NS} and MRE) are reported in Table **??** for discharge, loads and concentrations. Discharge was usually better predicted using distributed planting dates than using a single planting date based on temperature, even though the goodness of predictions did not change much for different planting schemes. On the other hand, for the biogeochemical model the MRE's relative to the three management schemes are not significantly different.

Chapter 5

Conclusions

This thesis aims at investigating the dominant controls on transport phenomena at the catchment scale by means of novel modeling tools applied to suitable case studies. Provided models are meant to give insight into physical processes that are still unclear, thus primarily acting as learning rather than predicting tools.

Long term effects of hydrologic fluctuations are captured by stochastic models in terms of steady state statistical distributions of relevant physical quantities. This modeling approach provides a causal relationship between daily rainfall random fluctuations and daily streamflow variability, this, in turn, relates to the variability of stream stage, in-stream nutrients removal, and the annual Horton index, which indicates the efficiency of vegetation water use.

Analytical expressions for the annual flow duration curve and for the exceedance probability of the annual minima in river basins have been derived through few physical (spatially and temporally averaged) parameters with clear physical meaning. The distributions depend upon the ratio between runoff frequency and the inverse of the mean catchment residence time, namely λ and k respectively, and on the parameter γ which defines the inverse of the mean runoff jump in correspondence to a rainfall event. While γ is simply a scale parameter, the ratio λ/k defines a 'wet' (when $\lambda/k > 1$) and a 'dry' (when $\lambda/k > 1$) condition of the catchment. The comparison of the analytical expression derived for the annual flow duration curve with the corresponding statistics obtained from field data measured in the Jacob Fork catchment suggests that the model developed is able to reproduce the observed flow duration curve for a broad range of durations. From the comparative analysis with flow observations, it is suggested that the use of a single, average timescale to model the underlying subsurface groundwater transport processes may often underestimate durations for both the highest and the lowest flows. Nevertheless, the duration of the smallest streamflows may be correctly reproduced by the analytical model by simply relating the transport parameter of the analytical model to the mean residence time of the slow groundwater contribution to runoff, which determines the probabilistic structure of the lowest flows.

The stochastic nature of the climate-landscape interactions has been linked to the intra-annual variability of the stream stage, h, and, in turn, to the effective removal rate constant, k_e by extending the presented ecohydrolgical framework. Accordingly, rainfall is seen as the major stochastic driver of the hydrologic processes occurring in a river basin. using the power function relationship between

stream discharge and stage ($h = aQ^b$) and the derived relationship between stage and first-order rate constant ($k_e = v_f/h$), novel exact expressions for the pdf's of h and k_e have been developed. Limited experimental data [*Doyle*, 2005] and deterministic modeling [e.g., *Bohlke et al.*, 2008] suggest intra-annual fluctuations in nutrient losses due to variability in stage. The stochastic framework presented helps to explore the full range of variability of hydrologic conditions. Quantifying the variability of k_e induced by stage fluctuations addresses the problem of the representativeness of k_e estimates derived from single-tracer measurements. Streamflow regimes characterized by larger λ/k values exhibit more stable h and k_e values and thus require fewer measurements within a year to characterize the mean annual nutrient loss dynamics. Dry streamflow regimes, on the other hand, exhibit more variable h and k_e, and larger number of measurements would be required to sample the entire range of inter-annual variability in hydrologic conditions.

This stochastic approach has been further extended to investigate the effect of the intra-annual variability of interactions between rainfall, soil moisture, and soil water-losses, on the inter-annual variability of water balance. The water balance was considered in terms of the annual Horton index, which has been characterized probabilistically through its analytical probability density function. The theoretical framework developed allows for the probabilistic structure of vegetation water use to be linked with spatially averaged parameters with clear physical meaning. The analytical solutions have been tested against estimates from 431 catchments distributed across the continental United States for which basic water balance data (i.e., precipitation, streamflow, potential evaporation) are available at the daily resolution for over 50 years. A generally good agreement has been observed between the model predictions of the mean of the Horton index and estimates from the data. Also the observed inter-annual variability, expressed as its standard deviation, was captured, although in this case higher uncertainties are observed when considering the single catchments.

The model was also used to estimate the catchment soil storage capacity, a key parameter of the model, through an inverse modeling procedure. The soil storage capacity was estimated for all the 431 sites and the estimates from the model showed clear regional patterns, which while interesting, remain to be validated through field explorations.

A sensitivity analysis showed that the climatic humidity index (i.e., the ratio of mean annual precipitation to mean annual potential evapotranspiration) is the main control on the mean of the Horton index, in agreement with the previous work of *Troch et al.* [2009]. The soil storage capacity (i.e., the ratio of soil storage capacity to mean annual precipitation) seems to have an important impact on the mean annual water balance only in water limited environments, whereas frequency of rainfall events within the year does not seem to affect the mean annual water balance under any circumstances. The inter-annual variability (i.e., standard deviation of the Horton index) is strongly related to both the humidity index, and the mean number of rainfall events, whereas it is affected by a dimensionless soil storage capacity only in dry climates.

An analysis on the errors of the model showed that there exist regions where the within-year variability of water partitioning is the major control on inter-annual variability of water balance as well as on the buffering effect, and regions where the role of within-year variability on inter-annual variability of the Horton index seems to be not so clear. This separation seems to be strongly related to the competition between the atmospheric demand and the water availability. This analysis shows that the observed inter-annual variability may arise from mechanisms other than the simple scaling-

up of short-term processes. In particular, in arid sites random daily rainfall variability is not the main control on inter-annual water balance variability and there exist other more important sources of variability that need to be taken into account. Since there is a consistent overestimation of the variability of the Horton index in drier regions we suggest, following previous work, that vegetation functioning, including likely adaptations to water stress in water limited environments, may be the cause of the observed low variability of inter-annual vegetation water use.

A deterministic approach was used to evaluate the water-mixing mechanisms within the soil, as well as the effect of anthropic management on solute transport at the catchment scale. The role of hydrologic and biogeochemical processes was explored by means of novel, process based models, which proved useful tools to evaluate the dominant controls of transport phenomena within catchments.

A catchment-scale tracer study using lithium from a point injection and nitrates from diffuse sources at catchment scales has been carried out and analyzed. The processes were modeled using a mass response function (MRF) approach, whose main idea is that the solute release from hydrologic units comprising soil is largely controlled by the time allowed for the exchange between immobile and mobile phases. The modeling framework adopted allows reproducing satisfactorily observed flux concentrations of different tracers resulting from localized or diffuse injections, and allows useful indirect inferences on the overall transport mechanisms determining solute release through runoff at the scale of the catchment.

Four different functional types of age-structures were examined and their impact on the flux concentration at a control section where runoff was collected is explored. The analysis suggested that runoff is composed by a collection of water particles with a mixture of ages. No clear signs of the presence of dominant ages have been tracked. The experiment also suggested that, in this case, the effect of unmixed preferential flows could be ruled out. the indirectly detected presence of old water proved crucial to mimic the flushing of solutes originally stored in soils, while new water underpins the behavior of non-native tracers deriving from point injections. Initial and boundary conditions of plot- and catchment-scale solute transport models have been shown to have major effects on modeling exercise.

The MRF modeling approach was then coupled with a 'source zone' model suitable to describe pesticide release from the top soil layer in intensively managed catchments. A decade-long water-quality monitoring dataset allowed to evaluate the ability of approach to predict pesticide fluxes at two very different spatial scales: tile and catchment scale. The model provided encouraging predictions at the tile station level, while prediction uncertainties increase at larger spatial scales. The greatest discrepancy lies in predicting the high concentration peaks at the start of the season. The LVRW case study highlighted overall considerations on predictions of pesticide export from managed agricultural catchments. At the scales of observation (i.e., fields and small catchments) prediction of the agro-chemical response seems to require an accurate knowledge of the management practices. Pesticide application dates, which are closely related to corn planting dates, constitute strong controls on the hydrologic and the biogeochemical response. However, as the spatial scale increases, it may be argued that these data become less important and the area studied can be more reliably represented by spatially averaged management indicators, such as the curves of acreage percent planted or an average distribution of land-use. From this point of view, the scale of the

river station perhaps represents a type of worst-case scenario for evaluating pesticide export, as the drainage area seems to be too small to use spatially average data, but too large to easily collect the required details from farmers and land owners.

In general, the application of the model to both tile stations and river station showed that the main control on atrazine losses prediction is the interval between application dates and the first large rainfall events, which is in agreement with several earlier studies [*Leaonard*,1990; *Chiovarou and Siewicki*, 2007; *Luo and Zhang*, 2009]. The highest discrepancies between model predictions were observed between the two assumptions on planting (and application) dates. Thus, reliable estimation of pesticide application dates is critical because the temporal window in which atrazine losses are observed is generally small with respect to the entire season. Usually high flow events from managed catchments are observed until up to 40-50 days after crops are planted, which approximately represents the period in which most of atrazine losses occur. In particular, the highest errors were made when applications are estimated later than they actually occur and some major flow event is not adequately predicted. Analogous conclusions were drawn by *Holvoet et al.* [2004], whose results showed that the accuracy in the estimation of the contaminant application dates is much more important than the accuracy in the estimation of other controls such as application rates and rainfall. It has been suggested how, to a certain extent, it is possible to deal with the uncertainties in application dates by relating them to mean air temperatures.

This was also corroborated by the GLUE analysis, which attributes to atrazine application dates and corn planting dates an important control on the atrazine loss process. Additionally, the GLUE analysis shows the predominance of the mass transfer rate constant, k_e, in the source zone on the other parameters of the model This parameter, which may be related to physical characteristics of the transport process (e.g. *Haggerty et al.*, 2004) is in fact difficult to estimate. Overall, the GLUE analysis showed that, in the hydrologic model, all the parameters considered have an important effect on predictions, although main controls are to be attributable to the depth of the soil and the water travel time. On the other hand, a certain level of equifinality was shown among some of the parameters of the biogeochemical model.

These considerations are particularly important when predicting contaminants such as herbicides and pesticides, because they are exclusively of anthropogenic origin. Therefore, the anthropogenic forcing, linked to stochastic rainfall patterns plays an important role in the exported pesticide loads, whereas for other chemicals, such as nutrients, the anthropic component (e.g., fertilizer application) is often clouded by the effect of the chemical soil production and legacy of nutrient sources in the catchment [*Basu et al.*, 2010b].

Overall, the present thesis has addressed several problems that are deemed relevant to the general framework of catchment hydrology. Catchment-scale transport processes were simulated by means of ad hoc modeling approaches, thus allowing for hypotheses testing, scaling analyses and, in certain cases, predictions over ranges of scales. Results were corroborated by robust analyses of extensive datasets, whose purpose was not simply to validate the approaches but rather to provide further insight into the processes.

Appendix A

Lists of Symbols

A.1 Symbols used in Chapter 2

Table A.1: List of symbols used in Chapter 2

Symbol	Description	Units	Symbol	Description	Units
λ_p	Mean rainfall frequency	T^{-1}	γ_p	Inverse of mean rainfall depth	L^{-1}
$\gamma'_p = \gamma_p n Z_r$	Inverse of normalized mean rainfall depth	$-$	I	Rainfall depth	L
n	soil porosity	$-$	Z_r	Rooting depth	L
s_1	field capacity	$-$	s	Relative soil moisture	$-$
PET	Maximum rate of evapotranspiration	$L\,T^{-1}$	s_w	wilting point	$-$
λ	Mean frequency of effective rainfall	T^{-1}	ET	Actual evapotranspiration rate	$L\,T^{-1}$
$\eta = PET/(nZ_r(s_1 - s_w))$	normalized maximum evapotranspiration rate	T^{-1}	Y	Effective rainfall depth	L
ξ_t	stochastic rate of rainfall	T^{-1}	k	inverse of mean residence time	T^{-1}
Q	Catchment scale runoff	L^3T^{-1}	ξ'_t	stochastic rate of effective rainfall	T^{-1}
$\gamma = \gamma_p/(kA)$	inverse of mean runoff jump after a rain event	$T\,L^{-3}$	A	Drainage area	L^2
p_Σ	Weighted average of catchment runoff pdf	$T^2\,L^{-3}$	p_Q	Catchment runoff pdf	$T\,L^{-3}$
P_m	Cumulative distribution of annual minima	$-$	h	Stream stage	L
b	$h - Q$ relationship coeff.	$-$	$f = P_Q$	Catchment runoff cumulative distribution	$-$
p_h	Stream stage pdf	L^{-1}	θ	Inverse of stage when $Q = 1/\gamma$	L
C_w	Nutrient concentration in water column	$M\,L^{-3}$	a	$h - Q$ relationship coeff.	$T^{3b}L^{1-3b}$
k_{eff}	Nutrient loss effective rate constant	T^{-1}	τ_L	Reach travel time	T
S	Stream cross sectional area	L^2	C_s	Nutrient concentration in storage zone	$M\,L^{-3}$
L_x	Reach length	L	k_{sed}	Nutrient loss specific rate constant	T^{-1}
α	Stream-storage exchange rate	T^{-1}	S_s	Storage zone cross sectional area	L^2
q_B	Average flow rate into the sediments	$L\,T^{-1}$	τ_L	Reach travel time	T
Ω	Inverse of k_{eff} when $Q = 1/\gamma$	T	$\beta = S/S_s$	Ratio between compartments	$-$
σ	Sediments porosity	$-$	q	Flow velocity	L/T
w	stream width	L	v_f	Uptake velocity	$L\,T^{-1}$
p_k	k_{eff} pdf	T	$\alpha = q_b/h$	Hyporheic exchange rate	T^{-1}
H	Annual Horton index	L	d_s	Storage zone depth	L
P	Annual precipitation	L	w_s	Storage zone width	L
p_U	Annual baseflow pdf	$1/L$	$r = w/w_s$	Widths ratio	$-$
L	Temporal scale for computing H	T	V	Annual vaporization	L
$\Sigma' = \lambda_p L$	Mean number of rainfall events	L	U	Annual baseflow	L
$\psi = L\langle ET\rangle\gamma_p$	$-$	$-$	p_{HI}	Horton index pdf	$1/L$
			$\phi = P/(PET\,L)$	Humidity index	$-$
			$\Sigma = \lambda L$	Mean number of eff. rainfall events in L	$-$
			$\gamma_s = \gamma_p n Z_r \cdot (s_1 - s_w)$	storage index	$-$

A.2 Symbols used in Chapter 3

Table A.2: List of symbols used in Chapter 3

Symbol	Description	Units
C	Concentration in the mobile zone	ML^{-3}
N	Concentration in the immobile zone	ML^{-3}
k_e	Mass transfer rate constant	T^{-1}
Q	Runoff	L^3T^{-1}
j	Effective rainfall intensity	LT^{-1}
A	Drainage area	L^2
g	System response function	T^{-1}
ϕ	Mass flux at the catchment outlet	MT^{-1}
ω	Age function	–
sur	Subscript indicating surface runoff	–
imp	Subscript indicating flow on impermeable areas	–
int	Subscript indicating interflow	–
sub	Subscript indicating subsurface flow	–
b	Subscript indicating baseflow	–
C_N	Nitrate flux concentration	ML^{-3}
C_L	Lithium flux concentration	ML^{-3}

A.3 Syimbols used in Chapter 4

Table A.3: List of symbols used in Chapter 4

Symbol	Description	Units
L_T	Total annual loads	M
Q_T	Total annual discharge	L^3
$C = L_T/Q_T$	Flow averaged concentration	$M\,L^{-3}$
C	Dissolved concentration	$M\,L^{-3}$
S	Sorbed concentration	$M\,M^{-1}$
$k_D = C/S$	Partition coefficient	$M\,L^{-3}$
Γ	Application coefficient	–
ρ	Bulk density	$M\,L^{-3}$
θ	Volumetric water content	–
ψ	Source/sink term	$M\,L^{-3}T^{-1}$
'i'	Subscript indicating the immobile phase	–
'm'	Subscript indicating the mobile phase	–
k_e	Mass transfer rate constant	T^{-1}
$R = 1 + k_D\rho/\theta$	Retardation factor	–
k_{deg}	Degradation rate constant	T^{-1}
i	Rainfall intensity	$L\,T^{-1}$
j	Effective rainfall intensity	$L\,T^{-1}$
g	System response function	T^{-1}
A	Drainage area	L^2
BF	Baseflow rate	$L^3\,T^{-1}$
ET	Actual evapotranspiration rate	$L\,T^{-1}$
T	Excess rainfall	$L\,T^1$
g_f	Fraction of groundwater recharge	–
S_t	Water content in the active soil layer	L^3
ϕ_j	Mass flux exiting the active soil layer	$M\,T^{-1}$
Q_M	Mass flux at the outlet of the drainage region	$M\,T^{-1}$
V	Characteristic volume for the mass-transfer mechanisms	L^3
N	Concentration in the immobile phase of the active soil layer	$M\,L^{-3}$
C_f	Perfectly mixed concentration in the mobile phase of the active soil layer	$M\,L^{-3}$
V_N	Volume of the immobile zone	L^3
Z	Depth of the active soil layer	L
θ_{fc}	Volumetric soil moisture field capacity	–
θ_{wp}	Volumetric soil moisture wilting point	–
DT_{50}	Solute half-life	T
f_{oc}	Fraction of soil organic carbon	–
k_{oc}	Sorption coefficient	$L^3\,M^{-1}$
τ	Water travel time	T
$k = 1/\tau$	Inverse of water travel time	T^{-1}
α	Baseflow recession constant	T^{-1}

Bibliography

[1] Abramowitz, M., and I. Stegun (Eds.) (1965), *Handbook of Mathematical Functions*, Dover, New York.

[2] Ahuja, L., A. Sharpley, M. Yamamoto, and R. Menzel (1981), The depth of rainfall-runoff-soil interactions as determined by 32P, *Water Resour. Res.*, 17(4), 969974, doi:10.1029/WR017i004p00969.

[3] Alexander, R. B., R. A. Smith, and G. E. Schwarz (2000), Effect of stream channel size on the delivery of nitrogen to the Gulf of Mexico, *Nature*, 403, 758761.

[4] Algoazany, A.S., P.K. Kalita, G.Z. Czapar,and J.K. Mitchell (2007), Phosphorus transport through subsurface drainage and surface runoff from a flat watershed in East Central Illinois, USA, *Journal of Environmental Quality*, 36, 3.

[5] Allen, R. G., L. S. Pereira, M. Smith, D. Raes, and J. L. Write (2005), FAO]56 dual crop coefficient method for estimating evaporation from soil and application extensions, *J. Irrig. Drain. Eng.*, 131, 2.13, doi:10.1061/(ASCE)0733-9437(2005)131:1(2).

[6] Anghel, I., H.J. Turin, P.W. Reimus, P.W. (2002), Lithium sorption to Yucca Mountain tuffs. *Appl. Geochem.* 17, 819824.

[7] Arnold, J. G., P. M. Allen, and G. Bernhardt (1993), A Comprehensive Surface-Groundwater Flow Model. *J. Hydrol.* 142:47-69.

[8] Arnold, J. G., and P. M. Allen (1999), Automated methods for estimating baseflow and ground water recharge from streamflow records, J. Am. Water Resour. Assoc., 35, 411424, doi:10.1111/j.1752-1688.1999. tb03599.x.

[9] Atkinson, S. E., R. A. Woods, and M. Sivapalan (2002), Climate and landscape controls on water balance model complexity over changing timescales, *Water Resour. Res.*, 38(12), 1314, doi:10.1029/2002WR001487

[10] Baldock, D., G. Beaufoy, G. Bennett, and J. Clark, J. (1993) *Nature Conservation and New Directions in the EC Common Agricultural Policy*. Institute for European Environmental Policy, London and Arnhem

[11] Baresel, C., and Destouni, G. (2005). Novel quantification of coupled natural and cross-sectoral water and nutrient/pollutant flows for environmental management. *Environmental Science and Technology*, 39(16): 6182- 6190, DOI: 10.1021/es050522k.

[12] Barry R.G., R.J. Chorley (1998), *Atmosphere, Weather and Climate*, 7th edn. Routledge, London

[13] Basu, N. B., P. S. C. Rao, H. E. Winzeler, S. Kumar, P. Owens, and V. Merwade (2010a), Parsimonious modeling of hydrologic responses in engineered watersheds: Structural heterogeneity versus functional homogeneity, *Water Resour. Res.*, 46, W04501, doi:10.1029/2009WR007803.

[14] Basu N. B., G. Destouni , J. Jawitz , S. Thompson , N. Loukinova, A. Darracq , S. Zanardo, M. Yaeger, M. Sivapalan , A. Rinaldo, and P. S. C. Rao (2010b), Nutrient Loads Exported from Managed Catchments Reveal Emergent Biogeochemical Stationarity, *Geophys. Res. Lett.*, in press.

[15] Battin, T. J., S. Luyssaert, L. A. Kaplan, A. K. Aufdenkampe, A. Richter, and L. J. Tranvik (2009), The boundless carbon cycle, *Nat. Geosci.*, 2, 598600.

[16] Belluck D.A., S.J. Benjamin, and T. Dawson (1991), Groundwater Contamination by Atrazine and its Metabolites: Risk Assessment, Policy and Legal Implications. *American Chemical Society*, Chapter 18, pp. 224- 273.

[17] Bencala, K. E., and R. A. Walters (1983), Simulation of solute transport in a mountain pool-and-riffle stream: A transient storage model, *Water Resour. Res.*, 19(3), 718.724.

[18] Beven, K. and Germann, P. (1982), Macropores and water flow in soils, *Water Resour. Res.*, 18, 13111325.

[19] Beven, K.J. (1996), Equifinality and Uncertainty in Geomorphological Modelling, in B.L. Rhoads and C.E. Thorn (Eds.), *The Scientific Nature of Geomorphology*, Wiley: Chichester, 289-313.

[20] Beven, K.J. (2001), Rainfall - Runoff Modelling: The Primer, *John Wiley & Sons*, England.

[21] Beven, K.J. (1996), Equifinality and Uncertainty in Geomorphological Modelling, in B.L. Rhoads and C.E. Thorn (Eds.), The Scientific Nature of Geomorphology, Wiley: Chich ester, 289-313.

[22] Birgand, F., R. W. Skaggs, G. M. Chescheir, and J. W. Gilliam (2007), Nitrogen removal in streams of agricultural catchments. A literature review, *Crit. Rev. Environ. Sci. Technol.*, 37, 381487.

[23] Bohlke, J. K., R. Antweiler, J. W. Harvey, A. Laursen, L. Smith, R. L. Smith, and M. A. Voytek (2008), Multi-scale measurements and modeling of denitrification in streams with varying flow and nitrate concentration in the upper Mississippi River basin, USA, *Biogeochemistry*, 93, 117.141, doi:10.1007/s10533- 008-9282-8.

[24] Bosch, N.S., 2008. The influence of impoundments on riverine nutrient transport: an evaluation using the soil and water assessment tool. *J. Hydrol.* 335, 14. doi:10.1016/j.jhydrol.2008.03.012.

[25] Botter, G., Bertuzzo, E., Bellin, A., Rinaldo, A., 2005. On the Lagrangian formulations of reactive solute transport in the hydrologic response. *Water Resour. Res.*, 41, W04008. doi:10.1029/2004WR003544.

Botter, G., Settin, T., Marani, M., Rinaldo, A. (2006), A stochastic model of Nitrate transport and cycling at basin scale. *Water Resour. Res.* 42, W04415. doi:10.1029/2005WR004599.

[26] Botter, G., A. Porporato, I. Rodriguez-Iturbe, and A. Rinaldo (2007a), Basin-scale soil moisture dynamics and the probabilistic characterization of carrier hydrologic flows: Slow, leaching-prone components of the hydrologic response, *Water Resour. Res.*, 43, W02417, doi:10.1029/ 2006WR005043.

[27] Botter, G., A. Porporato, E. Daly, I. Rodriguez-Iturbe, and A. Rinaldo (2007b), Probabilistic characterization of base flows in river basins: Roles of soil, vegetation, and geomorphology, *Water Resour. Res.*, 43, W06404, doi:10.1029/2006WR005397.

[28] Botter, G., F. Peratoner, A. Porporato, I. Rodriguez-Iturbe, and A. Rinaldo (2007c), Signatures of large-scale soil moisture dynamics on streamflow statistics across U.S. climate regimes, *Water Resour. Res.*, 43, W11413, doi:10.1029/2007WR006162.

[29] Botter, G., S. Zanardo, A. Porporato, I. Rodriguez-Iturbe, and A. Rinaldo (2008a), Ecohydrological model of flow duration curves and annual minima, *Water Resour. Res.*, 44, W08418, doi:10.1029/2008WR006814.

[30] Botter, G., F. Peratoner, M. Putti, A. Zuliani, R. Zonta, A. Rinaldo, M. Marani (2008b), Observation and modeling of catchment-scale solute transport in the hydrologic response: a tracer study. *Water Resour. Res.* 44, W05409. doi:10.1029/2007WR006611.

[31] Botter, G., E. Daly, A. Porporato, I. Rodriguez-Iturbe, and A. Rinaldo (2008c), Probabilistic dynamics of soil nitrate: the coupling of eco-hydrological and bio-geochemical processes. *Water Resour. Res.* 44, W03416. doi:10.1029/ 2007WR006108.

[32] Botter, G., S. Milan, E. Bertuzzo, S. Zanardo, M. Marani, and A. Rinaldo (2009), Inferences from catchment-scale tracer circulation experiments, *J. Hydrol.*, 369(3.4), 368.380, doi:10.1016/j.jhydrol.2009.02.012.

[33] Botter, G., S. Basso, A. Porporato, I. Rodriguez-Iturbe, and A. Rinaldo (2010a), Natural streamflow regime alterations: Damming of the Piave river basin (Italy), *Water Resour. Res.*, 46, W06522, doi:10.1029/ 2009WR008523.

[34] Botter, G., N. B. Basu, S. Zanardo, P. S. C. Rao, and A. Rinaldo (2010b), Stochastic modeling of nutrient losses in streams: Interactions of climatic, hydrologic, and biogeochemical controls, *Water Resour. Res.*, 46, W08509, doi:10.1029/2009WR008758.

[35] Botter, G., E. Bertuzzo, and A. Rinaldo (2010c), Transport in the hydrologic response: Travel time distributions, soil moisture dynamics, and the old water paradox, *Water Resour. Res.*, 46, W03514, doi:10.1029/2009WR008371.

[36] Bowman, R. S., and R. C. Rice (1986), Accelecated herbicide leaching resulting from preferential flow phenomena and its implications for ground water contamination, *Proc. Conf. on Southwestern Ground Water Issues*, pp. 413-425, National Water Well Association, Dublin, Ohio.

[37] Boyd, M. J. (1978), A storage routing model relating drainage basin hydrology and geomorphology, *Water Resour. Res.*, 14, 921 928.

[38] Boyer, E. W., C. L. Goodale, N. A. Jaworski, and R. W. Howarth (2002), Anthropogenic nitrogen sources and relationships to riverine nitrogen export in the northeastern U.S.A., *Biogeochemistry*, 5758, 137169.

[39] Brusseau, M.L., and P.S.C. Rao (1989), Sorption nonequlhbrmm during organic contaminant transport in porous media, *Crit Rev Environ Control*, 19 33

[40] Brusseau, M.L., R.E. Jessup, and P.S.C. Rao (1989). Modeling the transport of solutes influenced by multi-process nonequilibrium. *Water Resour. Res.*, 25: 1971.

[41] Brusseau, M.L. and Rao, P.S.C. (1990), Modeling solute transport in structured soils a review. *Geoderma* 46, 169192.

[42] Brutsaert, W. (2005), *Hydrology: An Introduction*, Cambridge Univ. Press, New York.

[43] Capel, P.D., S.J. Larson, and A.T., Winterstein (2001), The behaviour of 39 pesticides in surface waters as a function of scale. *Hydrological Processes* 15, 1251e1269.

[44] Castellarin, A., G. Galeati, L. Brandimarte, A. Brath, and A. Montanari (2004), Regional flow-duration curves: Reliability for ungauged basins, *Adv. Water Res.*, 27, 953 965.

[45] Cayan, D.R., R.H. Webb (1993), El Nino/Southern Oscillation and streamflow in the United States. In: Diaz, H.F., Markgraf, V. (Eds.), El Nifio: Historical and Paleoclimatic Aspects of the Southern Oscillation. *Cambridge University Press*, pp. 29-68.

[46] Chapra, S. C. (1997). Surface Water-Quality Modeling. New York, N. Y.: *McGraw-Hill*.

[47] Chiovarou, E. D., and T. C. Siewicki (2007), Comparison of storm intensity and application timing on modeled transport and fate of six contaminants, *Science of the Total Environment* doi:10.1016/j.scitotenv.2007.08.029

[48] Chow, V. T. (1964), *Handbook of Applied Hydrology*, McGraw-Hill, New York.

[49] Chow, V. T., D. R. Maidment, and L. W. Mays (1988), *Applied Hydrology*, McGraw-Hill, New York.

[50] Clapp, R. B., and G. M. Hornberger (1978), Empirical equations for some soil hydraulic properties, *Water Resour. Res.*, 14, 601604, doi:10.1029/WR014i004p00601.

[51] Creed, I.F., L.E. Band, N.W. Foster, I.K. Morrison, J.A. Nicolson, R.S. Semkin, and D.S. Jeffries, (1996), Regolation of nitrate-N release from temperate forests: a test of the n flushing hypothesis. *Water Resour. Res.* 32 (11), 33373354.

[52] Creed, I.F. and L.E. Band (1998a), Exploring functional similarity in the export of nitrate- N from forested catchments: a mechanistic model approach. *Water Resour. Res.* 34 (11), 30793093.

[53] Creed, I.F. and L.E. Band (1998b), Export of nitrogen from catchments within a temperate forest: evidence for a unifying mechanism regulated by a variable source area dynamics. *Water Resour. Res.* 34 (11), 31053120.

[54] Dagan, G. (1989), *Flow and Transport in Porous Formations*, Springer, New York.

[55] Darracq, A., F. Greffe, F. Hannerz, G. Destouni, V. Cvetkovic (2005), Nutrient transport scenarios in a changing Stockholm and Malaren valley region, Sweden. *Water Sci. Technol.* 51 (3-4), 3138.

[56] Darracq, A. and Destouni, G. (2007), Physical versus biogeochemical interpretations of nitrogen and phosphorus attenuation in streams and its dependence on stream characteristics. *Global Biogeochem. Cycles* 21 (3). doi:10.1029/2007GB3003.

[57] Darracq, A., G. Lindgren, G., and G. Destouni (2008). Long-term development of Phosphorus and Nitrogen loads through the subsurface and surface water systems of drainage basins, *Global Biogeochemical Cycles*, 22, GB3022, doi:10.1029/2007GB003022.

[58] Davidson, J. M., and R. K. Chang (1972), Transport of picloram in relation to soil physical conditions and pore water velocity, *Soil Sci. Soc. Am. Proc.*, 36, 257-261.

[59] Dingman, S. (2002), *Physical Hydrology*, Prentice-Hall, Upper Saddle River, N. J.

[60] Doyle, M. W. (2005), Incorporating hydrologic variability into nutrient spiraling, *J. Geophys. Res.*, 110, G01003, doi:10.1029/2005JG000015.

[61] Dubus, I.G., C.D. Brown, and S. Beulke (2003), Sources of un- certainty in pesticide fate modelling. *The Science of the Total Environment*, 317 (173), 5372.

[62] Dunne, T. (1982), Field studies of hillslope flow processes, in: *Hillslope Hydrology*, (edited by: M. J. Kirkby), John Wiley and Sons, Chichester, West Sussex, UK, 1978.

[63] Farnsworth R.K., E.S. Thompson, E.L. Peck (1982), Evaporation Atlas for the Contiguous 48 United States. *NOAA Technical Report*, NWS 33, NOAA: Washington, DC; 26.

[64] Fehlman, H. S. (1985), *Resistance components and velocity distributions of open channel flows over bedforms*, M.S. thesis, Colo. State Univ., Fort Collins.

[65] Flury, M., J. Leuenberger, B. Studer, and H. Fluhler (1995), Transport of anions and herbicides in a loamy and a sandy field soil, *Water Resour. Res.*, 31(4), 823 836, doi:10.1029/94WR02852.

[66] Fuortes L., M.K. Clark, H.L. Kirchner, and E.M. Smith (1997), Association between female infertility and agricultural work history, *Am. J. Industr Med.*, 31:445451

[67] Gish, T.J., A.R. Isensee, R.G. Nash, and C.S. Helling (1991), Impact of pesticides on shallow groundwater quality, *Trans. ASAE*, 34: 1745-1753

[68] Green, H. M., K. J. Beven, K. Buckley, and P. C. Young (1994), Pollution incident prediction with uncertainty, in *Mixing and Transport in the Environment*, edited by K. J. Beven, P. C. Chatwin, and J. H. Millbank, pp. 113137, John Wiley, New York.

[69] Gupta, A. and Cvetkovic, V. (2002) Material transport from different sources in a network of streams through a catchment. *Water Resour. Res.* 38 (3), 112.

[70] Guswa, A. J. (2008), The influence of climate on root depth: A carbon cost-benefit analysis, *Water Resour. Res.*, 44, W02427, doi:10.1029/2007WR006384.

[71] Haggerty, R., C. F. Harvey, C. Freiherr von Schwerin, and L. C. Meigs (2004), What controls the apparent timescale of solute mass transfer in aquifers and soils? A comparison of experimental results, *Water Resour. Res.*, 40, W01510, doi:10.1029/2002WR001716

[72] Hart, D. R. (1995), Parameter estimation and stochastic interpretation of the transient storage model for solute transport in streams, *Water Resour. Res.*, 31(2), 323328.

[73] Harvey, J. W., B. J. Wagner, and K. E. Bencala (1996), Evaluating the reliability of the stream tracer approach to characterize stream-subsurface water exchange, *Water Resour. Res.*, 32(8), 2441.2452.

[74] Henderson, N. E. (1963), *Open Channel Flow*, McMillan, New York.

[75] Holvoet, K., A. van Griensven, P. Seuntjens, and P.A. Vanrolleghem (2004), Sensitivity analysis for hydrology and pesticide supply towards the river in SWAT, *j. pce*, doi:10.1016/j.pce.2005.07.006

[76] Hornsby, A.G., R. D. Wauchope, A.E. Herner (1995), Pesticide Properties in the Environment. *Springer-Verlag*, New York, NY.

[77] Horton R.E. (1933). The role of infiltration in the hydrologic cycle. *Transactions of the American Geophysical Union* 14: 446-460.

[78] Huxman, T., M. Smith, P. Fay, A. Knapp, M. Shaw, M. Loik, S. Smith, D. Tissue, J. Zak, J. Weltzin, W. Pockman, O. Sala, B. Haddad, J. Harte, G. Koch, S. Schwinning, E. Small, and D. Williams, (2004), Convergence across biomes to a common rain-use efficiency. *Nature* 429, 651-654.

[79] Iacobellis, V., P. Claps, and M. Fiorentino (2002), Climatic control on the variability of flood distribution, *Hydrol. Earth Syst. Sci.*, 6(2), 229 237.

[80] Jury, W. A., H. Elabd, and M. Resketo (1986), Field study of napropamide movement through unsaturated soil, *Water Resour. Res.*, 22(5), 749-755.

[81] Kalita, P.K., A.S. Algoazany, J.K. Mitchell, R.A.C. Cooke, and M.C. Hirschi (2004), Subsurface water quality from a flat tile-drained watershed in Illinois, USA, *Agriculture, Ecosystems & Environment*, 115: 183-193.

[82] Kladivko, E. J., L. C. Brown, and J. L. Baker (2001), Pesticide transport to subsurface tile drains in humid regions of North America, *Crit. Rev. Sci. Technol.*, 31(1), 162, doi:10.1080/20016491089163.

[83] Knisel, W. G. (1980), CREAMS, A Field Scale Model for Chemicals, Runoff, and Erosion from Agricultural Management Systems. *U.S. Dept. Agric. Conserv. Res.*, Report No.26.

[84] Kramer, H., and M. R. Leadbetter (1967), *Stationary and Related Stochastic Process*, John Wiley, New York.

[85] Kucharik, C. J. (2006) A multidecadal trend of earlier corn planting in the central U.S. *Agronomy Journal*, Vol. 98, 15441550.

[86] Larose, M., G. C. Heathman, L. D. Norton, and B. A. Engel (2007), Hydrologic and atrazine simulation of the Cedar Creek watershed using the SWAT model. *J. Environ. Qual.*, 36(2): 521-531.

[87] Larsbo, M., S. Roulier, F. Stenemo, R. Kasteel, and N. Jarvis (2005), An Improved Dual-Permeability Model of Water Flow and Solute Transport in the Vadose Zone, 4:398406, *Vadose Zone J.*, doi:10.2136/vzj2004.0137

[88] Leonard, R. A., W. G. Knisel, and D. A. Still (1987), GLEAMS: Groundwater loading effects on agricultural management systems. *Trans. ASAE* 30(5): 1403-1428.

[89] Leonard, R.A., and W.G. Knisel (1989), Groundwater loadings by controlled-release pesticides: a GLEAMS simulation. *Trans. Am. Soc. Agric. Eng.* 32(6).

[90] Leonard, R. (1990), Movement of pesticides into surface waters, *Pesticides in the Soil Environment*, edited by H. H. Cheng, pp. 303 349, Soil Sci. Soc. of Am., Madison, Wis.

[91] Leopold, L. R., and T. Maddock (1953), The hydraulic geometry of stream channels and some physiographic implications, *U.S. Geol. Surv. Prof. Pap.*, 252, 57 pp.

[92] Leopold, L. B., M. G. Wolman, and J. P. Miller (1964), *Fluvial Processes in Geomorphology*, W. H. Freeman, San Francisco, Calif.

[93] Lindgren, G.A., G. Destouni, and A. Darracq (2007) Inland subsurface water system role for coastal nitrogen dynamics and abatement responses. *Environ. Sci. Technol.* 41 (7), 21592164.

[94] Luo, Y., and M. Zhang, (2009). A geo-referenced modeling environment for ecosystem risk assessment: organophosphate pesticides in an agriculturally dominated watershed. *Journal of Environmental Quality*, 38 (32), 664674.

[95] Maloszewski, P., and A. Zuber (1982), Determining the turnover time of groundwater systems with the aid of environmental tracers. Part 1. Models and their applicability, *J. Hydrol.*, 57, 207231.

[96] Maloszewski, P., W. Rauert, P. Trimborn, A. Herrmann, and R. Rau (1992), Isotope hydrological study of mean transit times in an alpine basin (Wimbachtal, Germany), *J. Hydrol.*, 140, 343360.

[97] Marion, A., M. Zaramella, and A. Bottacin]Busolin (2008), Solute transport in rivers with multiple storage zones: The STIR model, *Water Resour. Res.*, 44, W10406, doi:10.1029/2008WR007037.

[98] McDonnell, J. J. (1990), A rationale for old water discharge through macropores in a steep, humid catchment, *Water Resour. Res.*, 26, 28212832.

[99] McGrath G. S., C. Hinz, and M. Sivapalan (2007). Temporal dynamics of hydrological threshold events. *Hydrol. Earth Syst. Sci.*, 11, 923-938.

[100] McGrath, G.S., C. Hinz, and M. Sivapalan (2009), A preferential flow leaching index. *Water Resour. Res.* 45, W11405. doi:10.1029/2008WR007265.

[101] McGuire, K. J., M. Weiler, and J. J. McDonnell (2007), Integrating tracer experiments with modeling to assess runoff processes and water transit times, *Adv. Water Resour.*, 30(4), 824837.

[102] McKnight, D. M., G. M. Hornberger, K. M. Bencala, and E. W. Boyer (2002), in-stream sorption of fulvic acid in an acidic stream: A stream-scale transport experiment, *Water Resour. Res.*, 38(1), 1005, doi:10.1029/2001WR000269.

[103] Milly, P. C. D. (1993), An analytic solution of the stochastic storage problem applicable to soil-water, *Water Resour. Res.*, 29(11), 3755 3758.

[104] Mitchell, J.K., P.K. Kalita, M.C. Hirschi, and R.A.C. Cooke (2003), Upland drainagewatershed hydrology is different. Paper presented at the AWRA 2003 *Spring Specialty Conf. Agricultural Hydrology and Water Quality*, 1214 May 2003, Kansas City, MO.

[105] Mulholland, P.J. et al., 2008. Stream denitrification across biomers and its response to anthropogenic nitrate loading. *Nature* 452 (13), 202205. 06686.

[106] Nathan, R. J., and T. A. McMahon (1990), Identification of homogeneous regions for the purposes of regionalisation, *J. Hydrol.*, 121, 217 238.

[107] Neitsch, S.L., J.G. Arnold, and R. Srinivasan (2002),. Pesticides Fate and Transport Predicted by SWAT: Atrazine, Metolachlor and Trifluralin in the Sugar Creek Watershed. *BRC* Publication 2002-03, 96 pp.

[108] Nkedi-Kizza, P., P.S. C. Rao, R. E. Jessup, and J. M. Davidson (1982), Ion exchange and diffusive mass transfer during miscible displacement through an aggregated Oxisol, *Soil Sci. Soc. Am. J.*, 46(3), 471-476.

[109] Oishi, A.C., R. Oren, K.A. Novick, S. Palmroth, and G.G. Katul (2010), Interannual invariability of forest evapotranspiration and its consequence to water flow downstream, *Ecosystems* 13: 421-436 DOI: 10.1007/s10021-010-9328-3

[110] Önöz, B., and M. Bayazit (2002), Troughs under threshold modeling of minimum flows in perennial streams, *J. Hydrol.*, 258, 187 197, doi:10.1016/S0022-1694(01)00562-5.

[111] Packman, A. I., and K. E. Bencala (2000), Modeling surface-subsurface hydrologic interactions, in *Stream and Groundwater*, edited by J. B. Jones and P. J. Mulholland, pp. 174.183, Academic, New York.

Packman, A.I., N.H. Brooks, J.J. Morgan (2000) Kaolinite exchange between a stream and streambed: laboratory experiments and validation of a colloid transport model. *Water Resour. Res.* 36 (8), 23632372.

[112] Porporato, A., P. DOdorico, F. Laio, and I. Rodriguez-Iturbe (2003), Soil moisture controls on the nitrogen cycle. I. Modeling scheme. *Adv. Water Resour.* 26, 45 58.

[113] Porporato, A., E. Daly, and I. Rodriguez-Iturbe (2004), Soil water balance and ecosystem response to climate change, *Am. Nat.*, 164(5), 625632.

[114] Ralston-Hooper, K., J. Hardy, L. Hahn, H. Ochoa-Acuna, L.S. Lee, L. Mollenhauer, M.S. Sepulveda (2009), Acute and chronic toxicity of atrazine and its metabolites deethylatrazine and deisopropylatrazine on aquatic organisms, *Ecotoxicology*, Volume 18, Number 7, 899-905, DOI: 10.1007/s10646-009-0351-0

[115] Rao, P.S. C., R. E. Green, V. Balasubramanian, and Y. Kanehiro (1974), Field study of solute movement in a highly aggregated Oxisol with intermittent flooding, II, Picloram, *J. Environ. Qual.*, 3(1), 197-202

[116] Rao, P.S. C., J. M. Davidson, R. E. Jessup, and H. M. Selim (1979), Evaluation of conceptual models for describing non-equilibrium adsorption-desorptiono f pesticides during steady flow in soils, *Soil Sci. Soc. Am. J.*, 43(1), 22-28.

[117] Rao, P.S. C., D. E. Rolston, R. E. Jessup, and J. M. Davidson (1980), Solute transport in aggregated porous media: Theoretical and experimental evaluation, *Soil Sci. Soc. Am. J.*, 44(6), 1139-1146, 1980.

[118] Raymond, P. A., and N. H. Oh (2007), An empirical study of climatic controls on riverine C export from three major U.S. watersheds, *Global Biogeochem. Cycles*, 21, GB2022, doi:10.1029/2006GB002783.

[119] Ribaudo M.O., and A. Bouzaher (1994), Atrazine: Environmental Characteristics and Economics of Management, *Resources and Technology Division, Economic Research Service, U.S. Department of Agriculture*, Agricultural Economic Report No. 699.

[120] Rodhe, A., L. Nyberg, and K. Bishop (1996), Transit times for water in a small till catchment from a 16 step shift in the oxygen 18 content of the water input, *Water Resour. Res.*, 32(12), 34973511.

[121] Reddy, K. R., P. S. C. Rao, and R. E. Jessup (1982), The effect of carbon mineralization and denitrification kinetics in mineral and organic soils, *Soil Sci. Soc. Am. J.*, 46, 6268.

[122] Rodriguez-Iturbe, I., and A. Porporato (2004), *Ecohydrology of Water Controlled Ecosystems: Soil Moisture and Plant Dynamics*, Cambridge Univ. Press, New York.

[123] Rinaldo, A. and A. Marani (1987), Basin scale model of solute transport, *Water Resour. Res.*, 23, 21072118, doi:10.1029/WR023i011p02107

[124] Rinaldo, A., A. Bellin, and A. Marani (1989), On mass response functions, *Water Resour. Res.*, 25, 16031617, doi:10.1029/WR025i007p01603

[125] Rinaldo, A., A. Marani, and R. Rigon (1991), Geomorphological dispersion, *Water Resour. Res.*, 28, 513525.

[126] Rinaldo, A., G. Botter, E. Bertuzzo, A. Uccelli, T. Settin, and M. Marani (2006a), Transport at basin scales: 1. Theoretical framework, *Hydrol. Earth Syst. Sci.*, 10, 19 30.

[127] Rinaldo, A., G. Botter, E. Bertuzzo, A. Uccelli, T. Settin, and M. Marani (2006b), Transport at basin scales: 2. Applications, *Hydrol. Earth Syst. Sci.*, 10, 3148.

[128] Rodriguez-Iturbe, I., D. Entekhabi, and R. L. Bras (1991) Non-linear dynamics of soil moisture at climatic scales. I. Stochastic analysis. Water Resources Res. 27, 18991906.

[129] Rodriguez-Iturbe, I., and A. Rinaldo (1997), *Fractal River Basins: Chance and Self-Organization*, Cambridge Univ. Press, New York.

[130] Rodriguez-Iturbe, I., A. Porporato, L. Ridolfi, V. Isham, and D. Cox (1999), Probabilistic modelling of water balance at a point: The role of climate soil and vegetation, Proc. R. Soc. London, Ser. A, 455, 37893805.

[131] Runkel, R. L., and S. C. Chapra (1993), An efficient numerical solution of the transient storage equations for solute transport in small streams, *Water Resour. Res.*, 29(1), 211215.

[132] Rutherford, J. C. (1994), *River Mixing*, John Wiley, New York.

[133] Schilling, K. E., and M. Helmers (2008), Effect of subsurface drainage tiles on streamflow in Iowa agricultural watersheds: Exploratory hydrograph analysis, *Hydrol. Processes*, 22, 44974506, doi:10.1002/hyp.7052.

[134] Searcy, J. C. (1959), Manual of hydrology, 2, Low flow techniques, flowduration curves, *U. S. Geol. Surv. Water Supply Pap.*, 1542-A.

[135] Shaw, R.H. (1977), Climatic requirement, G.F. Sprague (ed.) Corn and crop improvement, *Agronomy*, 18: 591-623

[136] Sivapalan, M., G. Blschl, L. Zhang and R. Vertessy (2003). Down- ward approach to hydrological prediction. *Hydrol. Process.*, 17, DOI: 10.1002/hyp.1425

[137] Smakhtin, V. U. (2001), Low flow hydrology: A review, *J. Hydrol.*, 240, 147 186.

[138] Smith, M.C., J.L. Michael, W.G. Knisel, and D.G. Neary (1994), Using GLEAMS to select environmental windows for herbicide application in forests. *Proceedings of Second Conference on Environmentally Sound Agriculture*, 2022 April, Orlando, FL, pp. 506-512.

[139] Stall, J. B., and Y. Fok (1968), Hydraulic geometry of Illinois streams, *Water Res. Center Res. Rep. 15*, Univ. of Ill. at Urbana-Champaign, Urbana.

[140] Steenhuis, T.S., J. Boll, G. Shalit, J. S. Selker, and I. A. Merwin (1994), A simple equation for predicting preferential flow solute concentrations. *Journal of Environmental QuaLity*, 23, 1058-1064.

[141] Stewart, M. K., and J. J. McDonnell (1991), Modeling base]flow soil]water residence times from deuterium concentrations, *Water Resour. Res.*, 27(10), 2681.2693.

[142] Taylor, G. I. (1921), Diffusion by continuous movements, *Proc. London Math. Soc., Ser. A*, 20, 196211.

[143] Troch, P.A., G. Martinez, V. Pauwels, M. Durcik, M. Sivapalan, C. Harman, P. Brooks, H. Gupta, and T. Huxman (2009), Cli- mate and vegetation water use efficiency at catchment scales, *Hydrol. Process*, 23, 2409-2414, doi: 10.1002/hyp.7358.

[144] Van Genuchten, M. Th., and P. J. Wierenga (1977), Mass transfer studies in sorbing porous media: Experimental evaluation with tritium, *Soil. Sci. Soc. Am. J.*, 4(2), 272-278.

[145] Van Liew, M. W., and J. Garbrecht (2003), Hydrologic simulation of the Little Washita river experimental watershed using SWAT *J. Am. Water Resour. Assoc.* 39(2):413-426.

[146] Vasquez-Amabile, G., B.A. Engel, and D.C. Flanagan (2006), Modeling and risk analysis of nonpoint-source pollution caused by atrazine using SWAT. *Trans. ASAE* 49(3):667-678.

[147] Vogel, R. M., and N. M. Fennessey (1994), Flow-duration. I: New interpretation and confidence intervals, *J. Water Resour. Plann. Manage.*, 120(4), 485 504.

[148] Vogel, R. M., and C. N. Kroll (1989), Low-flow frequency analysis using probability plot correlation coefficients, *J. Water Resour. Plann. Manage.*, 115(3), 338 357.

[149] Wagener, T., M. Sivapalan, P. Troch, and R. Woods (2007), Catchment classification and hydrologic similarity, *Geogr. Compass*, 1, 901931, doi:10.1111/j.1749-8198.2007.00039.x.

[150] Wagner, B. J., and J. W. Harvey (1996), Solute transport parameter estimation for an injection experiment at Pinal Creek, Arizona, in *U.S. Geological Survey Toxic Substances Hydrology Program.Proceedings of Technical Meeting, Colorado Springs, Colorado, September*, 20.24, edited by D. W. Morganwald and D. A. Aronson, U.S. Geol. Surv. Water Resour. Invest. Rep., 94]4015, 186.194.

[151] Wallace, H.A., and E.N. Bressman (1937), Corn and corn growing, *John Wiley and sons*, New York, p. 93-94.

[152] Warner, T. J., T. V. Royer, J. L. Tank, N. A. Griffiths, E. J. Rosi]Marshall, and M. R. Whiles (2009), Dissolved organic carbon in streams from artificially drained and intensively farmed watersheds in Indiana, USA, *Biogeochemistry*, 95, 295.307, doi:10.1007/s10533-009-9337-5.

[153] Wauchope, R.D., T.M. Buttler, A.G. Hornsby, P.W.M. Augustijn-Beckers, and J.P. Burt (1992), The SCS/ARS/CES pesticide database for environmental decision-making. *Reviews of Environmental Chemistry and Toxicology*, 123:1-155.

[154] Weiler, M. and McDonnell, J.J. (2006), Testing nutrient flushing hyotheses at the hillslope scale: a virtual experiment approach. *J. Hydrol.* 319, 339356.

[155] Williams, J. R., C. A. Jones, and P. T. Dyke (1984), A Modeling Approach to Determining the Relationship Between Erosion and Soil Productivity. *Trans. ASAE*, 27:129-144.

[156] Winchester P.D., J. Huskins, and J. Ying (2009), Agrichemicals in surface water and birth defects in the United States. *Acta Paediatr.*, Apr;98(4):664-9.

[157] Wollheim, W. M., C. J. Vorosmarty, B. J. Peterson, S. P. Seitzinger, and C. S. Hopkinson (2006), Relationship between river size and nutrient removal, *Geophys. Res. Lett.*, 33, L06410, doi:10.1029/2006GL025845.

[158] Wondzell, S. M. (2006), Effect of morphology and discharge on hyporheic exchange flows in two small streams in the Cascade Mountains of Oregon, USA, *Hydrol. Processes*, 20, 267287.

[159] Wörman, A., A. I. Packman, H. Johansson, and K. Jonsson (2002), Effect of flow-induced exchange in hyporheic zones on longitudinal transport of solutes in streams and rivers, *Water Resour. Res.*, 38(1), 1001, doi:10.1029/2001WR000769.

[160] Ye, W., B.C. Bates, N.R. Viney, M. Sivapalan, and A.J. Jakeman (1997), Performance of conceptual rainfall-runoff models in low-yielding ephemeral catchments. *Water Resour. Res.*, 33, 153-166.

[161] Yuan, Y., J. K. Mitchell, S. E. Walker, M. C. Hirschi, and R. A. C. Cooke (2000), Atrazine losses from corn fields in the Little Vermilion River watershed in east central Illinois, *Appl. Eng. Agric.* 16 (1), 5156.

[162] Zanardo, S., C. J. Harman, P. A. Troch, P. S. C. Rao, and M. Sivapalan (2011a), Climatic and landscape controls on inter-annual variability of water balance and vegetation water use: a stochastic approach, *in review at Water Resour. Res.*

[163] Zanardo, S., N. B. Basu, G. Botter, E. Bertuzzo, A. Rinaldo, and P. S. C. Rao (2011b), Dominant controls on pesticide transport from tile to catchment scale: lessons from a minimalist model, *in review at Water Resour. Res.*

[164] Zhang, L., N. Potter, K. Hickel, Y. Zhang, and Q. Shao (2008), Water balance modeling over variable time scales based on the Budyko frameworkModel development and testing, *J. Hydrol.*, 360, 117 131, doi:10.1016/j.jhydrol.2008.07.021.